AD

TECHNICAL REPORT ECOM-03743-9

HYDROCARBON-AIR FUEL CELL

FIFTH SEMI-ANNUAL REPORT

By

C. E. HEATH
H. H. HOROWITZ
G. CIPRIOS
E. H. OKRENT
W. J. ASHER
J. S. BATZOLD
M. BELTZER
B. BROYDE
A. A. ZIMMERMAN

OCTOBER 1966

ECOM

UNITED STATES ARMY ELECTRONICS COMMAND • FORT MONMOUTH, N. J.

CONTRACT DA 36-039 AMC-03743 (E)

ESSO RESEARCH AND ENGINEERING COMPANY
GOVERNMENT RESEARCH LABORATORY
Linden, N. J.

NOTICES

DISCLAIMERS

The findings in this report are not to be construed as an official Department of the Army position, unless so designated by other authorized documents.

The citation of trade names and names of manufacturers in this report is not to be construed as official Government indorsement or approval of commercial products or services referenced herein.

DISPOSITION

Destroy this report when it is no longer needed. Do not return it to the originator.

Technical Report ECOM-03743-9

October 1966

HYDROCARBON-AIR FUEL CELL

Fifth Semi-Annual Report
1 January 1966 to 31 July 1966
Report No. 9

Contract No. DA 36-039 AMC-03743(E)
Task No. 1C622001A053-04

Prepared by

Carl E. Heath
Hugh H. Horowitz
George Ciprios
Eugene H. Okrent
William J. Asher
John S. Batzold
Morton Beltzer
Barret Broyde
Abraham A. Zimmerman

Esso Research and Engineering Company
Government Research Laboratory
Linden, New Jersey

For

Electronic Components Laboratory
United States Army Electronics Command, Fort Monmouth, N. J.

SUMMARY

The research discussed in this report is a continuation of studies aimed at determining the feasibility of a direct hydrocarbon-air fuel cell capable of widespread military application. These investigations have been concerned with the mechanism of electrochemical oxidation of hydrocarbons, the search for non-noble metal electrocatalysts, the improvement of platinum catalyst utilization, and the development of new intermediate temperature electrolytes.

2.1 Task A, Mechanism Studies

Studies of the mechanism of the adsorption and oxidation of hydrocarbons were continued with the aim of understanding limiting electrode processes and uncovering leads to their solution. The effect of trace quantities of poisons on the electrocatalysis of butane oxidation on platinum was examined. It was proposed that selective blockage of sites or electronic interactions between adsorbed species would influence the adsorptive or oxidative processes. Sulfuric acid electrolyte was mostly used in these studies; however, other electrolytes were also investigated.

With iodide ion or triphenyl phosphine as selective "poisons" butane adsorption equilibrium, butane adsorption rate, and butane electrochemical oxidation rate were measured by cyclic voltammetry. Iodide was found to adsorb so strongly relative to butane that there was essentially no interaction. The poison merely occupied surface sites indiscriminately; butane adsorbed and reacted on the remaining sites and reaction rates were reduced proportionately. The weaker poison, triphenyl phosphine, was oxidized in the same potential range as the hydrocarbon and its effects could not be distinguished. Other adsorbates should be investigated.

Attempts to study the fundamental effects of other electrolytes on hydrocarbon adsorption and oxidation were unsuccessful. Impurities or reactive components in phosphoric acid and several buffer electrolytes interfered with adsorption rate determinations. Several purification methods were evaluated but were not effective. Since electrolyte interactions have an important effect on hydrocarbon oxidation, further efforts to study the basic reaction steps should be made.

2.2 Task B, Non-noble Metal Electrocatalysts

Research on non-noble metal electrocatalysts as substitutes for the platinum metals used thus far followed three approaches:

(1) Investigation of mixed metal oxides and carbides.

(2) Studies to apply the two site catalysis mechanism based on platinum for selecting non-noble metal alloys for use in buffer electrolytes.

(3) Research on applying the electronic theory of metals and semi-conductors to catalyst development.

Two classes of compounds which meet the electrocatalyst requirements of conductivity and corrosion resistance are the tungsten bronzes and the eta-carbides. Furthermore, catalytic transition metals might be incorporated into the lattices of the compounds in a way similar to the perovskites previously studied in this program. The tungsten bronzes have the general formula A_xWO_3 where A is an alkali or alkaline earth metal or lead, silver, copper or thallium. The eta-carbides have a stoichiometric formula approximated by M_6C, where M can be a combination of two or three elements.

The bronzes and their modifications proved to be most promising. Nickel was incorporated into a modified tungsten bronze structure with an extremely complex X-ray diffraction pattern. Probably, the material consists of mixed bronze and oxide phases. $Ni_{0.237}WO_3$ was an electrical conductor, was not corroded, and was an active hydrogen electrocatalyst. The catalytic activity was established by potentiostatic and voltage scan methods. Current densities of 1-5 ma/cm^2 were observed in sulfuric acid at 90°C. Oxide [illegible]ining larger quantities of nickel are also catalytic, although there is some initial corrosion in these materials. Europium tungsten bronze, a true bronze, is also catalytic. The mechanism of electrocatalysis has not been established; however, voltage scans suggest that the fuel reduces an electrochemically regenerable tungsten oxide.

Performance of these catalysts appeared to be limited by two factors. Surface areas were low, < 5 m^2/gm, in comparison with 30-100 m^2/gm for platinum black. While pellets have high conductivity, interparticle electrical resistance is large. Electrodes made from powders may, therefore, have unacceptably high local resistance. Light sintering does restore conductivity. Thus, special electrode fabrication techniques must be developed to exploit this development.

Further work on these compounds is clearly justified to optimize catalyst and electrode structure.

The eta-phase carbides investigated have not shown definite activity. However, surface areas are unusually low. Method to decrease particle size should be explored.

The two-site electrocatalysis mechanism has been useful in the development of multicomponent noble metal catalysts and could provide a rationale for selecting non-noble metal hydrocarbon catalysts for buffer electrolytes. To determine the validity of this approach the interactions of nickel, ruthenium, and ethylene in alkaline and buffer electrolytes were studied. Nickel was chosen to provide the adsorption site; ruthenium was selected as a model redox site to be replaced by a non-noble metal later. These studies have shown that ethylene is adsorbed on nickel in potassium carbonate, but not in potassium hydroxide. This finding explains the lack of activity previously observed for nickel catalysts and suggests that electrolyte modification is a fruitful area for further work. Research on mixed nickel-ruthenium catalysts has begun, but carbonate deposition in the electrodes interfered with the studies.

Application of the electronic theory of metals and semi-conductors to fuel cell catalyst development has been suggested frequently, but most efforts have been haphazard. As the first step, a series of Raney alloys chosen from the first row transition elements and having known magnetic properties were prepared. Alloys were chosen to continuously vary magnetic moment (and hence d- or s-band occupancy) while maintaining a constant crystal structure. These alloys were evaluated as hydrogen and hydrocarbon electrocatalysts and olefin hydrogenation catalysts.

Hydrogen electrocatalytic activity was observed for Ni-Cu, Ni-Co, and Ni-Fe solid solution alloys. Activity correlated with magnetic moment, and, consequently, d-band occupancy. Maximum catalysis was obtained at 1.0 Bohr magnetons. No hydrocarbon activity was found, probably because, as discussed above, ethylene will not adsorb on nickel in alkaline electrolytes. All the catalysts prepared were highly active for olefin hydrogenation and the tests were diffusion rather than activation limited. Further investigations will be concerned with extending the alloy range and improving the evaluation procedures.

2.3 Task C, Noble Metal Catalyst Studies

Studies to improve platinum utilization continued to show promise. The initial target for this program is a liquid or gaseous hydrocarbon electrode capable of 150 ma/cm^2 with less than 2 mg/cm^2 noble metal. Potential catalyst supports, co-supports, and treatments which would increase inherent catalytic activity and dispersion were investigated as well as methods which would increase platinization levels in the interface zones.

Adsorption of platinum salts on to carbon supports yielded high utilization, but limited adsorption capacity reduced the catalyst quantity which could be located at the interfaces. Temperature studies did not uncover better adsorption isotherms, but ozonation did deactivate ineffective adsorption sites. Using this technique, electrodes yielding 80 ma/cm^2 on butane at 3.2 mg/cm^2 loading have been developed. Analysis has also confirmed that platinum utilization is inversely proportional to crystallite size.

The carbon co-support also affects utilization. Sodium tungsten bronze and silica have been found to be effective. Also, a new system based on alumino-silicate molecular sieves, now under investigation, may make even smaller catalyst crystallites than now possible.

2.4 Task D, New Electrolytes

Hydrocarbon electrodes are limited by activation rather than diffusion limited phenomena. Higher temperature operation, within the constraints of engineering practical field batteries, should significantly improve fuel cell power densities for both non-noble metal and platinum catalyzed electrodes. Previous studies confirmed this hypothesis using an intermediate electrolyte such as pyrophosphoric acid.

Mixed alkali metal dihydrogen phosphates were studied. These electrolytes were not likely to be corrosive and in contrast with the alkali metal bisulfates, previously evaluated, should be invariant and not exhibit unwanted redox potentials. A 25 wt % $NaH_2PO_4 \cdot H_2O$, 75 wt % KH_2PO_4 electrolyte, which is a supercooled viscous liquid at about 100°C, was primarily studied.

These melts were stable; insoluble metaphosphates did not form over ten days at 260°C. Furthermore, a theoretical analysis indicated that they reject CO_2. Electrolytic conductivity was 16 ohm-cm at 275°C, requiring closer cell spacing than often used in fuel cell design. But improved electrode performance should more than offset such debits. The ability of these electrolytes to minimize ionic concentration polarization, i.e., buffer capacity, is satisfactory. Most encouraging, however, is the noncorrosiveness of these electrolytes, even at 250-300°C. Tantalum, nickel-cobalt, and glass, all severely attacked by acid electrolytes at these temperatures are quite stable in mixed alkali phosphates.

High current densities were obtained on both hydrocarbon and oxygen electrodes. At 250°C, butane was polarized 0.35 v at 200 ma/cm^2 and oxygen, 0.18 v, at the same current density. Humidification improved cathode performance. It is particularly significant that unlike aqueous, non-acid electrolytes, excellent hydrocarbon performance was obtained in these weak acid melts.

Based on these results, mixed alkali phosphate electrolytes warrant further development.

CONTENTS

ILLUSTRATIONS

TABLES

APPENDIX TABLES

SECTION 1

INTRODUCTION

The objective of these investigations is to determine the feasibility of a direct hydrocarbon-air fuel cell capable of widespread military application. Such fuel cells must use fuels which react to carbon dioxide, which must be reasonably available, and pose no unusual corrosion, toxicity, or handling problems. Also, the cell must use a CO_2-rejecting electrolyte and operate at temperatures consistent with reasonable start-up characteristics and which would be thermally self-sustaining without excessive loss in efficiency. Other desired requirements include high electrical output per unit volume and weight, high efficiency, long life, high reliability, reasonable cost, particularly catalyst cost, and ruggedness.

Previous research under this program has established that liquid hydrocarbons can be directly oxidized to carbon dioxide in CO_2 rejecting electrolytes. Performance levels are satisfactory, 17-21 mw/cm^2 and 14-17 mw/cm^2 having been demonstrated on oxygen and air, respectively. The fuel was decane, representative of a jet fuel. Suitable electrode structures have been developed and multicell units operated. However, only platinum had given suitable electrocatalytic activity and the quantities required preclude any extensive application.

Current work is directed toward finding non-noble metal electrocatalysts to replace the platinum or to reduce substantially the quantity of platinum required. Since catalytic activity would be enhanced by higher temperature operation than is possible with the sulfuric or phosphoric acid electrolytes now used, efforts have also been aimed towards new intermediate temperature electrolytes for the 150-300°C range.

The program is thus divided into four parts, referred to as Tasks A through D in this report. Task A describes electrocatalytic mechanism studies, Task B, studies on non-noble metal catalysts, and Task C, research on noble metal catalyst improvement. Task D discusses new electrolyte research.

SECTION 2

EXPERIMENTAL STUDIES AND DISCUSSION

2.1 Task A, Mechanism Studies

Studies of the mechanism of adsorption and oxidation of hydrocarbons continued along two lines. First, the effect of very small amounts of poisons on the behavior of platinum black toward butane was determined, in the hope that partial coverage of the surface with strongly adsorbed materials might promote hydrocarbon absorption. Secondly, an attempt was made to carry out similar studies in other electrolytes such as concentrated phosphoric acid and buffer.

Phase 1 - Effect of Poisons on Butane Adsorption on Platinum

The effect of adsorbed "poisons" on the adsorption of butane on platinum was studied, to determine whether selective blockage of sites, electronic effects of the adsorbed species, or interactions between the adsorbates would affect the adsorption or oxidation processes. The electrolyte was 3.7 M sulfuric acid at 80 to 95°C, the catalyst was Engelhard platinum black and the poisons were first iodide ion, and, second triphenyl phosphine. The extent of adsorption, the rate of adsorption and the shape of the oxidation curve of the adsorbed butane were measured in the iodide case.

Part a - Saturation Butane Coverage of Iodide Treated Platinum

Experiments were run using platinum black on a flag electrode to measure the relation between total iodide and butane coverage. One fourth of one cc of 0.01 M potassium iodide solution (2.5×10^{-6} moles) was added to electrolyte (about 120 cc) containing a platinum flag screen electrode covered with platinum black. The catalyst surface area amounted to about 7.5×10^{-6} moles of hydrogen atom sites. (Equivalent to 15 mg of Pt black with ten percent of all atoms in the surface). After 30 minutes to 2 hours adsorption time, one fifth to one third of the surface was covered with iodide ion, as shown by a decrease in the platinum hydride peaks in a linear voltage scan. The iodide also manifested itself by an anodic peak on top of the oxide formation wave and a smaller cathodic peak. The potential between the two waves, 1.2 volts, indicated that iodate, IO_3^-, was the oxidation product of the iodide, and that the cathodic peak was the reduction of some of the iodate formed. The ratio of the iodide oxidation wave to the decrease in hydride coulombs was 3.18, suggesting that one iodide blocks about two hydrogen sites. (See Appendix A-1 for details and Figure A-1 for an illustrative scan.)

With this as a background, butane adsorptions were run with and without adsorbed iodide. The wetted electrode was held for varying periods of time in the butane gas phase with its lower edge touching the electrolyte. At the end of the adsorption period the electrode was totally immersed in electrolyte, so that adsorption thereafter was negligible, and then voltammetrically scanned up to one volt from reversible hydrogen. These scans measured almost all of the adsorbed butane without oxidizing the iodide. Between butane adsorptions hydrogen coverage was checked, in one series of experiments, to be sure that iodide coverage was remaining constant. After a series of adsorptions was completed a complete scan was run to 1.4 volts versus hydrogen to determine the iodide coverage.

Figure A-1

Diagrammatic Butane-Iodide Scans

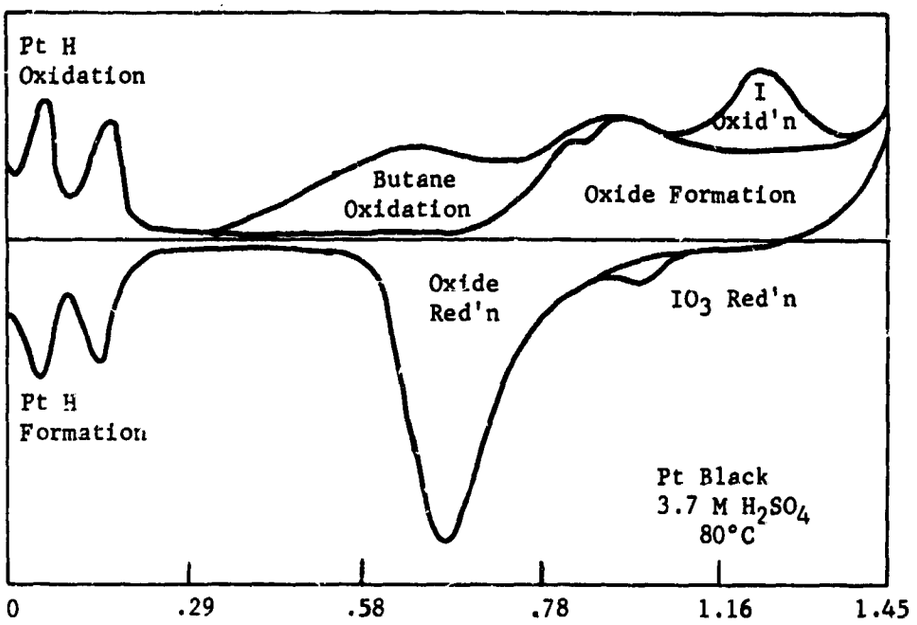

The result simply stated was that partial coverage of the surface with iodide was equivalent to having correspondingly less platinum. Saturation coverage with butane was reached in about 30 minutes, and was equal to that fraction of the surface not covered by iodide. This is illustrated in Table A-1, calculated from the data in Appendix A-1.

Table A-1

Fraction of Sites Covered by Butane and Iodide

Iodide Coverage	Fraction Uncovered	Saturation Butane Coverage
0	1.0	1.0
0.33	0.67	0.65
0.46	0.54	0.51

Assuming that the butane covers only Type I platinum sites (8) it appears that the iodide does not cover either the Type I or Type II sites of platinum selectively, but covers them both in equal proportion. This suggests that the two types of hydrogen are closely associated on each platinum atom and each iodide covers them both at once. This is corroborated by the facts that each iodide does occupy about two hydrogen sites, and that the scans show that both hydrogen peaks are decreased simultaneously by iodide adsorption.

Part b - Oxidation Characteristics of
Butane on Iodide Treated Platinum

At the same time that the total butane coverage was obtained, the scans were examined for the detailed shape of the butane oxidation wave. The peak current was measured, along with the voltage at the peak current, and the current at a fixed potential, 0.45 volts versus calomel or 0.60 volts versus reversible hydrogen. The butane currents were generally less on the iodide treated electrodes and the peak voltages generally higher on the iodide treated electrodes. However, if the butane coverages were expressed as fractions of the iodide-free sites and the currents also corrected for iodide coverage (Appendix Table A-2), then all the data fell on the same curves. Figure A-2 gives the corrected maximum current as a function of corrected butane coverage; a simple linear relation was found.

Figure A-2

Maximum Scan Current on Iodide Treated Platinum

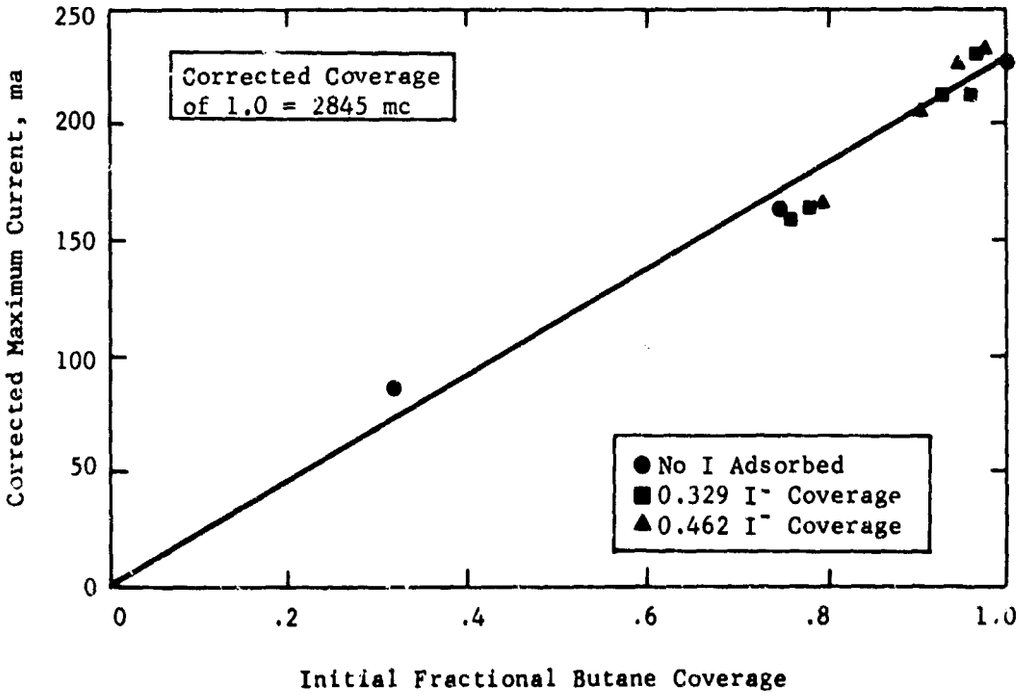

The peak voltage becomes more anodic with increasing initial coverage (Figure A-3). This is probably because very high fuel adsorption restricts the number of sites available for water discharge and thereby inhibits oxidation.

Figure A-3

Butane Peak Voltage on Iodide Treated Platinum

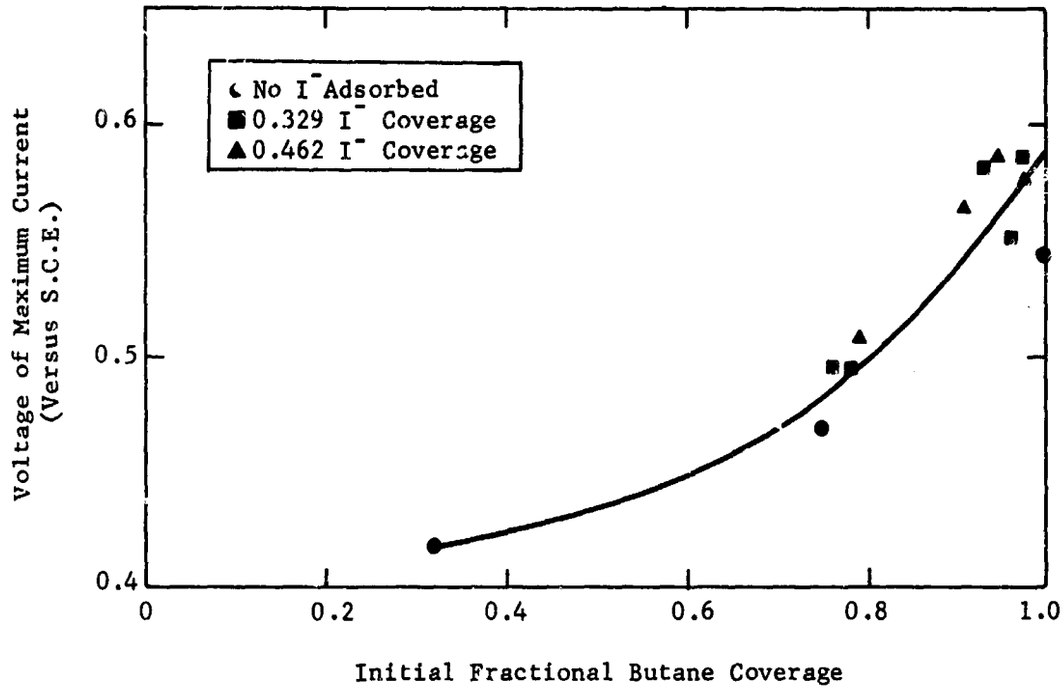

The same factor causes the current at the fixed voltage before the peak to rise with coverage and then drop again. Again the presence of iodide has little effect on the shape of the curve. See Figure A-4.

Thus, it appears that adsorbed iodide ion does not interact with adsorbed butane so as to affect the latter's oxidation rate, other than to make fewer active platinum sites available.

Part c - Adsorption Rates of Butane
on Iodide Treated Platinum

Previous results had indicated that the flag electrodes are not suitable for measuring adsorption rate limits, since they are limited by diffusion. However, the data from which Figures A-2 to A-4 were taken (Appendix A-1) appeared to indicate a more rapid approach to equilibrium coverage at low adsorption time for the iodide treated electrodes than for the controls. However, a more extensive repetition of this data showed that this was not generally the case (Appendix A-2).

Figure A-4

Butane Scan Current at Fixed
Voltage on Iodide Treated Platinum

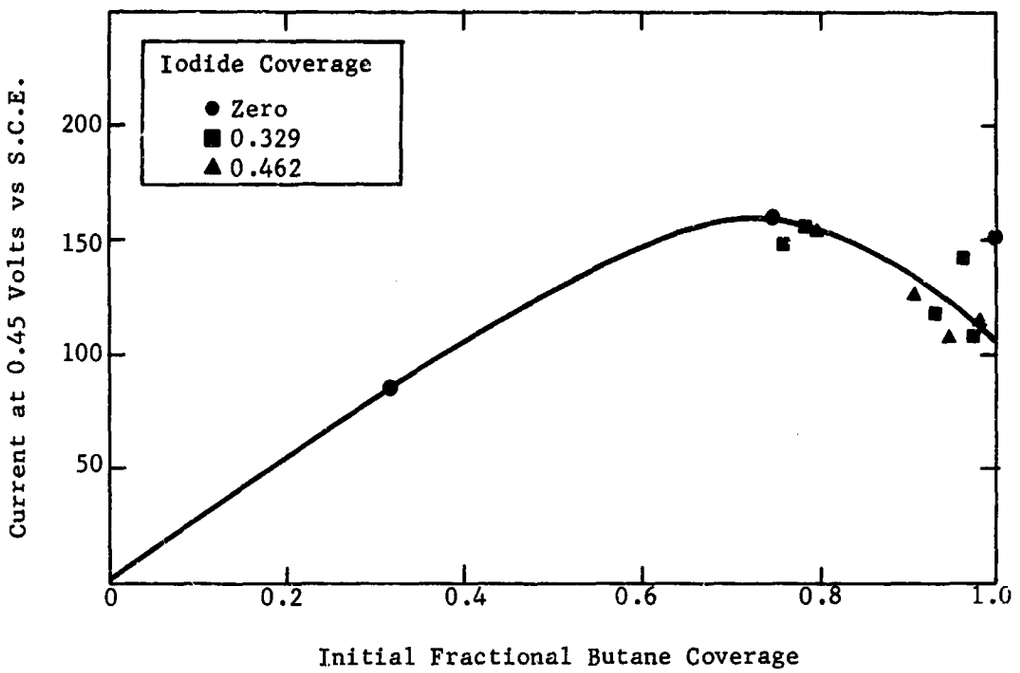

Figure A-5 shows that approach to equilibrium was the same with and without iodide treatment, with the exception of two unexplained instances where high coverages were obtained after short exposures.

Two methods were used to obtain more valid measures of the adsorption rates. In one, the flowing electrolyte system described in an earlier report (7) was used. Electrolyte saturated with butane was flowed through the catalyst, mounted on a sintered gold disk, at a high enough rate not to be diffusion limited. While there were problems with the system, described in Appendix A-3, with adequate base line and flow rate corrections it was possible to determine the total amount of butane adsorbed in a continuous short scan and to estimate the iodide coverage at the same time. The rate of butane adsorption was decreased by the adsorption of iodide in roughly the same ratio as the decrease in surface sites, as shown in Table A-2.

Figure A-5

Adsorption of Butane on Flag Electrode

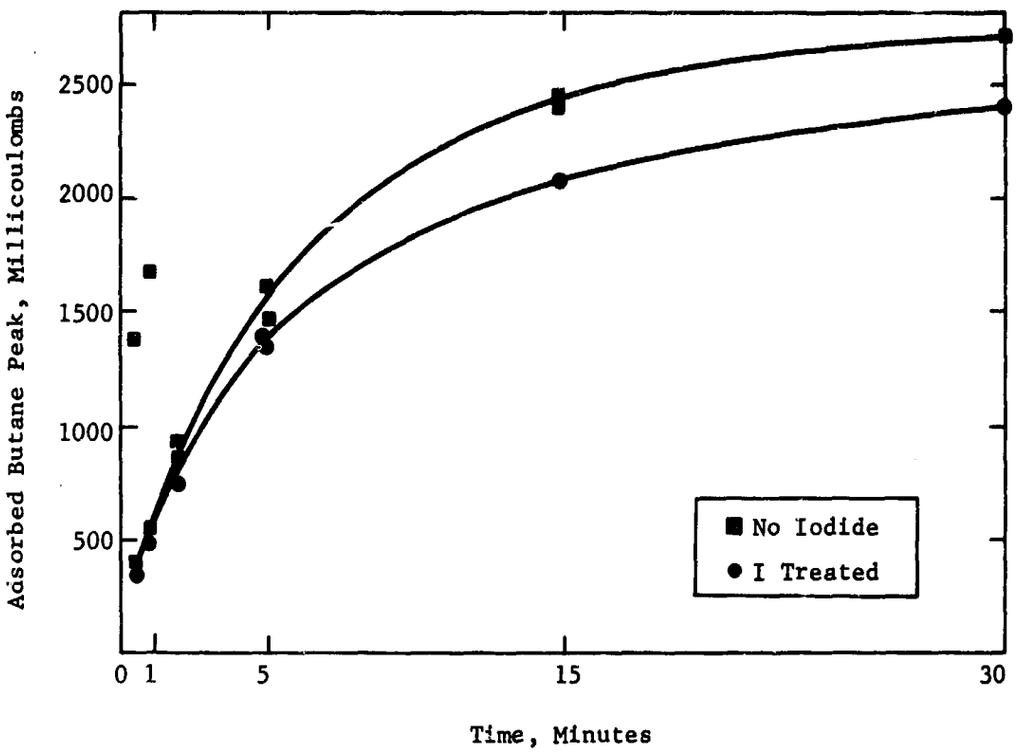

Table A-2

Relative Butane Adsorption Rates on Iodide Treated Platinum

Fractional Iodide Coverage	Fractional Free Surface	Relative Butane Adsorption Rate
0	1.0	1.0
0.42	0.58	0.46
0.73	0.27	0.37

There appears to be no large accelerative effect of adsorbed iodide ion on the rate of butane adsorption within a rather large experimental error. In view of the previous results with total coverage and with oxidation rates it is most likely that iodide has no effect on butane adsorption rate other than to change the number of sites available.

A second method for estimating adsorption rate was simply to measure the butane limiting current on a porous diffusion electrode, since previous work has shown this to be determined by the adsorption rate (7). A standard 50 mg/cm^2 Engelhard platinum black electrode, supported on a platinum screen and sintered with gelled Teflon emulsion, was used. In galvanostatic performance runs the precise limiting current was difficult to establish, but little difference was noted between an iodide free and the same iodide treated electrode. Both polarized 0.4 volts at 20 ma/cm^2. The steady state method was also used potentiostatically with iodide in other electrolytes and with triphenyl phosphine, as discussed below.

Part d - Adsorption of Triphenyl Phosphine

Triphenyl phosphine (TPP) proved to be very slightly soluble in 3.7 M sulfuric acid. Nevertheless, a platinum flag electrode in contact with TPP saturated electrolyte showed virtually complete elimination of the platinum hydrogen peaks in a voltage scan, indicating a high surface coverage. Unfortunately, the oxidation of triphenyl phosphine did not occur in a narrow potential range at highly anodic potentials as in the case of iodide, but covered a wide range which overlapped the butane oxidation potentials.

A platinum flag electrode exposed to electrolyte that was 10% saturated with TPP showed about 15-20% coverage of hydrogen sites (1326 mc total anodic and cathodic hydrogen peaks without TPP, 1026 mc with TPP). After a 30 minute exposure to butane in the gas phase with the lower edge of the flag touching electrolyte, the electrode when untreated showed 2096 mc in the butane peak, when treated with the TPP showed 2156 mc. The latter peak had a different shape, indicating that some of the 2156 mc was due to oxidation of the TPP. Thus, the total coverage figures indicated no notable effect of TPP on butane adsorption.

A measure of the effect of adsorbed TPP on butane adsorption and oxidation was obtained from steady state runs on a standard platinum-Teflon electrode. Exposure of the electrode to electrolyte saturated with TPP prior to the start of the butane run produced a decided drop in performance as shown in Figure A-6.

The results with triphenyl phosphine indicate no performance benefits due to its presence. They also illustrate the point that only under fortunate circumstances is it possible to obtain independent oxidation and adsorption measurements with two adsorbed substances using the voltage scan technique.

Part e - Modification of Flowing Electrolyte System

In view of the difficulties encountered with the flowing electrolyte system, mentioned in part c, the system was improved in a number of ways. The electrolyte head was raised from nine to eighteen inches without increasing its volume appreciably by using a longer and narrower flanged vessel. This provided greater flow rates to insure overcoming diffusion limits. The counter electrode was encased in a tube with a fritted glass bottom to avoid the entrance of gases evolved at the counterelectrode into the working electrode region. A large "Varibore" stopcock was added to the system to allow the flow to be shut off during a scan to avoid unexplained flow rate effects on blank scans. A mixing chamber was included in the system to allow liquid fuels to be used. A number of other improvements were made, so that valid measurements of the important factor, hydrocarbon adsorption rate, can be made on future catalysts.

Figure A-6

Butane Performance on TPP Treated Electrode

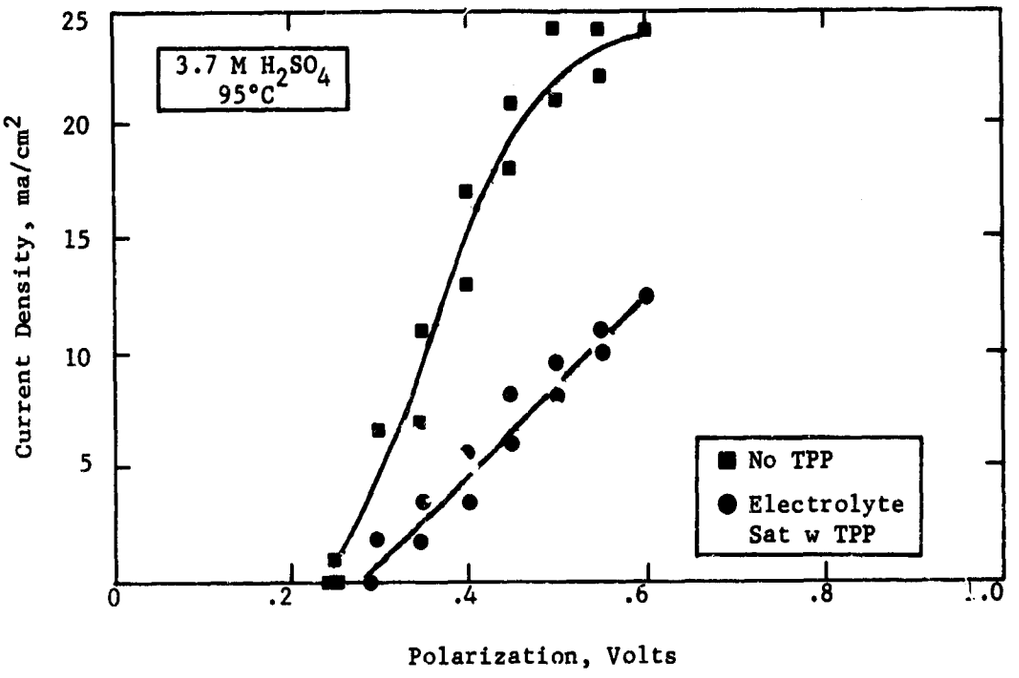

Part f - Decane Adsorption

An attempt was made to determine whether decane adsorption could be measured in the flowing electrolyte system. Decane was placed in a mixing chamber upstream of the vessel containing the platinum catalyst mounted on the porous gold disk. Electrolyte saturated with decane was flowed from the mixing chamber through a glass wool plug and eventually through the catalyst bed. After thirty minutes no decane adsorption could be detected. This result, if confirmed, would be very significant. It would indicate that, unlike butane, decane does not reach the electrode surface via a solubility-diffusion process, but by some other means, such as surface diffusion.

Phase 2 - Other Electrolytes

Attempts were made to carry out voltammetric adsorption-oxidation studies in electrolytes other than sulfuric acid. Phosphoric acid was examined to determine whether the same adsorption effects would be obtained in this more active electrolyte as were obtained in sulfuric acid earlier (7). Various buffer electrolytes were also examined to learn more about the apparent failure of saturated hydrocarbons to

adsorb in non-acidic media. However, in all cases the adsorption rate measurements were stymied by the presence of oxidizable impurities in the electrolytes. With 13.7 M phosphoric acid at 150°C as the electrolyte, an oxidation peak was observed in blank runs at the same potential that fuel peaks are ordinarily observed. The impurity wave peaked near 0.5 volts versus S.C.E. This occurred both in the flowing electrolyte system and in the dipping flag system, after exposure times of two to forty minutes. Replacement of the porous gold plate and the circulating Mace pump, and elimination of the Viton gasketing and all non-Teflon tubing failed to improve the situation. Treatment of the Baker phosphoric acid with hydrogen peroxide, nitric acid and by pre-electrolysis had no effect. Using argon, nitrogen or laboratory air as the atmosphere had no effect. It began to be suspected that the phosphoric acid itself was being reduced to an oxidizable impurity when the electrode was cathodized. This hypothesis was supported by the fact that addition of 1 gm of sodium phosphite pentahydrate to 120 cc of electrolyte produced a very large impurity wave.

Similarly a pH 7 phosphate buffer, consisting of one molar each potassium mono- and dihydrogen phosphate showed a strongly adsorbing impurity. This electrolyte was intended to be used to study the effect of adsorbed iodide in non-acidic media. However, exposure of the electrode to the buffer containing a small amount of potassium iodide showed a complete elimination of the Type II hydrogen peak, a long drawn out impurity oxidation wave, and no iodide peak. The use of butane or argon atmospheres or the elimination of the added iodide had no effect on the scans. Hence an impurity was adsorbing so strongly it blocked the surface to both iodide and butane adsorption.

Steady state performance runs using a flange cell and a porous diffusion electrode containing 50 mg platinum black per cm^2 were carried out 95°C in the near neutral phosphate buffer. Maximum currents in the range of only 3 ma/cm^2 were obtained with or without added iodide (Figure A-7). This esult raised the possibility that adsorbable impurities might be limiting the activity of non-acidic electrolytes.

To avoid reducible anions carbonate and borate buffers were next examined. A buffer of one molar each potassium carbonate and bicarbonate also showed elimination of the hydrogen peaks on platinum black and an oxidation wave in a blank run with no fuel added. This may be the same as Giner's reduced carbon dioxide (9).

Finally, a pH 7 buffer of sodium tetraborate and sulfuric acid was prepared, which showed no hydrogen peak elimination on standing and no growth of an impurity wave on a static dipping flag electrode. It also showed a butane adsorption wave in the presence of that fuel and an iodide oxidation wave after iodide adsorption. Borate apparently did not contain or form oxidizable impurities.

Steady state butane runs were made in pH 7.6 borate-sulfuric acid buffer with and without adsorbed iodide. The buffer consisted of 175 cc of 0.5 M sulfuric acid and 1 M sodium tetraborate, to which 2.5 cc of 0.01 M potassium iodide was added in half the cases. In duplicate pairs of runs using a porous diffusion type electrode, butane gave up to 23 ma/cm^2 limiting current. However, the polarizations at which appreciable current densities were reached were extremely high, 0.5 to over 1.0 volts (Table A-3). It was concluded from the shape of the curve that the buffer was failing at the anode, allowing acidity to build up, which in turn provided the high activity, but at high polarizations. Due to this effect, electrode performance was not very reproducible and the small apparent benefit for iodide was not considered significant.

Figure A-7

Steady State Butane Performance
Phosphate Buffer, pH 6.7, 95°C

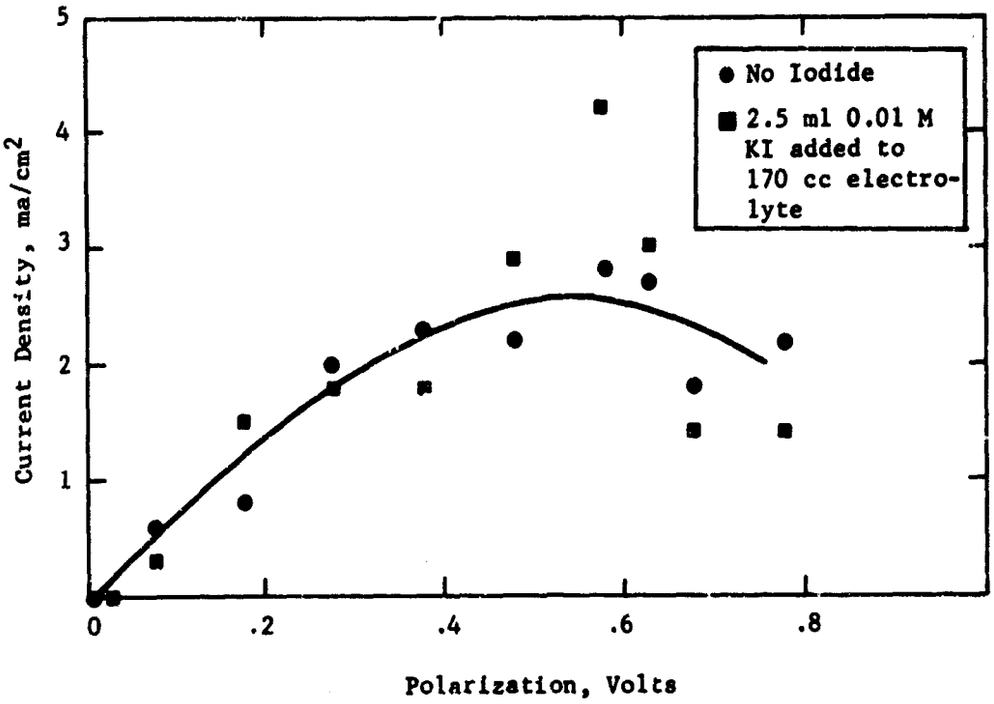

Table A-3

Activity of Butane in pH 7.6 Borate Buffer

Flange Cell, Potentiostatted Runs, 95°C

Current Density, ma/cm²	Polarization, volts			
	No KI		With KI	
	Run 1	Run 2	Run 1	Run 2
0	0.13	0.14	0.08	0.15
5	0.68	0.59	0.57	0.49
12	0.83	0.85*	0.77	0.75
13.5	0.85	--	0.81	0.80*
11	1.05*	--	0.90	--
23	--	--	1.05*	--

*Limiting current reached.

When a borate buffer containing more of the basic buffering component was used, the maximum current dropped back to 3 ma/cm^2, as with the phosphate buffer (Figure A-8). Hydrogen in the same electrolyte performed considerably better despite the transport difficulties of this buffer indicated by its 26 ohm cm resistivity. Thus, it appears that pH per se limits hydrocarbon performance and that impurities in the electrolyte, while hampering adsorption measurements, do not affect the steady state performance of hydrocarbon fuels.

Figure A-8

Performance in pH 9.2 Borate Buffer

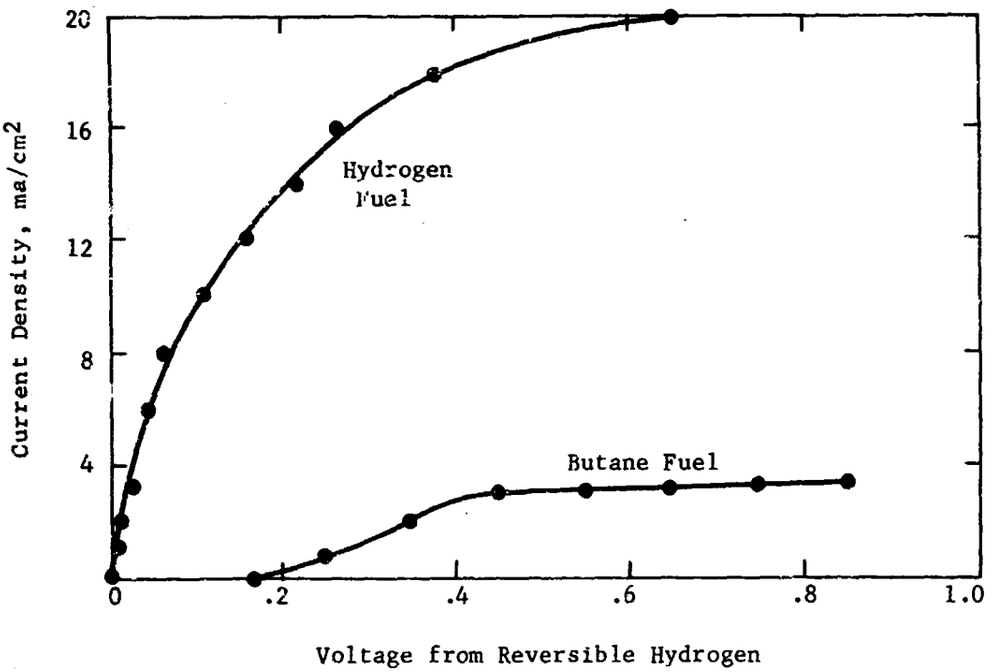

Despite the fact that the alkaline borate buffer performed well in steady state performance runs and showed no impurities on flag electrodes, it did show impurities in the flowing electrolyte system when attempts were made to measure butane adsorption rates. The difference in sensitivity to impurities is understandable from the geometry of the latter two systems. Adsorptions on flag electrodes are carried out by holding most of the wetted electrode in the vapor phase above the electrolyte. Gaseous fuel then dissolves and diffuses through an electrolyte film with a thickness in the micron range, whereas the competing impurities must diffuse from the bulk electrolyte long distances through the thin film. In the flowing electrolyte system, however, both the butane and the impurities reach the electrode via the same route, thereby giving the impurities a much greater chance to compete.

Attempts have been made to purify non-acidic electrolytes by charcoal treatment and by recrystallization. As of this writing, however, no satisfactory adsorption rate measurements have been carried out in electrolytes other than sulfuric acid.

Phase 3 - Conclusions

The effect of electrolyte composition on the rates of adsorption of saturated hydrocarbons remains as an important area to be studied in the development of successful direct hydrocarbon fuel cells. The studies reported here indicate that iodide in the electrolyte is adsorbed so strongly relative to butane that there is no interaction between the two. The iodide simply makes a fraction of the sites unavailable to butane. Butane adsorbs and oxidizes on the remaining sites exactly as it would on fresh platinum. The lack of selectivity of the iodide adsorption and the saturation coverage of one iodide per two hydrogen sites suggests that the two types of hydrogen sites are spaced closely on the platinum surface. They may represent the two different types of d-orbitals of each platinum atom. To affect hydrocarbon adsorption, materials should be chosen which are more selectively and less strongly adsorbed. Unfortunately, triphenyl phosphine, a likely candidate, oxidized in the same range as the hydrocarbon so that its effects could not be determined readily. As far as electrolytes other than sulfuric acid are concerned, all, including phosphoric acid, phosphates, carbonates and borates showed impurity contents high enough to preclude meaningful adsorption rate measurements. Efforts to purify such electrolytes should be made to permit competitive adsorption studies in electrolytes other than sulfuric acid. However, it may be that these other electrolytes are themselves reducible to adsorbable impurities so that complete purification may not be possible.

2.2 Task B, Non-Noble Electrocatalysts

Development of a practical hydrocarbon fuel cell system depends upon reducing the catalyst cost by replacing the present platinum systems with either more effective or less expensive materials. The development of active non-noble replacement materials offers one a route towards this goal.

The search for non-noble catalysts was divided into three areas. The first area deals with the examination of mixed metal oxides and carbides as potential electrocatalysts. Previous work has shown that these materials are conductive and provide an acid resistant media for incorporation of catalytic elements. Secondly, considerable effort was spent to determine if the two-site catalysis mechanism predicated on platinum mechanism studies could be extended to non-noble systems, which would utilize carbon dioxide rejecting buffer or molten salt electrolytes. In the third area high surface area metal alloys were prepared by the Raney technique to determine how best to apply the electronic theory of metals and semi-conductors to catalyst development. This would provide a series of guidelines for other catalyst studies as well as providing catalysts for use with non-acidic carbon dioxide rejecting electrolytes.

Phase 1 - Acid Resistant Metal Oxide and Carbide Catalysts

Non-noble electrocatalysts for use in hydrocarbon fuel cells must meet two important requirements. They must be conductive, acid resistant materials suitable for use in carbon dioxide rejecting electrolytes. Two classes of materials which meet these two requirements are the tungsten bronzes and the eta-phase carbide systems, since they allow incorporation of a non-noble catalytic element in an inert structure. The following paragraphs will deal with studies aimed at incorporating catalytic elements into these conductive, acid resistant structures.

Part a - Investigation of Tungsten Bronzes as Electrocatalysts

The tungsten bronzes are compounds having the general formula A_xWO_3 where A is an alkali or alkaline earth metal or lead, silver, copper or thallium. The tungsten bronzes show metallic conductivity and are acid resistant (10). They are usually characterized by a crystal structure having less vacancies than that shown by ReO_3 (classified as DO_9 or Pm3m) and more vacancies than those shown by the perovskite (E2, or Pm3m) structure although other crystal structures have been reported (11). These tungsten bronzes should not be confused with the metallic bronze alloys. The latter are alloys of copper, zinc, tin, lead, etc. and are not acid resistant.

Preliminary work here (8) showed that small amounts of transition metals might be incorporated into the tungsten bronze structure along with sodium or lead. An acid resistant form of the transition metal is thus produced. Unfortunately, the electrical conductivity of these samples was rather low and no definite electrochemical activity could be found. Furthermore, the exact nature of the species produced could not be elucidated. In an effort to expand the work commencing during the last period an attempt was made to prepare tungsten bronzes of the transition and post-transition elements only. These materials would not only maintain the acid resistance and conductivity of the well-known bronzes, but, further, would have d or p electrons available to enhance catalysis.

The method of preparation was as follows. The desired proportions of reactants to make a tungsten bronze of the stoichiometry T_xWO_3 (T = transition metal, $0 < x \leq 1$) were ballmilled together for two hours and then pressed into pellets at 50 tons/in^2. The pellets were dried in an oven at 110°C. The dried pellets were sealed in an evacuated quartz test tube and heated. The heating conditions varied from sample to sample and are given in Appendix B-1.

Only two elements of all those examined may have formed a cubic lattice that is characteristic of tungsten bronzes. However, even these compounds were not pure and existed with other as yet unidentified phases. Furthermore, a previously prepared thallium tungsten bronze (12) was also found to be impure. The following lines found for $Nb_{0.2}WO_3$ and $In_{0.2}WO_3$ are believed to arise from a cubic form. These are listed in Table B-1.

Table B-1

X-Ray Characterization of
Indium and Niobium Tungsten Bronzes

$In_{0.2}WO_3$			$Nb_{0.2}WO_3$		
Possible hkl	d, obs	a, calc	Possible hkl	d, obs	a, calc
300	3.35	10.05	200	5.25	10.50
310	3.21	10.15	300	3.475	10.43
322	2.144	10.05	310	3.265	10.32
422	2.04	9.99	330	2.435	10.33
520	1.853	9.97	332	2.234	10.47
420	1.807	10.22			avg = 10.40 Å
610	1.66	10.10			
611	1.622	9.98			
533	1.535	10.07			
731	1.317	10.11			
		avg = 10.085 Å			

The lattice constants found for these two materials are much larger than the 3.8 Å lattice characteristic of the tungsten bronzes characterized in the literature. The niobium and indium compounds may just be mixed oxides with a cubic structure. All the materials reported in Appendix B-1 showed a large number of compounds present. In fact this mixture of products was similar to those found for the nickel tungsten oxygen system discussed in part b.

All of these prepared materials were fabricated into foraminated Teflon bonded electrodes supported on tantalum screens and tested in 3.7 M sulfuric acid at about 90°C. In some cases cathodic currents were found on oxygen but these may have been due to oxidations (Appendix B-2).

None showed activity in the Brown[2] hydrogenator. The lack of catalytic activity in these systems led to a study of the nickel ‹ tem which is described in the next section.

Part b - Nickel Tungsten Bronzes

The nickel-tungsten oxide system received a good deal of attention since it was hoped to prepare a nickel tungsten bronze. This material could contain a catalytic nickel atom in an acid resistant matrix. By analogy with the alkali metal tungsten bronzes (13,14) the nickel would be present as nickel metal (that is, there would be free electrons associated with the crystal lattice). The tungsten bronze structure is characterized by its acid resistance, and if a known catalyst such as nickel could be incorporated into it there would be a good chance for developing a non-noble metal catalytic system usable in a CO_2 rejecting medium.

The first attempts at nickel tungsten bronze preparations were made with a mixture of nickelous oxide, tungsten and tungsten trioxide corresponding to the stoichiometry $Ni_{0.2}WO_3$. The mixed materials were pelletized at 100,000 psi and sintered in an evacuated quartz ampule at 982°C for 24 hours in order to produce the desired bronze through the reaction, $3\ NiO + W + 14\ WO_3 \rightarrow 15\ Ni_{0.2}WO_3$. An examination of the fired pellets indicated a most striking color change.

The initial pellets are a greenish yellow while the heated ones are blue or purple throughout. Further it was found that the blue pellets are electrically conducting ($>$ 100 mhos/cm) while the initial mix has a very poor conductivity ($<$ 10^{-3} mhos/cm).

The blue pellets were ground in an agate mortar and examined by X-ray powder crystallography. These showed that in addition to a structure like tungsten trioxide there were materials similar to other tungsten oxides present. These resembled $WO_{2.90}$ (15), $WO_{2.72}$ (16), and $WO_{2.96}$ (17) and nickel tungstate (18) (Appendix B-3). Neither tungsten metal nor nickelous oxide could be detected in the fired material although they were found in the unfired pellet. No cubic or tetragonal forms that are characteristic of the tungsten bronzes (19) could be found. Furthermore, the resultant product mixtures was independent of whether the preparation was made from nickelous oxide, tungsten and tungsten trioxide or just nickel and tungsten trioxide. In some cases, in addition to these forms, a cubic form with a lattice parameter of 3.80 Å was observed. These cubic samples appeared to be ferromagnetic. It is possible that nickel tungsten bronze was formed. This will have to be examined more fully. However, the resultant mix was not active as a fuel cell catalyst on either hydrogen or oxygen in 3.7 M sulfuric acid at 90°C.

When slightly higher concentrations of nickel are incorporated into the tungsten oxide structure then the resultant material shows activity on hydrogen (Appendix B-4). For example $Ni_{0.237}WO_3$ gives anodic current with hydrogen in acid. The amount of activity depends not only on polarization but also on electrode structure. All five preparations of $Ni_{0.237}WO_3$ have shown some degree of activity on hydrogen. Some have shown a small cathodic current on oxygen. This may not be true activity as these electrodes always developed yellow spots of tungsten trioxide. Thus, the oxygen may have caused the catalyst to be reoxidized to tungsten trioxide. No unquestionable activity on hydrocarbons has been found in the period covered by this report. The gross X-ray powder spectra of this active acid stable catalyst is not different than that found for the inactive samples of $Ni_{0.2}WO_3$ (Appendix B-3).

The nature of the active species is unclear at the present time. It does not appear to be a classical tungsten bronze as there is not evidence of a cubic or tetragonal species present. It may be that the nickel is incorporated into a number of tunnel structures (20) in which the nickel atoms sit in a polyhedron whose faces are composed of tungsten oxide groups sharing corners. This would explain the acid stability of the nickel and the conductivity of the crystals.

Physical mixtures of other metals and tungsten oxide have shown catalysis in chemically oxidizing hydrogen. Indeed, a series of hydrogen tungsten bronzes have been reported (21). These are made by contacting hydrogen with mixtures of tungsten trioxide, platinum and water. A recent study (22) of the reaction postulates that the platinum serves as a site for adsorbing and dissociating the hydrogen while the tungsten oxide lattice causes the oxidation. Presumably the nickel in our system serves the same function as the platinum does in theirs.

The catalytic activity that has been found here does not appear to be restricted to $Ni_{0.237}WO_3$; it occurs at higher nickel concentrations as well. For example, two samples of $NiWO_3$ (prepared from nickel metal and tungsten trioxide) also gave anodic currents with hydrogen. These materials showed high corrosion currents under nitrogen when they were first put into acid but after a while the corrosion became small and the hydrogen activity persisted. A sample of $Ni_{0.4}WO_3$ also was examined in sulfuric acid at 90°C but it gave very high corrosion currents and the solution turned green. Apparently, all the nickel in this system dissolved for no hydrogen activity was detected. This sample showed cathodic currents with oxygen but this may have been due to the substoichiometric oxides reoxidizing to tungsten trioxide. Appendix B-5 summarizes the materials prepared thus far with the nickel-tungsten-oxygen system.

Part c - Voltage Scan Characteristics of Tungsten Bronzes

The encouraging results obtained with the nickel tungsten bronze catalysts prompted an examination of the response of materials of this type to voltage scans. Three compounds were investigated, (1) material showing some activity for electrochemical hydrogen oxidation, $Ni_{0.237}WO_3$, (2) a similar material of lower nickel content, $Ni_{0.2}WO_3$, showing no activity, and (3) a nickel free material consisting of a fired sample of 10% W, 90% WO_3. These materials were each mixed with 5 wt % Teflon powder, and 100 mg of the mixture pressed at 1000 psi on gold flag electrodes. Slow voltage scans, 5 mv/sec, were run in 3.7 M sulfuric acid at 80°C, the maximum voltage of the scan being 1 volt polarized from standard hydrogen.

All of these compounds showed both anodic and cathodic areas in the region within a few hundred millivolts of the standard hydrogen potential. The active material, $Ni_{0.237}WO_3$, was distinguished only by an apparent sharpening of the anodic peak compared to the broader, less well-defined peaks obtained with the two inactive materials. The current potential traces are illustrated in Figures B-1, B-2 and B-3.

Figure B-1

Voltage Scan of Active Nickel Tungsten Bronze

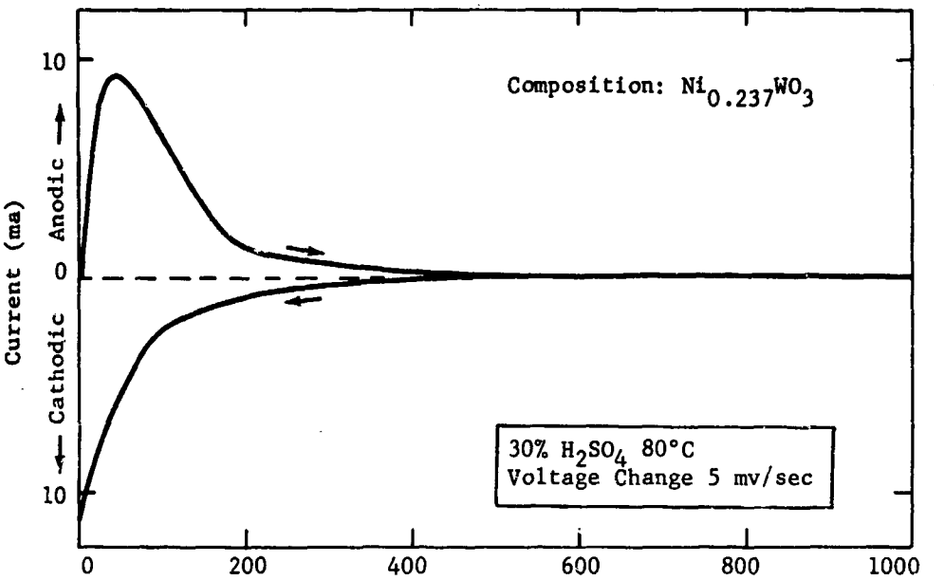

Potential vs. Standard Hydrogen (mv)

Figure B-2

Voltage Scan of Inactive Nickel Tungsten Bronze

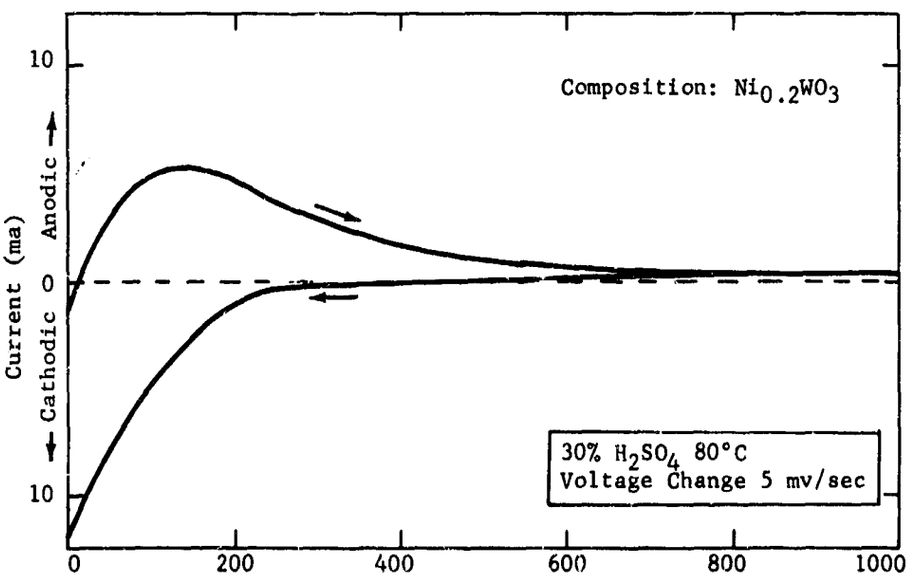

Potential vs. Standard Hydrogen (mv)

Figure B-3

Voltage Scan of Inactive Tungsten Oxide

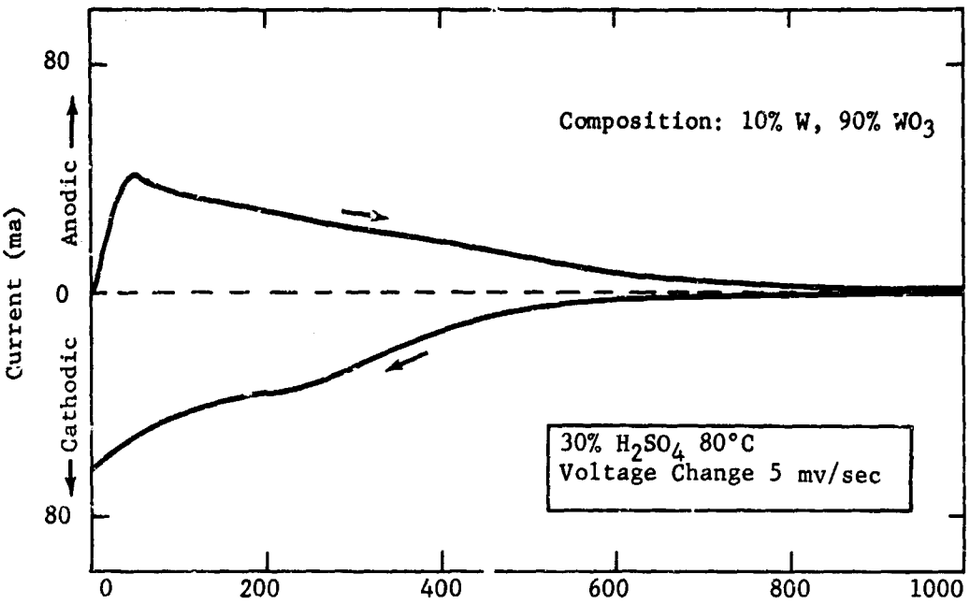

The reaccions leading to the appearance of these peaks have not been definitely established. Two obvious choices exist, the discharge of hydrogen ion and its subsequent oxidation, the reaction occurring on platinum in this potential region, or an electrochemical reduction and subsequent oxidation of the material itself. The latter could, for example, occur through partial valence changes in the tungsten oxides, which are known to exist in nonstoichiometric forms (23) and to undergo reduction and oxidation in this region (24). This latter explanation is supported by the appearance of similar areas in the non-nickel containing compound tested.

The activity of the $Ni_{0.237}WO_3$ compound for hydrogen oxidation was substantiated during the course of this study. Voltage scans taken in the presence of hydrogen bubbled through the electrolyte were displaced in the anodic direction by approximately 10 milliamperes compared to those taken with nitrogen bubbling, as shown by comparison of the curves in Figure B-4.

Figure B-4

Hydrogen Activity of $Ni_{0.237}WO_3$ by Voltage Scan

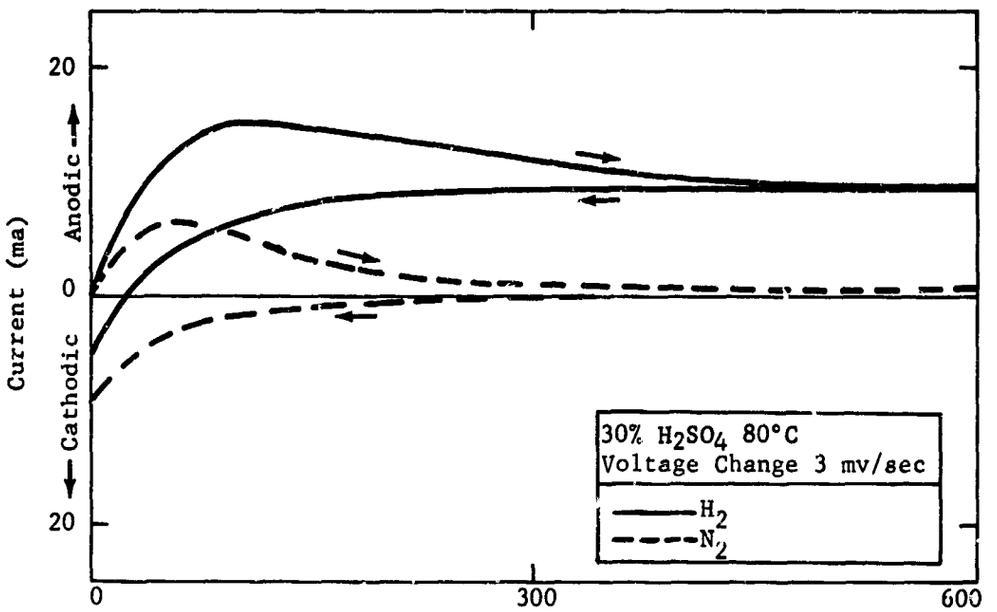

A possible explanation for the electrocatalytic effect shown by the tungsten bronze involves a chemical interaction between the hydrogen and the bronze, producing a lower valence state material which may then be electrochemically oxidized.

$$Ni_{0.237}WO_3 + xH_2 \longrightarrow Na_{0.237}WO_{3-x} + xH_2O$$

$$Ni_{0.237}WO_{3-x} + xH_2O \longrightarrow Ni_{0.237}WO_3 + 2xH^+ + 2xe$$

Since the transition metal concentration is critical, judging by the data obtained to date, the mechanism is not likely to be this simple. Perhaps the nickel concentration is critical in introducing vacancies in the lattice. Not enough information is available concerning the detailed structure of compounds of this type to allow more definitive statements concerning the origin of the catalytic activity to be made at this time. However, the occurrence of demonstrated electrochemical activity for a material consisting exclusively of non-noble components, stable in sulfuric acid, is very encouraging. The known occurrence of a wide variety of these materials, allowing for tremendous variation in the type and concentration of the components, gives strong encouragement that increased performance can be achieved.

Part d - Catalyst Structure Problem

The amount of activity obtained from different samples of $Ni_{0.237}WO_3$ varied markedly with the method of preparation of the electrodes. Indeed electrodes prepared in the same way from the same fired sample show differences in performance that are not readily explainable. It does appear, though, that the low activity levels found thus far are due to their low surface areas since the 325 mesh powders used in some of the electrodes are roughly 40 microns in diameter. Finer powders prepared by grinding in a tungsten carbide ballmill (Spex Mill) are not much smaller. Both probably have surface areas less than 5 m^2/gm. The desired surface area is about 30-100 $meters^2/gm$, the range of values obtained with platinum catalysts.

A more serious problem arises from the poor electrical conductivity of the prepared electrodes. The original blue pellets of tungsten bronze are very conductive. When these pellets are ground to 325 mesh and then pressed into pellets again at 100,000 $pounds/in^2$ their conductivity is reduced. Further size reduction and pelletization under the same conditions results in a nonconductive material. Previous workers have found this sort of conduction anomaly (compare references 13 and 27 with references 25 and 26). It would appear that interparticle electron transport between this class of crystals is poor when there is no bonding at all between them. If there is even a small amount of bonding between the crystals, conductivity is restored. Thus, sintering a nonconductive pellet (made from a finely ground powder) for only a few minutes at 1000°C in vacuum seems to fully restore the conductivity.

The decrease in electrical conductivity in going from pellet to a powder causes a serious problem in electrode fabrication. Electrodes made from powders are not very conductive. For example, a small bit of $Ni_{0.237}WO_3$ was pressed onto a tantalum screen and the conductivity from the catalyst to the screen was measured. It was found to be about a thousand ohms, with a few spots having lower conductivity even though the electrode was only a few mills thick. This type of electrode has poor structural stability and falls apart at the slightest disturbance. If Teflon emulsion is added to the catalyst powder and then fabricated into an electrode on a tantalum screen by either hot or cold pressing better structural stability results, but the electrical conductivity is still about the same.

It is believed that the low activities found with electrodes containing the nickel-tungsten oxides arises from a combination of comparatively low surface areas and poor electrical conductivity across crystal faces. Research is now under way to fabricate electrodes incorporating both high surface areas and high conductivity. One way of doing this is by containing small particles of catalyst in a porous conductive support. Another way would be to form the catalyst into a semi-porous electrode. The catalyst appears to show structural properties similar to ceramics and these techniques as well as powder metallurgical ones could probably be used to develop an interface maintaining electrode containing only the nickel tungsten bronze.

None of fired mixes showed any activity in hydrogenation experiments on 1-hexene in the Brown[2] hydrogenator.

Part e - Europium Tungsten Bronze Catalysts

Recently Ostertag (28,29) has synthesized and characterized cubic tungsten bronze systems containing rare earth elements. During the period covered in this report the tungsten bronze $Eu_{0.1}WO_3$ was synthesized here, according to the procedure in reference (28) and studied in 3.7 M sulfuric acid at 90°C. The rare earth bronze prepared here showed a crystal lattice with a parameter of 3.814 Å (reference (28)

gives 3.815 Å). This bronze gave a current under hydrogen after it was fabricated into an electrode with Teflon emulsion. Typical data are summarized in Table B-2.

Table B-2

Performance of Europium Tungsten Bronzes

(5 cm^2 electrode - 3.7 M H_2SO_4)

Gas	Cell Temp, °C	Current, ma	Polarization from Theoretical Hydrogen, Volts
N_2	92	0.37	0.54
H_2	92	0.51	0.54
N_2	89	0.125	0.94
H	92	0.95	0.94

It is planned to synthesize and study other rare earth tungsten bronzes. These materials offer an opportunity to study the effect of magnetic moment on catalytic activity as the magnetic susceptibility (molar) varies eighteenfold from $Ce_{0.1}WO_3$ to $Dy_{0.1}WO_3$ (29).

Part f - Eta Phase Carbides

Eta phase carbides are those carbides having a stoichiometric formula close to M_6C and possessing a cubic Fd3M structure (Structurbericht type E93), where M can be a combination of two or three elements. Appendix B-6 summarizes the eta-phase carbides reported in the literature thus far. The eta phase carbides are potentially electrocatalysts for hydrocarbons because they are acid resistant, electrically conductive, and a catalytic element can be incorporated in their structure.

Eta-phase carbides were prepared from powdered starting materials which were ballmilled to insure homogeniety. These were then pelletized and fired in a carbon crucible using a vacuum induction furnace which had been equipped with a quartz tube or a specially constructed water cooled bell jar. The installation of this latter unit has increased the induction furnace capability such that it can sustain 2000°C for several hours without loss in vacuum or structural damage. In addition, some of the materials were sintered in evacuated quartz ampules. Detailed preparation conditions are summarized in Appendix B-7.

After the samples were heated in the vacuum furnace for the required time, they were cooled and ground to 325 mesh and washed in 3.7 M sulfuric acid at 100°C for six hours. X-ray spectra were taken after the acid wash. Using this procedure many eta phase carbides have been prepared. These are listed in Appendix B-7 along with compositions which did not lead to the desired products.

X-ray analysis indicated that except for a sample of Ni_3W_3C (Appendix B-7) no change in X-ray pattern was found on acid washing.

The acid washed powders were then fabricated into Teflon bonded foraminated electrodes and tested in 3.7 M sulfuric acid. Both galvanostatic and potentiostatic techniques were used as indicated in Appendix B-7 . Potentiostatic techniques were used if no method is specified.

Only one sample (Ni_3W_3C) of all the eta phase carbides showed activity in acid. The activity could not be repeated with other samples. It may be that the particle size of that eta carbide preparation was unusually low and the high surface area gave rise to the activity.

Future efforts in the eta carbide area will be in examining the carbides containing copper, preparing fine particles of eta carbides from oxide starting materials, and examining ultrasonic techniques for reducing particle size of these very hard materials.

Phase 2 - Potential Application of Two Site Mechanism to Non-noble Electrocatalysis

In previous reports (1, 2, 3, 4) work aimed at gaining an understanding of the mechanism of platinum electrocatalysis has been described. This work has led to the conclusion that the mechanism involves a two site process combining adsorption at one site and oxidation at an adjacent site having "redox" capability. Considerable progress in enhancing methanol catalysis has been made by incorporating two materials having different properties into an electrode (5,6). For example, platinum, iridium and palladium in combination with ruthenium, rhenium, or molybdate are many times as active as platinum alone for methanol electrocatalysis. It is postulated that the former materials serve as methanol adsorption sites, while the latter serve as the "redox" sites. Unfortunately, none of these mixed catalysts appear to enhance saturated hydrocarbon oxidation, at least for the platinum system where studies have been concentrated.

Recent work has shown that platinum may be quite unique for saturated hydrocarbon oxidation because it possesses a built-in balance between hydrocarbon adsorption sites ($\sim$50% of the surface) and free sites available for the oxidation reaction (30). Thus, where extra redox sites can be utilized to advantage in the methanol case, where high fuel surface coverage greatly reduces the number of free "redox" sites available, the relatively lower surface coverage exhibited by saturated hydrocarbons on platinum may make additional redox sites unnecessary or even undesirable.

This general principle may, however, still be applicable to hydrocarbon catalysis when other metals are considered as catalysts especially for the hypothetical case of a metal where adsorption may occur but no electrochemical oxidation step is available.

Part a - Working Hypothesis

This picture provides a rationale which can be used for the development of a lower cost catalyst for hydrocarbons by the combination of two materials chosen for adsorption and redox capability. Initial efforts were directed toward a demonstration of this principle in buffer or basic electrolyte where a wider choice of materials was available. For instance, adsorption sites could then be provided by cobalt or nickel, and oxidation sites by ruthenium, silver oxide or cobalt molybdate. Since adsorption of hydrocarbons is known to be more difficult in high pH electrolyte, ethylene was chosen as the test fuel initially since olefin adsorption occurs more readily than saturated hydrocarbon adsorption. Since the adsorption step is, of

course, a major requirement for such a catalyst system considerable effort was made to study factors affecting this step as discussed in a later section of this report.

Part b - Evaluation of Nickel-Electrolyte Interactions

The anticipated use of nickel as a catalyst component prompted studies aimed at investigating the activity and stability of this material in potassium hydroxide electrolyte. It had already been established (6) that passivation of nickel resulting in loss of performance could result from overpolarization of electrodes. It was thus of interest to obtain more specific data on the stability of nickel with respect to anodic polarization and obtain as much information as possible regarding electrochemical reactions of the nickel itself.

Electrodes were prepared from commercial Raney nickel and Teflon emulsion (approximately 10 wt % Teflon) by cold pressing on flag type supports. Some data was also obtained on similar electrodes using a nickel-cobalt catalyst containing 25 atom % cobalt prepared by the Raney technique as discussed in phase 3 of this task.

The passivation data were obtained by recording sets of anodic and the corresponding cathodic voltage scans which began at the hydrogen potential and had steadily increasing end points. Steady state measurements of hydrogen activity, at a fixed potential of 40 millivolts polarized, were obtained after each scan. Thus, the magnitude of the polarization loss suffered by the electrode, corresponding to the point of reversal of the individual traces, was steadily increased, and a value of the activity of the electrode as measured by its hydrogen activity obtained after each increase. A sharp drop in hydrogen activity was observed when the polarization exceeded 250 millivolts. Data illustrating this conclusion are listed in Table B-3.

Table B-3

Effect of Polarization on
Nickel Electrochemical Activity

3 M KOH, 75°C

H_2 Performance 40 millivolts polarized ma/cm^2	Maximum Polarization During Preceeding Scan, mv
45	150
30-40	200
25-30	250
2-5	300

Thus, the activity of the nickel electrode is indeed very sensitive to overpolarization. Examination of the scans themselves indicates that the loss in performance is associated with polarization of the nickel electrode into a large anodic peak situated between 150 and 400 millivolts polarized. This as shown in Figure B-5 where the peak has been adjusted for the succeeding scans to the same size for purposes of clarity. In practice, this peak decreases rapidly on succeeding scans, and Figure B-5 represents the situation where each scan is made with a fresh electrode.

Figure B-5

Voltage Scans on Nickel with Variable End Point

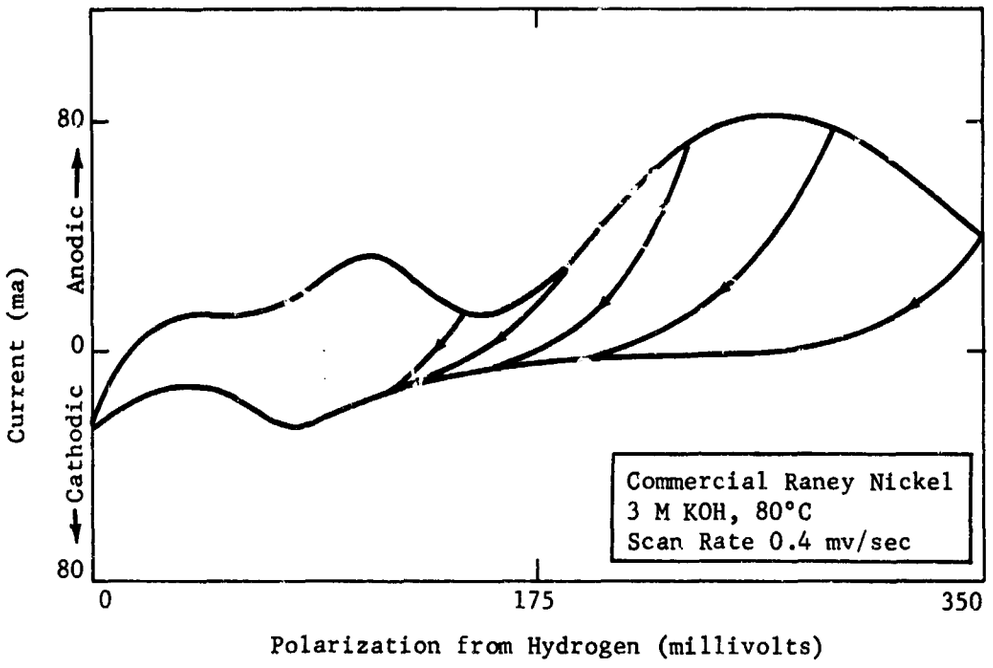

It seems clear that the reaction represented by the large peak is associated with the loss of activity of the nickel catalyst. Two possible reactions can be postulated, namely, oxidation of "internal" hydrogen associated with the Raney nickel during its preparation and an electrochemical oxidation of the nickel surface. Since massive nickel (screen) also shows a peak in this area, and would not likely contain hydrogen, while Raney nickel is known to contain considerable quantities of hydrogen which can be electrochemically oxidized, it is probable that both of these processes occur. Also, either of these processes could lead to deactivation of the nickel. "Internal" hydrogen loss could cause drastic changes in the crystal parameters of the nickel, while surface oxidation could easily destroy catalytic activity.

As mentioned previously, the size of the peak decreased drastically from the first to the second scan, when the potential of the nickel was returned only to hydrogen open circuit. However, after cathodization of the nickel electrode, the peak reappeared, showing that the reaction leading to its formation was reversible at potentials negative to the hydrogen potential. This phenomenon is shown in Figure B-6 although the faster scan rate used in this experiment (5 mv/sec) compared to the approximately 0.4 mv/sec in the preceeding figure, causes loss of detail and "tailing" of the peak. This is an indication that the reaction leading to the appearance of these peaks is relatively slow, and supports the contention that diffusion of "internal" hydrogen to the surface followed by its oxidation may be rate controlling.

Figure B-6

Effect of Cathodization on Nickel Scan

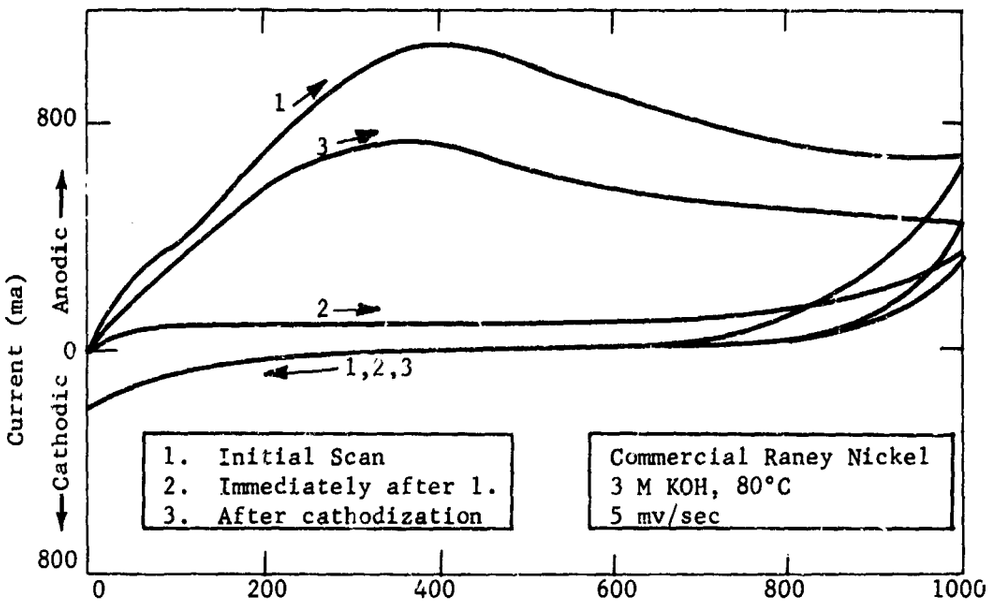

The demonstrated ability to recover a significant fraction of the peak associated with fresh nickel suggested that the loss in performance might not be irreversible and that activity could also be regained by cathodization. However, this technique, when tried on a number of deactivated electrodes, showed no promise in restoring activity. Thus, the loss of activity of nickel electrodes through over-polarization appears to be permanent and thus represents a serious obstacle to the use of nickel as a fuel cell catalyst where polarizations greater than 200 to 300 millivolts might be xpected.

A more detailed scan on nickel can be obtained by operating at a much slower rate of voltage change. This scan shows clearly three anodic peaks, two of which are mall and occur at less polarized potentials than the large peak discussed previously. At potentials more anodic than the large peak, the nickel surface appears inert up to at least 1 vol polarized. The scan obtained in this study is shown in Figure B-7.

Figure B-7

Slow Scan on Nickel

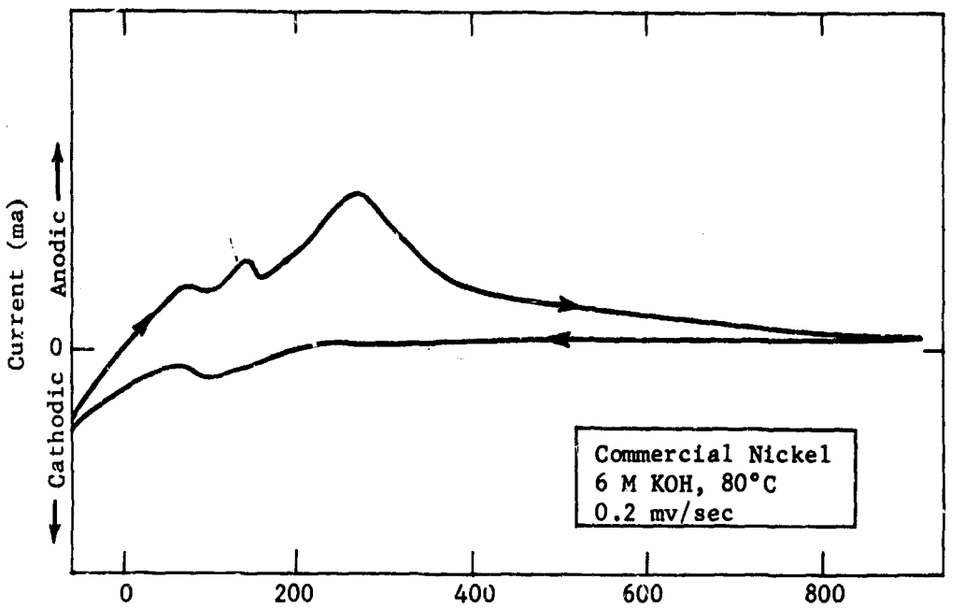

The origins of the two smaller peaks which are observed is open to question. Brieter and Weininger (31) suggest, on the basis of capacitance data on polycrystalline nickel, that three reactions are possible in this polarization range, namely

$$Ni\text{-}H + OH^- \longrightarrow Ni + H_2O + e^- \quad (1)$$

$$Ni + OH \longrightarrow NiOH + e^- \quad (2)$$

and $$Ni + 2OH^- \longrightarrow Ni(OH)_2 + 2e^- \quad (3)$$

The last reaction can be considered as a gross oxidation of the nickel surface, and has already been considered with reference to the large peak. Reactions (1) and (2), the oxidation of hydrogen adsorbed on the surface and the adsorption of hydroxyl radicals, might be expected to occur only on active sites and thus lead to smaller peaks. For instance, surface coverage of nickel by weakly adsorbed hydrogen occurs on only a small fraction of the total sites (32). Although the available information does not allow specific designations of the reactions associated with the peaks observed, a qualitative investigation of the coulombic relationships between anodic and cathodic scans was undertaken to shed light on the "reversibility" of the peaks.

Taking the reversible hydrogen electrode (RHE) potential in 3 M potassium hydroxide at 80°C as -1.05 volts versus standard calomel (SCE), it was found that the first detectable shoulder occurred at about 50 mv from the RHE. This shoulder may correspond to oxidation of Ni·H described by Breiter (Reaction 1) and others for crystalline nickel. Scans from -1.10 to -0.95 volts including only this shoulder were fairly reversible, with a tendency to grow cathodically. In the absence of well-defined peaks, the entire anodic and cathodic portions were integrated as in Table B-4.

Table B-4

Voltage Scans in "Nickel Hydride" Range

50 mg Raney Nickel Pressed into Gold Flag-Screen
3 M KOH, 80°C, -1.10 to -.95 volts vs
S.C.E., 207.7 sec/1/2 cycle

	Total Millicoulombs	
	Anodic	Cathodic
Run 1	1550	1860
Run 2	1670	2110

As will be shown below the cathodic growth was probably due to the reduction of nickel oxide to nickel at these potentials. The relatively close correspondence between the anodic and cathodic coulombs suggest that the reaction in this potential range, presumably the adsorption and oxidation of hydrogen is reversible.

When the scan range was extended to -0.80 volts versus S.C.E., the second sharp peak is detected at 0.125 volts versus the R.H.E. This one was also reversible since it was accompanied by a broad cathodic wave on the return half of the voltage sweep at .09 to .04 versus R.H.E. These peaks may correspond to the adsorbed hydroxyl radical, Ni·OH (Reaction 2). Table B-5 illustrates the reversibility of the total anodic and cathodic reactions in this voltage range and relative size of the peaks described.

Table B-5

"Nickel-Hydroxyl Radical" Scans

-1.07 to -0.88 volts versus S.C.E.

Scan Time, sec/1/2 cycle	Total Coulombs		Peak Coulombs	
	Anodic	Cathodic	Anodic	Cathodic
207.7	1575	1400	240	260
825	1888	1710	342	241
1656	1716	1685	289	260

The differences due to scan rate are not considered significant in view of the difficulties involved. Comparison of the absolute values in Tables B-4 and B-5 should not be made because of probable loss of nickel from the electrode. Further details are given in Appendix B-8.

As discussed previously, the third peak, occurring at still more anodic potentials, was large relative to the other two, and was largely irreversible, probably corresponding to the formation of NiO or $Ni(OH)_2$ (reaction 3). Repeated scanning from -1.08 to -0.78 volts versus S.C.E., including this peak at -0.865, would cause a steadily diminishing scan thickness, in each case with the anodic coulombs exceeding the cathodic coulombs, in distinct contrast to the "Ni·H" scans of Table B-6. In addition there appeared to be no difference in the behavior of the electrode when ethylene was bubbled into the solution rather than nitrogen. These points are illustrated in Table B-6, and Appendix B-8.

Table B-6

Formation and Reduction of "Nickel Oxide"

Scan Range -1.08 to -0.78 volts versus S.C.E.,
825 sec/1/2 cycle 3 M KOH, 80°C

Treatment	Total Coulombs	
	Anodic	Cathodic
None, N_2 atmosphere	1746	1352
Repeated Scanning under N_2	1300	1090
45 min of C_2H_4 at -0.98 volts versus S.C.E.	1554	1312
Repeated scanning under C_2H_4	1110	996
45 min of N_2 at -1.08 volts versus S.C.E.	2360	1402
Repeated scanning under N_2	1080	967
30 min of C_2H_4 at -1.08 volts versus S.C.E.	1430	1030

Thus, nickel exhibits characteristics that are similar to those of platinum, but there are important differences. Like platinum, nickel may form a hydride, a half oxide (adsorbed hydroxyl) and a complete oxide. Unlike platinum, the voltage range over which these reactions occur is narrow, leading to oxidation of the surface at relatively low polarizations with resulting deactivation. Fortunately, the formation and reduction of the "half oxide" appears to be fairly reversible and adsorption of hydrocarbons could take place competitively with hydroxyl radical in this region. Thus, attempts were made to evaluate hydrocarbon adsorption on nickel, since without this step further work on nickel would not be justified.

Part c - Potential Techniques for Detection of Ethylene Adsorption on Nickel in the Presence of Electrolyte

Although hydrocarbon adsorption on nickel from the vapor phase is well established (33) measurement of such adsorption in the presence of electrolyte has not been reported. It is well known, however, that adsorption of hydrocarbons on platinum is severely hindered in high pH electrolytes compared to acid electrolytes.

This difficulty may involve competition by anion adsorption in the higher pH range. Since nickel is unstable in acid solution, the use of such electrolytes for this study was unfortunately necessary, and since hydrocarbon adsorption was felt to be an important but difficult step in the proposed mechanism, a technique was developed to at least qualitatively measure the ability of ethylene to adsorb on nickel immersed in high pH electrolyte. Several techniques are potentially useful.

(a) Anodic oxidation

Detection of adsorbed species by electrochemical oxidation, either by voltage scanning (34) or by chronopotentiometry (35) can be used to advantage for noble metal catalysts. For a catalyst such as nickel, passivation of the surface itself through oxidation at the anodic potentials necessary to detect oxidation of adsorbed species was felt to seriously limit the applicability of this technique. Such passivation of the nickel surface is, in fact, a serious drawback to the use of this metal in a practical system, as is discussed in a later section of this report.

(b) Radio tracer techniques

Techniques involving detection of adsorbed layers using radio tracers have been developed (36). However, the fairly elaborate equipment and technology development required for its use discouraged its application to this study.

(c) Hydrogenation reaction of olefins

A technique based on the known fact that olefin hydrogenation (37) can be detected electrochemically on platinum was chosen for study. The applicability of this method was checked both by detection of ethylene adsorbed on platinum, and the examination of nickel as a possible electrocatalyst for the reaction. Detection of the reaction itself on nickel was not felt to be conclusive since at least gas phase catalytic olefin hydrogenations can proceed on surfaces not normally catalysts for the reaction, such as gold, provided atomic hydrogen can be delivered to the surface (38). Thus, the basis for the measurement of ethylene adsorption was chosen as an examination of the reaction

$$C_2H_4 \text{ ads} + 2H^+ + 2\ e^- \xrightarrow{\text{cat}} C_2H_6$$

by detection of the current consumed during a cathodic scan. This method potentially avoids the difficulty of passivating the catalyst surface associated with anodic scans.

Part d - Application of Cathodic Scan Method to Platinum

A short study of the applicability of the proposed method was made using platinum as the catalyst. This allowed a direct comparison of the proposed method with the conventional oxidation scan method on the same electrode. The electrode consisted of 50 mg of commercial platinum black pressed on a platinum screen backed with foil, immersed in 6 M KOH electrolyte at a temperature of 75°C. A gas sparger in the cell allowed saturation of the electrolyte with the appropriate gas. The scanning equipment was the same as that described previously. Ethylene was sparged through the cell with the electrode held at a potential in the double layer region (0.35 volts vs standard hydrogen) for ten minutes followed by a nitrogen sparge for five minutes to reduce the

ethylene concentration in solution to very low values undetectable by steady state measurements. Then the potential was moved either anodic or cathodic to oxygen or hydrogen evolution respectively. The results are depicted in Figures B-8 and B-9.

Figure B-8

Cathodic Scan of Platinum Black with Adsorbed Ethylene

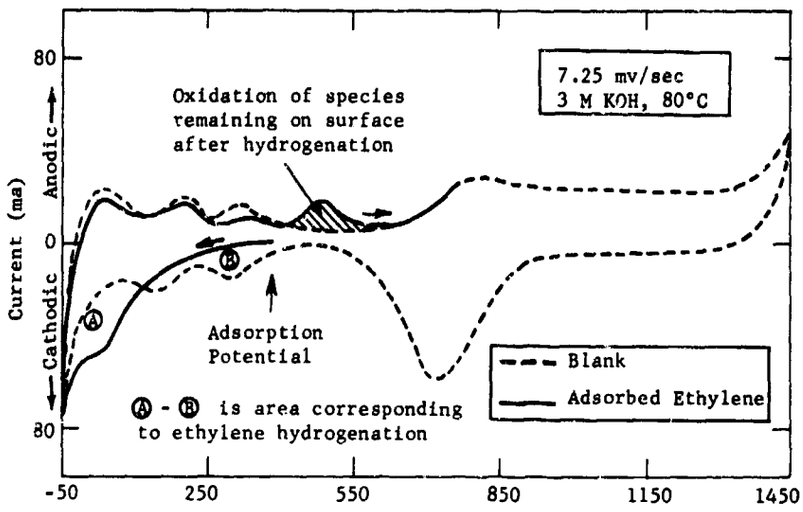

Figure B-9

Anodic Scan of Platinum Black with Adsorbed Ethylene

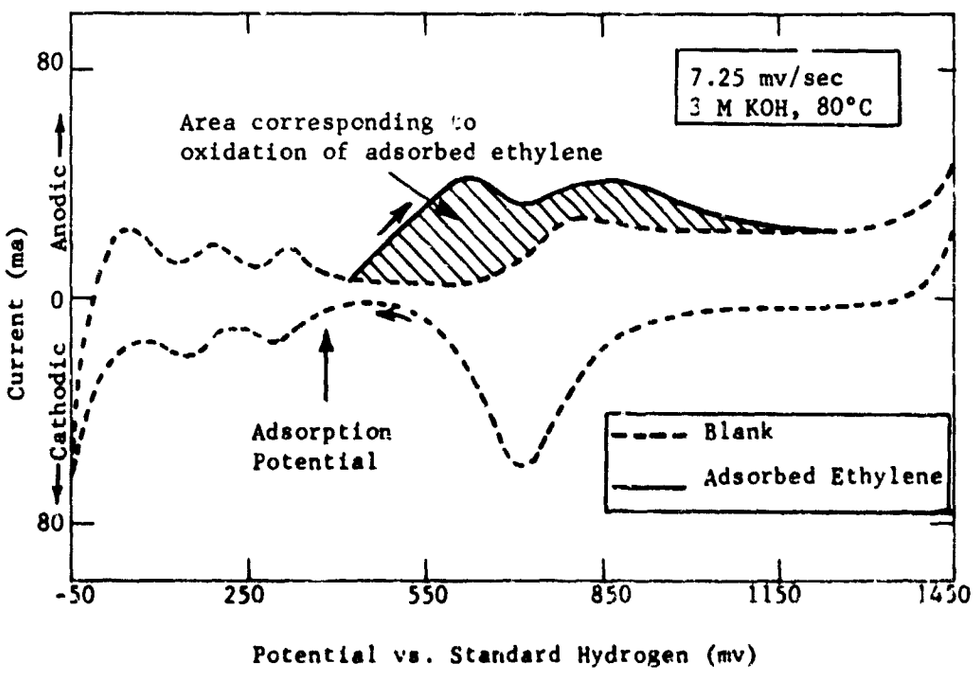

It is immediately obvious that the cathodic scan (from the adsorption potential toward hydrogen evolution) is quite different when ethylene is preadsorbed compared to the base case. Inhibition of the deposition of hydrogen normally occurring in a peak at about 0.25 volts polarized is followed by a steadily increasing cathodic current becoming equivalent to the base case in the hydrogen evolution region. The overall area of the peak to this point is greater than the base case area, the difference presumably being the coulombs consumed in the hydrogenation reaction. It is also apparent that desorption of surface species is not complete since the anodic scan immediately following the hydrogenation scan shows a depression of the normal hydrogen oxidation peaks and, in addition, a small oxidation wave at slightly more anodic potentials, characteristic of the influence expected from a low surface coverage species. Whether this material is unreacted ethylene, ethane not desorbed, or carbonaceous residues from possible ethylene cracking was not established.

The anodic oxidation scan is typical of that expected for the oxidation of an adsorbed material at high surface coverage, where rather large polarizations are required for oxidation.

A check on the quantitative aspects of the technique can be obtained by comparison of the coulombs consumed during the anodic and cathodic scans. Since the complete anodic oxidation of ethylene involves 12 electrons, while the hydrogenation involves only 2, the ratio of the anodic to cathodic coulombs should be 6/1. The presence of material remaining on the electrode after the cathodic sweep interferes with a simple analysis of the data. Coulombic ratios calculated for several assumptions are shown in the following table.

Table B-7

Anodic/Cathodic Area Relationship

Assumption	Anodic/Cathodic Area
Simple ratio of observed anodic and cathodic area	8.5/1
Material remaining on electrode is unreacted ethylene	7.2/1
Material remaining on electrode is nondesorbed ethane	6.7/1

Although further effort to optimize this technique would be possible, the main objective of demonstrating the applicability of the technique in a known system had been met. The requirement that nickel catalyze the hydrogenation reaction in the presence of electrolyte was then examined.

Part e - Catalysis of Ethylene Hydrogenation by Nickel

In view of the difficulties associated with preparing and maintaining active nickel catalysts and electrodes, a supply of commercial Raney nickel was obtained and used in this study. This material was supplied by the Raney Catalyst Division of the W. R. Grace and Company and identified as Raney No. 28 Active Catalyst. A convenient electrode form, minimizing the exposure of the active catalyst

to air during preparation, consisted of a Teflon coated magnetic stirring bar, wrapped with gold coated tantalum foil attached to a gold current lead. By partially dipping this structure into the magnetic catalyst, a small clump of catalyst in electrochemically usable form could be introduced into the nitrogen blanketed cell in a few seconds. Attempts to prepare more conventional structures by pressing mixtures of nickel and Teflon onto flag electrodes did not always produce active electrodes. Since the object of this experiment was a demonstration of electrochemical activity rather than a high performance gas electrode, the use of the "magnetic" electrode was considered justified.

In 3M KOH, at 75°C, the ability of the nickel catalyst to hydrogenate ethylene was demonstrated both by steady state current measurements and by voltage scans in the presence and absence of ethylene, supplied by sparging.

Typical steady state measurements in this system are shown in Table B-8.

Table B-8

Ethylene Hydrogenation Catalyzed by Nickel

100 mg Commercial Raney Nickel, 3 M KOH, 80°C

Potential Millivolts from Standard Hydrogen	Current, ma	
	Ethylene	Nitrogen
40	-1.8	+1.5
0	-14	-0.5
-30	-22	-3.5
-60	-45	-30

The larger cathodic currents obtained close to the hydrogen open circuit potential are evidence for the occurrence of ethylene hydrogenation. The postulated mechanism involves consumption of hydrogen atoms supplied by the nickel catalyst, and replacement of these hydrogen atoms by electrochemical discharge of hydrogen ion.

Typical voltage scan data showed similar behavior, and, in addition, showed that the electrode was active for hydrogen oxidation. The current was shifted anodically in the presence of hydrogen by a relatively constant amount, independent of potential over the range studied. Similarly the current with ethylene is shifted cathodically, providing evidence of the hydrogenation reaction, as shown in Fig. B-10.

These results with ethylene showed that the hydrogenation reaction, in theory at least, could be used to detect the presence of ethylene adsorbed on the nickel surface. Thus, experiments to investigate this possibility were undertaken.

Figure B-10

Commercial Raney Nickel Activity by Voltage Scan

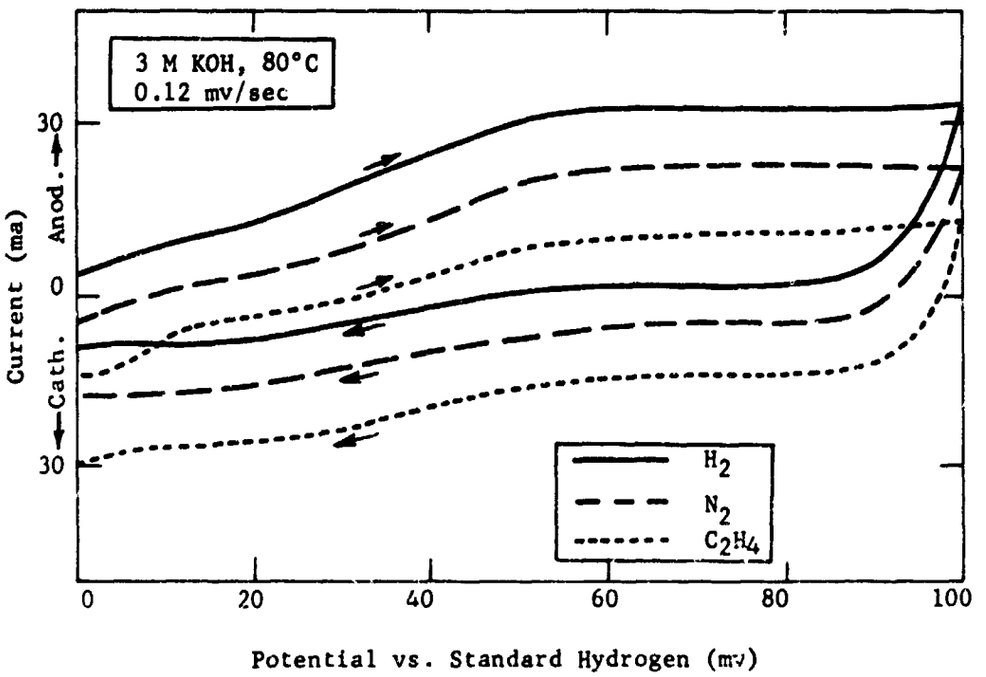

Part f - Ethylene Adsorption on Nickel

Conditions for the adsorption experiments were chosen as follows. Cathodic voltage scans were run with nitrogen sparging until reproducible values were obtained. This was more of a problem with nickel than with platinum due to the relative slowness of the hydrogen discharge and oxidation reactions compared with platinum, and necessitated rather slow voltage changes with time. The potential at which adsorption was allowed to occur, which also served as the potential for starting the cathodic scans (250 mv polarized from H_2) was chosen to be sufficiently anodic such that the ethylene hydrogenation reaction was absent, but sufficiently cathodic such that irreversible catastrophic passivation of the nickel surface could be avoided. Adsorption times of ten minutes, in the presence of ethylene, followed by a nitrogen sweep time of five minutes before starting the scan were used. Steady state experiments had shown that about two minutes of nitrogen sparging was sufficient to reduce the contribution of ethylene initially present in the cell to vanishingly small values. Three electrolytes, 3 M potassium hydroxide, 2 M potassium carbonate and 1M potassium phosphate were used at 75°C.

In the potassium hydroxide and potassium phosphate electrolytes, no evidence of ethylene hydrogenation was found. In the latter electrolyte, a greenish discoloration developed which indicated that the nickel catalyst was unstable under the conditions used, as would be expected from the Pourbaix diagram (24). In the

potassium carbonate system, however, the cathodic voltage scans showed the predicted higher cathodic currents indicative of hydrogenation of adsorbed ethylene.

Figure B-11

Evidence for Adsorption of Ethylene on Nickel

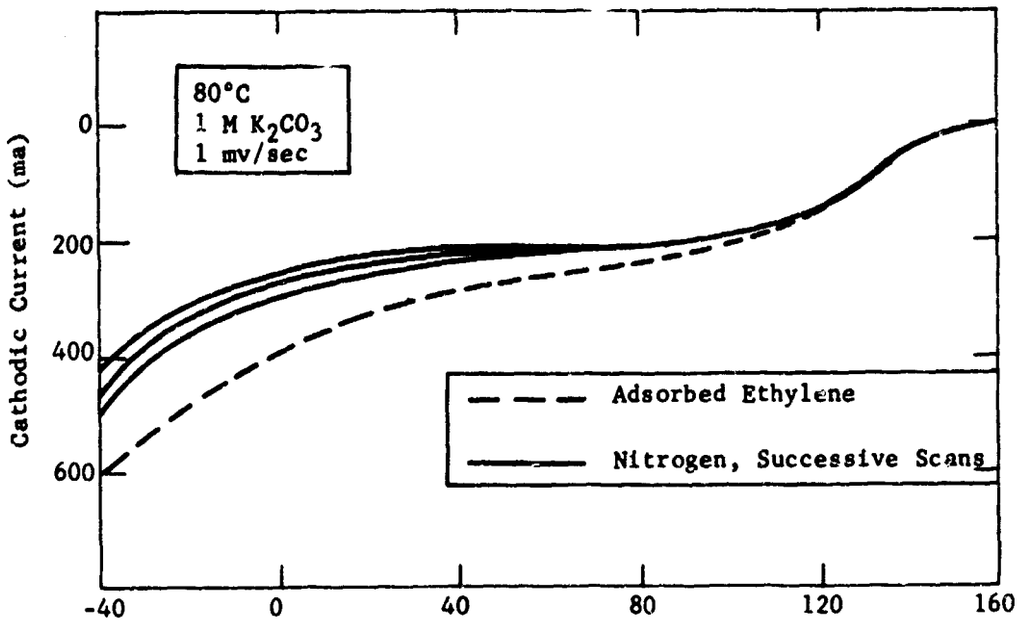

Much less detail is available in the scans that is present with platinum due mainly to the absence of well-defined hydrogen peaks. For this reason, it is difficult to estimate the degree of surface coverage, since hydrogen atoms from layers well below the surface can take part in electrochemical reactions. Presumably, additional work could be done to define the electrode surface area by independent methods, and to obtain more data on the adsorption itself. However, for the purposes of the present experiment, this further work was not felt to be justified.

The lack of evidence for ethylene adsorption in the potassium hydroxide electrolyte is attributed to relatively high surface coverage of an ionic species, presumably hydroxyl ion. In the potassium phosphate buffer solution, the apparent corrosion of the nickel did not justify further examination of this electrolyte. The rather encouraging evidence of ethylene adsorption in the potassium carbonate electrolyte justified examination of the mixed nickel-ruthenium system.

Part g - Activity of Mixed Nickel-Ruthenium Catalysts

Some preliminary work had been done with mixed nickel-ruthenium and palladium-silver catalysts prepared by hydrogen reduction. Since the results of the adsorption study were not then available, evaluation of these catalysts was attempted in both 2 M

potassium carbonate and 3 M potassium hydroxide. Electrodes were prepared by pressing gelled mixtures of catalyst and Teflon emulsion onto tantalum screen and evaluated in the interface maintaining mode. It was quickly evident that modification of the electrode structure would be necessary for operation with the carbonate electrolyte due to buildup of carbonate salt residue on the gas side of the electrode. This was a result of evaporation of water from the gas side of the electrode, leaving a solid residue of the carbonate salt. Because of this difficulty the majority of the catalyst testing was done in 3 M KOH.

No evidence for hydrocarbon oxidation was obtained and in fact the overall activity of the electrodes was poor even on hydrogen. The data obtained in this study is tabulated in Appendix B-9. Thus this early work was terminated in favor of work aimed at a more systematic evaluation of suspected problems in the system, described previously. Base on this further work, it is apparent that evaluation of hydrocarbon oxidation on nickel catalysts in potassium hydroxide is doomed to failure due to the ineffective hydrocarbon adsorption step. Work done in the future on this mixed catalyst system will be restricted to electrolytes such as carbonate, where at least olefin adsorption can occur.

Phase 3 - <u>High Surface Area Alloys</u>

Studies aimed at evaluating the potentialities of non-noble metal alloys as hydrocarbon electrocatalysts have been extended to include an investigation of the role of electronic configuration on catalyst effectiveness. The objective of this program is to determine how to apply the electronic theory of metals (39) and semi-conductors (40,41,42) to catalyst development. As a first step towards this goal, a series of high surface area alloys with known magnetic properties have been prepared and evaluated as electrocatalysts to determine if a correlation with band occupancy could be found. Consequently, alloy compositions were chosen with a view towards obtaining a smooth variation in electronic structure while keeping the alloy crystal structure constant.

Inter-alloys of the first row transition elements were selected for this initial phase of the program since their atomic diameters are all within 15% of each other and adjacent elements have the same crystal structure, thus insuring a continuous range of solid solution alloys. In addition, only alloy systems with known electronic and magnetic properties (43) were selected since initially no magnetic measurements were contemplated.

Alloy selection was also limited by the requirement that these materials have sufficient surface area to allow effective chemical and electrochemical evaluation. This requirement precluded the use of simple alloying techniques. Several methods of alloy preparation were considered including co-reduction of mixed salts(7), coprecipitation and reduction of mixed oxides and carbonates (44), and a modified Raney alloy procedure (8). All of these techniques have significant weaknesses. However, previous work (8) has indicated that the modified Raney alloy procedure can best produce the desired alloys. This modified procedure depends upon the existence of a single phase region in the ternary aluminum-alloy phase diagram somewhat below the alloy melting point to allow for the high temperature annealing step. Consequently, this procedure was adopted for this phase of the program. As a result of the foregoing considerations, the inter-alloys of iron, cobalt, nickel and copper were selected for study.

Part a - Electronic Considerations

The catalytic activity of transition metals are generally attributed to the state of occupancy of the d-band (43, 44, 7). Indeed, all the fundamental chemisorption and catalytic properties of their surfaces are dictated by the relative position of the surface Fermi level. However, the degree to which the bulk electronic configuration affects these surface properties depends upon the degree of isolation. Of course, with metal catalysts, the surface state is more dependent on bulk properties than in a true semi-conductor catalyst. This is fortunate, since the surface properties of metals are quite difficult to define.

Vol'kenshtein (40) argues that the problem of associating catalytic activity with electronic structure is further complicated by the fact that chemisorption and reactivity are dictated by the relationship between the free adsorbate energy levels and the surface Fermi energy. Thus, the type of chemisorption (electron donor or acceptor) is dictated by this energy difference (Figure B-12). The presence of the adsorbate can also alter the surface Fermi level for subsequent reactions (although this is a less important factor for metal catalysts because of the large influence of the bulk energy levels). Thus, it is possible for a fuel adsorbate to appear as an electron donor with one metal alloy and an electron acceptor with another. Furthermore, the electrochemical oxidation of hydrocarbons probably proceeds through a number of electron acceptor and donor stages. Thus, it is not possible to predict a priori what the required band occupancy should be. Therefore, it will be necessary to develop a correlation of reactivity with occupancy for the specific hydrocarbon fuel in question.

Figure B-12

Role of Fermi Surface in Hydrocarbon Adsorption

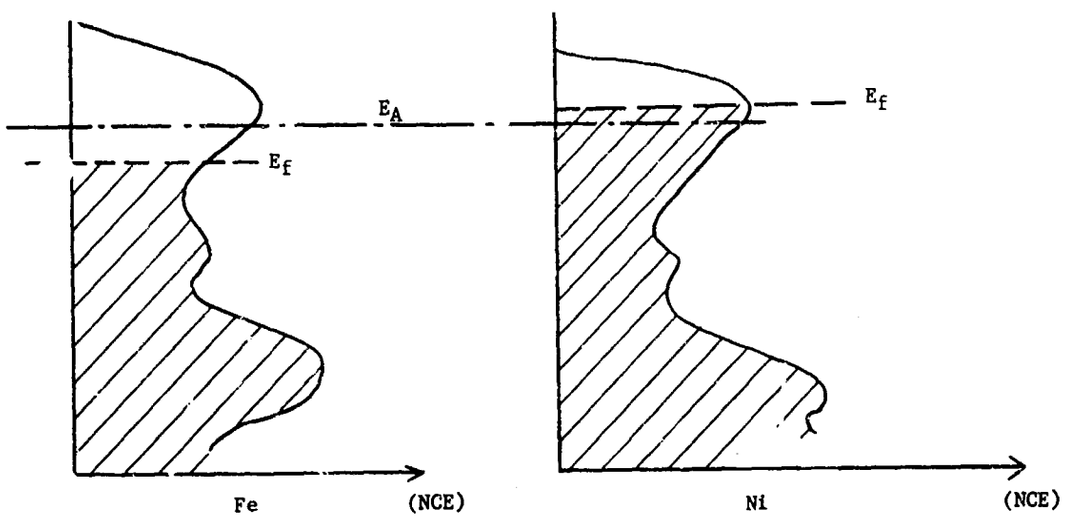

$E_A - E_f > KT$
Adsorbate Donates
Electron to Lattice

$E_f - E_A > KT$
Adsorbate Accepts
Electron from Lattice

Alloying, of course, can alter the d-band occupancy. For the first row transition elements, these changes are generally reflecced directly in the intrinsic magnetic moment. Hence if this concept is correct, it should be possible to find a correlation between catalytic activity for a given reaction and magnetic moment. Our analysis of some Russian data (45) on the hydrogenation of benzene on Raney alloy catalysts indicates that this may indeed be a valid contention. This is illustrated in Figure B-13 which is a plot of benzene hydrogenation rate per gram of catalyst versus magnetic moment. The magnetic data are from Bozworth (43). Notice that the data for Ni-Fe, Ni-Co, Ni-Cr, Ni-Mo and Ni-Ti alloys form a smooth curve with a maximum at 0.4-0.5 Bohr magnetons. No such correlation is as yet available for the electrochemical oxidation of hydrocarbons.

Figure B-13

Effect of Magnetic Moment on Benzene Hydrogenation

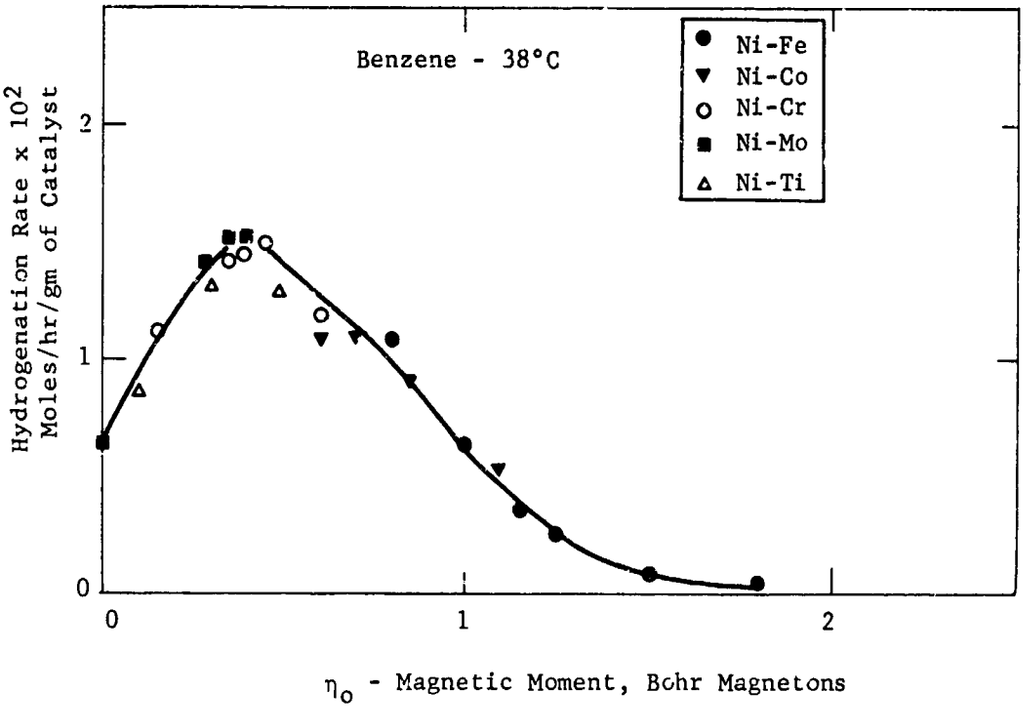

Part b - Raney Alloy Preparation

Previous studies have indicated that a modified Raney alloy technique could successfully produce high surface area metal alloys. Consequently, a number of interalloys of first row transition elements (Ni-Co, Ni-Cu, Ni-Fe) were prepared by melting a 50 wt % mixture of the desired alloy and pure aluminum in an electric arc furnace under a helium atmosphere. These crude melts were then annealed at 800-850°C for 72 hours in evacuated quartz ampules. This was then followed by a water quench to prevent phase separation. Microscopic examination of the solid metal samples indicated that the annealing process had been successful. The resultant alloys were then activated by hydrolysis and digestion in 6 M KOH after grinding to 200 mesh in a Spex mill.

Two hydrolysis procedures were briefly examined, one involving a rapid high temperature hydrolysis in 6 M KOH, the other utilizing a controlled low temperature ture procedure. In both cases a 90°C digestion step followed the hydrolysis. As indicated in Table B-9, these two techniques appear to produce different catalysts despite the fact that the crystallite size was the same.

Table B-9

Effect of Hydrolysis Temperature
on Catalyst Activity - Raney Nickel Catalyst

Hydrolysis Temperature, °C		Surface Area, m^2/gm	X-Ray Crystallite Size, Å	Hexene-1 Hydrogenation millimoles/min/gm	Hydrogen Limiting Current,(1) ma/cm^2
Initial	Final				
25	80-90	53	53-59	2.62	120
5	15	25	59	4.20	44

(1) Nickel - 15% Teflon electrode 50 mg/cm^2, cold pressed at 5000 psi.

Surface area measurements can explain the difference in hydrogen activity However, they do not account on the differences in hydrogenation rate.

The low temperature hydrolysis (5-15°C) was adopted as standard procedure since it was felt that this would produce the more repeatable catalyst, especially since the high temperature reaction is an uncontrolled reaction with some detonation hazard. In this procedure, the powdered alloy was first prewet with water and cooled to 5°C prior to admitting the 6 M KOH. The addition rate was controlled to maintain the temperature below 15°C. After the hydrolysis is complete (at 15°C), the slurry is held at 25°C until hydrogen evolution stops. The material is then washed and digested at 90°C for one hour. The final material is then stored under absolute alcohol until required for X-ray characterization, surface area measurement, and chemical and electrochemical evaluation. This was necessitated by the fact that all of these materials were pyrophoric.

Part c - Alloy Characterization

As indicated in previous studies, it is important to establish if the residual material,after aluminum dissolution, is a true solid solution alloy or merely a mechanical mixture of the two metals. X-ray crystallographic data, such as lattice parameter, are generally used for this purpose. However, with the Raney alloys, lattice expansion due to adsorbed hydrogen tends to complicate matters. For example, solid nickel gives a lattice constant of 3.517 Å while Raney nickels can give values of 3.525 to 3.547 depending upon the amount of adsorbed hydrogen. Thus, a second criteria, the existence of a single crystal phase in the X-ray spectra must be used in combination with simple lattice constants.

Table B-10

X-Ray Data Analysis of Raney Alloys

Alloy Composition	X-Ray Crystallite Size, Å	Lattice Parameter, Å		Remarks
		Observed	Literature Value	
Pure Nickel	53,59	3.525	3.517	Prepared by high temperature hydrolysis, very clean spectra, no Al, NiAl of Ni_2Al_3 observed.
Pure Nickel	59	3.547	3.517	Some NiAl and Al present in spectra.
90 Nickel-10 Copper	59	3.526	3.526	Small amount of Ni_2Al_3 and NiAl phase observed, single cubic phase of Ni-Cu alloy only detectable.
70 Nickel-30 Copper	32	3.547	3.543	Some copper not in Ni-Cu lattice as indicated by the 2.1 Å line in spectra. Significant quantities of Ni_2Al_3 also present.
Pure Cobalt	43	3.559	3.537	Parameters are for cubic cobalt; normal structure at room temperature is hexagonal close packed. Cubic phase normally exists only above 450°C. Resultant alloy appears to be mixture of 68% cubic cobalt and 38% hexagonal.
89 Nickel-11 Cobalt	58	3.550	3.549	Only well-defined f.c.c. lattice observed, no hexagonal cobalt was observed, no NiAl, or Ni_2Al_3 detected, only expanded f.c.c. lattice observed, no hexagonal Co lines present, no NiAl or Ni_2Al_3 phase.
40 Nickel-40 Cobalt	71	3.567	3.528	Only expanded f.c.c. lattice observed, no hexagonal Co lines, no NiAl or Ni_2Al_3.
Pure Iron				Only Fe_3O_4 lines observed possibly due to X-ray florescence--to be checked.
15 Nickel-85 Iron				" " ", no nickel lines observed.
30 Nickel-70 Iron				" " "

Applying these criteria, only the nickel-copper and nickel-cobalt systems actually can be said to produce the desired solid solution alloys. As indicated in Table B-10 both the 90Ni-10Cu and 70Ni-30Cu mixtures did form true alloys, yielding lattice parameters which were in good agreement with the literature. The 38Ni-62Cu alloy failed to form since two distinc crystal lattices (Cu and Ni) were observed. All of the nickel-copper alloy spectra showed Ni_2Al_3 inclusions which had not been (or could not be) removed in the hydrolysis step.

The nickel-cobalt alloys on the other hand formed clean face centered cubic lattices with no NiAl or Ni_2Al impurities present. However, as indicated earlier, the lattice parameters for the 75Ni-25Co and 40Ni-60Co did not agree with literature values due to the hydrogen adsorbed in the lattice. Further evidence of alloy formation in this case can be found if one remembers that cobalt's normal configuration is hexagonal, and Raney cobalt preparations yield mixtures of the cubic and hexagonal phases.

X-ray data on the nickel-iron system indicates that this system failed to produce alloys since only Fe_3O_4 lines were observed. However, this work will have to be rechecked as copper X-ray emissions were used, and this is known to produce spurious lines due to X-ray florescence. Furthermore, no nickel lines were observed and the material was a good conductor. Fe_3O_4 would be expected to be an insulator.

In addition to the X-ray spectra work, physical characterization also included determination of crystallite size and surface area. Crystallite measurements indicate that these materials range in size from 30 to 70 Å, with the majority of the alloy in the 50-60 Å range. The surface area measurements, although not complete, indicate that the alloys have surface areas between 40 and 60 m^2/gm, which is a quite respectable level for unsupported catalysts.

Part d - Catalyst Evaluation

In view of the problems associated with electrode structure, and hydrocarbon adsorption in high pH electrolytes (8) both chemical and electrochemical evaluations are required to establish the existence of hydrocarbon activity, and determine if a correlation with electronic properties exist. Consequently, the Raney alloys were evaluated for electrochemical activity on hydrogen and ethylene as well as for hydrogenation activity. Future evaluation of these Raney allovs will include evaluation using the gas phase reformer since this would allow the examination of hydrocarbon activity in the absence of problems with competing ions.

All of the Raney alloys were evaluated as hydrogenation catalysts using the Brown[2] hydrogenator. Only the 38Ni-62Cu melt failed to show hydrogenation activity. Furthermore, for the alloys actually formed (part c) the hydrogenation rate ranged from 2.6 to 3.3 millimoles/min/gm of catalyst with no trend observed for magnetic moment except that no activity was observed below 0.5 or above 1.3 Bohr magnetons. This lack of definition is probably due to the fact that the hydrogenation of hexene-1 in the Brown[2] hydrogenator is diffusion, rather than catalyst limited. A critique of the application of the Brown[2] apparatus to catalyst evaluation may be found in Appendix B-10.

The Raney alloy catalysts all show hydrogen activity when incorporated into a modified Teflon bonded (unsintered) electrode. Limiting currents of 26 to 160 ma/cm^2 were obtained in 90°C 6 M potassium hydroxide electrolyte. In testing these electrodes, a small performance decay was observed. However, stable values were obtained after 30 minutes provided the electrode was not driven beyond 160 mv

from theoretical hydrogen. Tests were generally run for several hours. As with most Raney alloys, these systems had enough adsorbed hydrogen to operate for some time in the absence of fuel (nitrogen blanket). However, under these conditions, the current would drop to zero in less than an hour. Returning to hydrogen would restore much of the lost performance, indicating that the steady state values reported correspond to true catalytic activity. Unfortunately, no ethylene or hydrocarbon activity was detected in potentiostatic measurements. This is probably a reflection of the adsorption problem discussed previously, and therefore, tests with alternate electrolytes is planned.

Part e - Correlation with Magnetic Moment Data

The hydrogen activity data summarized in Appendix B-11 was found to correlate with alloy magnetic moment. This is shown in Figure B-14, which is a plot of hydrogen limiting current density versus magnetic moment. The open symbols represent values for alloys which either failed to form or where actual alloying is in question. The observed correlation is quite good considering that it is uncorrected for the effect of catalyst surface area and variations in electrode fabrication. Notice that the maximum hydrogen activity, 160 ma/cm^2, was obtained with the 75Ni-25Co alloy having a magnetic moment of 1.0 Bohr magnetons. This correlation is equivalent to a correlation with occupancy of the d-band since for the first row transition elements magnetic moment is correlatable with d-band vacancies. Thus, it appears that it may well be possible to ultimately establish what the optimum electronic configuration for hydrocarbon oxidation is.

Figure B-14

Correlation of Hydrogen
Activity and Magnetic Moment

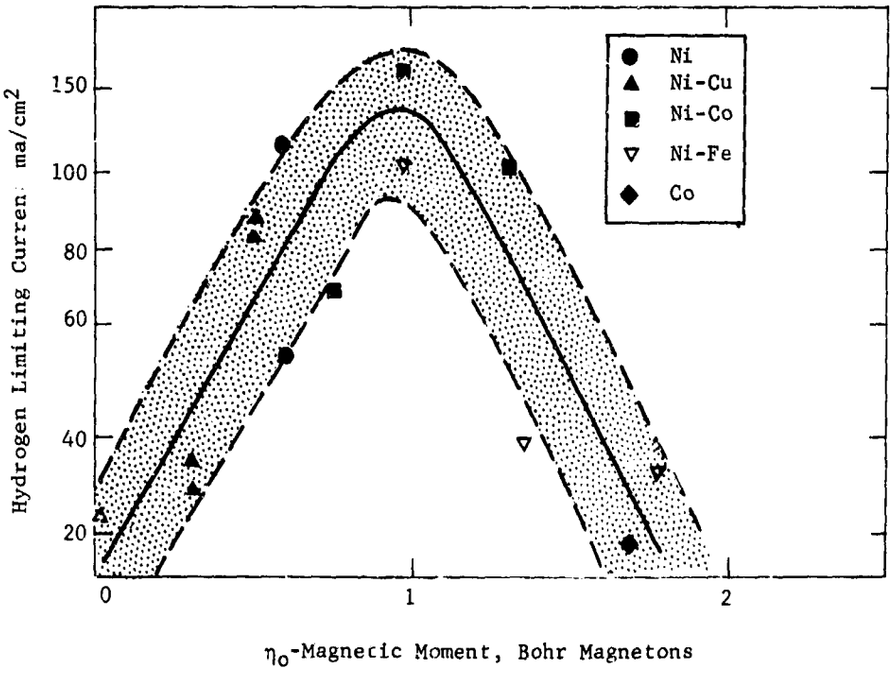

Phase 4 - Conclusions

Part a - Acid Resistant Metal Oxide and Carbide Catalysts

Studies aimed at determining the potentialities of the metal tungsten oxygen system as hydrocarbon electrocatalysts have shown that transition metals can be incorporated in this structure to produce conductive acid resistant materials. Data presented indicates that the metal-tungsten-oxygen system does indeed protect the catalytic transition elements while still allowing them to retain their catalytic properties. For example, hydrogen activity was observed with the nickel tungsten oxygen system. Thus, a material corresponding to $Ni_{0.237}WO_3$ has shown significant hydrogen activity despite problems with catalyst structure, and this activity has been confirmed using the voltage scan technique. In view of these results further work on the transition metal-tungsten oxygen system is warranted, especially since it is evident that both the catalyst and electrode structure have not been optimized for these systems. Examination of the potentialities of the rare earth tungsten bronzes was also initiated with the preparation of an europium tungsten bronze. This material has shown activity on hydrogen in acid media. Furthermore, X-ray analysis indicates that this is a true tungsten bronze rather than a mixed oxide system. Other rare earth bronzes should be examined to determine if this electrochemical activity is a general property of this class of material.

The eta phase carbides prepared thus far have not shown any definite activity as electrocatalysts. However, examination of these materials may be hampered by their inherent low surface areas, since one of the fired samples (Ni_3W_3C) did show detectable hydrogen activity. Methods for increasing the surface area are just now being explored.

Part b - Potential Application of Two Site Mechanism to Non-Noble Electrocatalysts

Research aimed at demonstrating catalysis of hydrocarbons by the two site mechanism using non-noble components have shown that a nickel electrode can adsorb ethylene when the electrolyte used is potassium carbonate. This is an important finding since the sensitivity to electrolyte may allow increased adsorption by electrolyte modification, and since it demonstrates that past failures to observe activity in potassium hydroxide may be due to lack of adsorption and not lack of activity. The sensitivity of nickel to deactivation has been more clearly established and is recognized as a serious problem. Further studies of adsorption as a function of electrolyte, and of variation in the second catalyst component in a suitable electrolyte are indicated.

Part c - High Surface Area Alloys

Hydrogen activity data obtained on the solid solution alloys of Ni-Cu, Ni-Co and Ni-Fe indicate that hydrogen performance correlates with magnetic moment, and hence d-band occupancy. A maximum hydrogen activity of 160 ma/cm^2 was obtained at about 1.0 Bohr magnetons. More work will be required to establish the validity of this maximum with an alloy which does not contain nickel (Co-Cu). No hydrocarbon or ethylene activity was observed with these materials. However, this may be due to the electrolyte, since it has been previously demonstrated that ethylene would not adsorb on nickel catalysts in 6 M KOH. Although the modified Raney procedure is a useful one for solid solution alloys of the first row transition elements, its general applicability may be limited. Consequently, it appears that investigations of other procedures for producing high surface area alloys will be required in the future.

2.3 Task C, Noble Metal Catalyst Studies

Current studies in noble metal catalysis are aimed at raising the effectiveness of carbon supported materials for hydrocarbon oxidation. Our initial objective was the development of a liquid or gaseous hydrocarbon anode capable of 150 ma/cm^2 with a platinum loading of under 2 mg/cm^2. Previous studies (6, 7) have shown that improved utilization can be obtained by placing the maximum platinum concentration at the three phase fuel-catalyst-electrolyte interface. Electrode structure studies have shown that a threefold improvement in utilization could be obtained with thin interface maintaining electrode structures. However, at low platinization the amount of platinum present in the active zone was insufficient to give practical currents. Further results (8) demonstrated that alteration in the "catalyst-support system" could also effect large improvements in platinum utilization. These data indicated that platinum utilizations as high as 40 ma/mg could be obtained at low platinization levels (and hence low platinum loadings). Since both performance and utilization improvement are required to attain the target goals, the current program is aimed at producing platinized carbon catalysts with increased platinization while retaining or improving the overall platinum utilization levels. Consequently, the approach involved first exploring potential catalysts supports, co-supports and treatments which would improve catalyst utilization. This was then followed by an examination of potential ways of increasing platinization with these materials. Electrode and catalyst structure factors were also briefly examined.

Phase 1 - Supported Platinum Catalysts

Studies reported previously indicated that high carbon surface area was advantageous for adsorbed platinum on FC-30C catalysts. In these studies increased surface area was achieved by carbon dioxide burn-out. However, as indicated in Table C-1, the surface area reached a limit of about 200 m^2/gm by CO_2 burnout.

Table C-1

Effect of Carbon Burnout of Performance

% Addition Burnout	Surface Area, m^2/g	Pt Utilization at 0.4 volts Polarized, ma/mg(1)
--	180(2)	37
--	112	25
20	192	39
28	172	20

(1) Platinization procedure discussed in Part a.
(2) Original batch of FC-30 carbon.

Accordingly, other carbons with surface areas of up to 900 m^2/gm were examined in an effort to achieve the higher performance levels required. In most of these studies, three carbon materials were examined; FC-20 (700 m^2/gm), FC-30 (110-200 m^2/gm) and FC-50 (450 m^2/gm).

The resultant supported catalysts were evaluated for butane activity at 150°C in 14.7 M H_3PO_4. All tests were conducted using the standard sintered carbon Teflon emulsion electrodes described previously (7) except that Teflon 42 (DuPont trademark for polytetrafluoroethylene suspension) was substituted for the original Teflon 41 BX.

Part a - Platinization Techniques

Various platinization procedures (on carbon supports) have been examined, including: (a) impregnation of a platinum salt, (b) adsorption of a platinum salt, (c) multiple adsorptions, and (d) co-precipitation methods. The impregnation procedure had been used in most of the earlier supported Pt studies. It involved deposition of a concentrated solution of a Pt salt onto a carbon support. By this technique, a limiting Pt utilization of about 10 ma/mg had been previously attained.

The advantage of adsorption from a dilute solution over the usual impregnation technique is that it eliminates the possibility of crystallization of trapped platinum salt during the drying operation. Ammonium chloroplatinate was found to be suitable for these adsorptions. Utilizations of up to 40 ma/mg were obtained when a silica co-support was used. It appears that platinum adsorption on the carbon is connected with a partial reduction of the platinum which occurs during this step. This is demonstrated by a decrease in the pH of the solution during the adsorption step. Furthermore, the adsorbed material contains only about three chlorine atoms per platinum instead of the original six.

For catalysts containing more than 6% platinum on carbon, single impregnations or adsorption resulted in increased Pt crystallite size with corresponding decrease in platinum activity. Use of a double adsorption procedure was effective in preventing appreciable platinum crystallite growth. In this procedure, ammonium chloroplatinate was adsorbed on carbon, then reduced at 149°C with hydrogen, and a second adsorption carried out before the final reduction and activation steps. Using this technique, performance levels as high as 85 ma/cm^2 were achieved, with some loss in Pt utilization at the higher platinum loadings. These results are discussed in detail in Phase 2.

Some additional studies aimed at increasing the platinum content of supported catalysts, involved variation of the temperatures used during the chloroplatinate adsorption step, in order to uncover a more favorable adsorption isotherm. Adsorption temperatures of 0°, 30° and 60°C were used with FC-30 carbons that contained 0 to 10% silica as co-support. Platinum pickup ranged from 1.9 to 2.6 wt % and utilization ranged from 17 to 26 ma/mg on butane at 0.4 volts polarized. No discernable trend was present. However, the highest Pt adsorption and utilization was obtained with the standard 30°C preparation and this temperature was used in subsequent preparations.

All of the prepared carbon catalysts were subjected to a final elevated temperature reduction-activation step independent of mode of platinization. While some of these materials were pretested prior to activation, it is safe to assume that all catalysts tested received this activation step unless specifically noted otherwise.

Part b - Carbon Activation Treatments

As indicated, burnout with carbon dioxide at 1000°C was effective in improving the activity of FC-30 carbon. In addition to increasing surface area, this treatment also improved the hydrophilicity of the carbon surface by introducing

oxygenated sites. As a result of this success, other methods for introducing oxygenated sites were investigated.

Ozonization at room temperature was,therefore, examined as a method for introducing oxygenated sites without burnout and hence without altering the inherent carbon surface area or pore distribution. Improvements in platinum utilization were obtained even when using a low surface area form of FC-30 carbon (110 m^2/gm). As shown in Table C-2 (and Appendix C-1) the ozonization decreased the platinum adsorption. This result was partly due to a greater tendency to colloid formation during catalyst preparation. This effect was not found for FC-20 carbon.

Table C-2

Effect of Ozone
Treatment on FC-30 Carbon

(Butane, 14.7 M H_3PO_4, 150°C)

Platinum Content wt % After Activation	Ozone Treatment gms Ozone/gm Carbon Treated	Limiting Current, ma/cm^2	Platinum Utilization ma/mg Pt
1.9	0	20	25
1.5	0.02	25	40
1.3	0.06	20	38
0.6	0.28	8	35

Activation of FC-20 carbon was also attempted with either carbon dioxide at 1000°C or ozone at room temperature. While the carbon dioxide treatment did increase the surface area from 700 to 900 m^2/gm it had no effect on Pt activity (Appendix C-1), apparently the CO_2 treat does not produce an increase in active pores. Ozone treatment on the other hand was clearly beneficial as shown in Table C-3.

Table C-3

Effect of Carbon
Activation on Platinum Utilization

(5% Pt on FC-20 Carbon with/without 10% SiO_2 Co-Support)

Treatment	Platinum Utilization, ma/mg Pt (at Limiting Current)
None	5-15
CO_2 Burnout	5-12
Ozone	17-30

Optimization studies on the ozone treatment indicated that the best utilizations were obtained at an ozone treatment level of 0.1 gms O_3/gm C independent of the presence of the SiO_2 co-support. This is illustrated in Figure C-1 below.

Figure C-1

Optimization of Ozone
Treatment on FC-20 Carbon

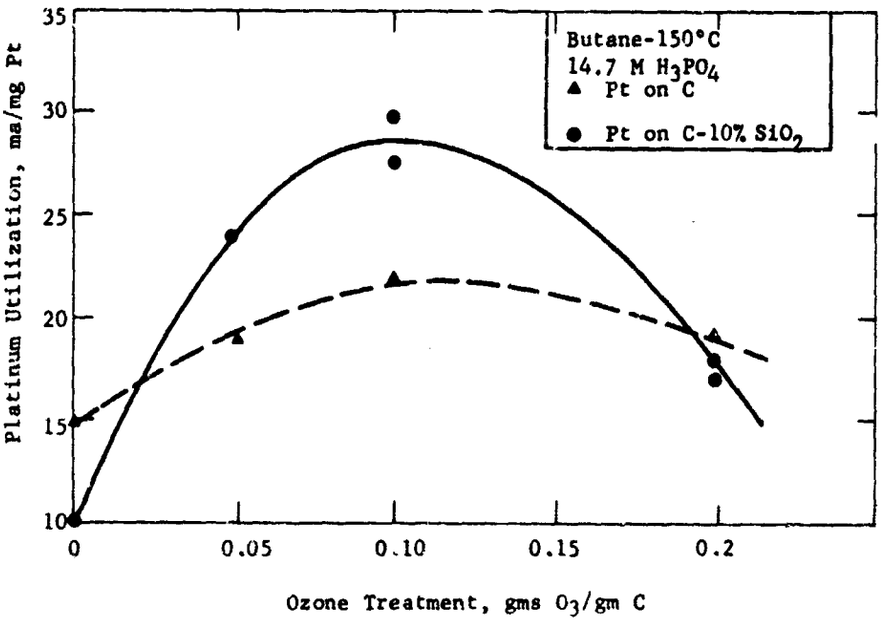

The reason for the ozone treatment effects is not fully understood. However, it is believed to be connected with the initial platinum adsorption step. As discussed in Part a, platinum adsorption on the carbon is connected with a partial reduction of the chloroplatinate by active sites on the carbon. Because of its high reactivity, the ozone attack occurs at relatively accessible pores, oxidizing the active sites and thereby eliminating their ability to reduce chloroplatinate. Accordingly, the platinum deposition in the less accessible sites in the smaller pores should be favored. This deactivation is best seen in examining Table C-2 which shows a decreasing platinum content on increasing ozonization.

Since the FC-20C has a higher adsorption capacity due to its high surface area and microporosity, the deactivating effect of the ozone presumably acts merely to shift adsorption to the less accessible sites. Accordingly, there is no drop-off in total platinum adsorption in this case.

During the activation treat of the catalyst, the platinum redistributes itself on the carbon surface, accompanied by platinum crystallite growth. In this step, transfer of the platinum from the smaller pores into the larger pores probably occurs, making the platinum more accessible to hydrocarbons. Evidence for this

conclusion is the fact that hydrogen performance is extremely good in the absence of the activation treat, despite the poor hydrocarbon performance. Diffusion of hydrogen into the micropores occurs readily.

However, the extent of crystallite growth during the activation treat appears to be extremely dependent on the initial location of the platinum. Thus, adsorption of colloidal platinum onto carbon would be expected to restrict itself to larger pores than for salt adsorption because of the size of the colloid particles After activation the colloidal material crystallites grow to 100-200 Å, although X-ray diffraction shows that initially the Pt crystallite size is less than 50 Å.

The ideal support would therefore appear to be one which has a high percentage of both small and intermediate pores for optimum final platinum dispersion (minimal crystallite growth). Generally speaking carbon supports with high intermediate porosity (50-200 Å) are not available, but can be prepared using the procedure of Dubinin (45). This will be examined in the future.

Part c - Co-support Studies

Increased platinum utilization was obtained using FC-30C supported catalysts by the introduction of 10% SiO_2 as a silicic acid gel. The benefit obtained by the use of the silica co-support disappeared with the higher surface FC-20 carbon unless the carbon was ozonized. This suggests that the silica co-support benefit may be related to the high surface area ($\sim$600 m^2/gm) introduced by this material, thus favoring small pore adsorption with a subsequent reduction in crystallite growth on activation. The higher surface area carbons do not require this increased surface area.

Alternatively, the silica benefit may be related to an interaction with the carbon. X-ray diffraction data shows the presence of a series of silica peaks for the FC-30 case, but not with the FC-20 and FC-50 carbons. The benefit of ozonization (Figure C-2) on the FC-20 carbon-silica system may be related to increased interaction between the silica with the more hydrophilic carbon surface.

Other co-support systems were also examined. These included alumina, sodium tungsten bronze, and a mixed nickel tungsten oxide ($Ni_{0.2}WO_3$). The results of this study are summarized in Table C-4.

Table C-4

Effect of Co-Support on
Platinum on Carbon Utilization

(Butane, 150°C, 14.7 M H_3PO_4, FC-30 Carbon)

Co-Support	Limiting Platinum Utilization, ma/mg Pt
7% Al_2O_3	16
10% WO_3	11
5% Sodium Tungsten Bronze	33
50% $Ni_{0.2}WO_3$	15
10% SiO_2	40
None	20

None of these materials shows any advantage over the 10% SiO_2 co-support. However, sodium tungsten bronze did show some improvement over the base case. In addition, the $Na_{0.2}WO_3$ co-support improved electrode stability at limiting current, allowing operation for eight hours with little increased polarization.

The search for other co-support systems has lead to the development of the alumino-silicate carbon system. This material is related to the well-known molecular sieves and it is believed to be a new composition of matter. The key step in developing this substrate for maximum platinum utilization is the deposition of a thin layer of ion exchange (Na^+) alumino-silicate in the pores of the carbon support. The Na^+ ion is then exchanged for the catalytic element prior to reduction. This insures the presence of discrete individual platinum ions prior to the reduction step, which should minimize platinum crystallite size.

The deposition of alumino silicates on carbon proceeds with surprising ease. The carbon particles were put in solution of sodium silicate, sodium hydroxide and sodium aluminate similar to those used to grow crystals of molecular sieve. The rate of deposition was so rapid that it was nearly complete in the first five minutes even at ambient temperature. See Table C-5 and Appendix C-2.

Table C-5

Effect of Deposition Time
on Alumino-Silicate Content

Time of Deposition, min	Amount of Alumino-Silicate Deposited (wt % of carbon)
5	84
20	109
120	122

This rate of deposition is ten times faster than the growth of molecular sieve crystals from similar solutions. Deposits of up to 140 wt % were readily formed. A deposit of 70 wt % would represent a monolayer of the alumino silicate tetrahedra, which consist of aluminum or silicon surrounded by four oxygen atoms, evenly spread over the surface area of the carbon. Deposits of from 0.5 to 140 wt % could be made by changing the ratios of salts to carbon and water to carbon. See Table C-6 and Appendix C-2.

Table C-6

Effect of Solution Composition on
Weight of Deposited Alumino-Silicate

gm of Salts / gm of Carbon	gm of Water / gm of Carbon	Deposit of Alumino-Silicate (wt % of Carbon)
4.64	220	0.5
.264	22	11.6
.925	22	24.5
4.64	22	148

The alumino-silicate deposits appear to have all four characteristics required of an effective co-support. Microscopic examination indicates that all of the alumino-silicate is on the carbon particles rather than in separate aggregates. This is important since any catalyst deposited on alumino-silicate agglomerates would not be in good electrical contact and could not contribute to the electrochemical reaction. Conductivity tests indicated that the alumino-silicate deposit was inside the catalyst pores. The conductivity of a 25% alumino-silicate on carbon was 2/3 that of the pure carbon. Had surface multilayer deposition occurred, much lower conductivity would have been observed.

The absence of this thick multilayer is important to both the charge transfer from the catalyst on alumino-silicate to the conductive carbon co-support and the conduction of these electrons through the carbon co-support to the electrode current collector.

Furthermore, large crystal deposits were not formed in a few pores as the X-ray scans indicated that the deposits were amporphous. If large crystals had been formed in the pores the electrical conductivity from the catalyst in the crystals to the carbon would have been a problem.

Finally exchangeable Na^+ ions were found. Powders formed were first contacted with water and then $CaCl_2$ solutions. The solution from the water contacting step showed no sodium in the flame test but the solution from $CaCl_2$ treat did show Na^+ indicating that ion exchange had occurred. Thus, all four of the characteristics required for effective catalyst utilization have been met.

A quick test of this new catalyst substrate was made using a solution of platinum as $(Pt(NH_3)_4Cl)^+Cl^-$ and ruthenium as $(Ru(NH_3)_4OHCl)^+Cl^-$. Loading of 0.5 of each element was achieved. However, the electrode was unsuccessful as it polarized severely at less than 1 ma/cm^2 on methanol in sulfuric acid. This could be attributed to the alumino-silicate not being distributed uniformly enough on the surface of the pores with the conditions used and therefore causing an insulating effect. It could also be attributed to a large concentration of unidentified impurities in the complex ruthenium salt used for the ion exchange.

Part d - Coprecipitation Techniques

The technique of coprecipitation of Pt with alumina followed by leaching of the alumina had been used to obtain a Pt black with very high activity (7). An

attempt was now made to extend this approach to a Pt on carbon catalyst. A solution of sodium aluminate and chloroplatinic acid at 70°C was neutralized to appearance of cloudiness, then carbon was added. The resulting slurry was slowly reduced with formaldehyde with simultaneous coprecipitation of alumina. Leaching of the alumina at room temperature was attempted with 8 M KOH, 20% H_2SO_4, and 20% H_3PO_4. The order of effectiveness was $H_3PO_4 > KOH > H_2SO_4$. However, even with the H_3PO_4, 28% of the alumina was still present. By leaching with hot H_3PO_4 the alumina content was reduced to 1%, and the limiting Pt utilization increased from 5 to 15. Nevertheless, the procedure did not offer any advantage over the Pt adsorption technique.

Part e - Effect of Crystallite Size

The primary advantage of supported catalyst systems lies in their ability to create and maintain the active material in a fine state of subdivision during activation and use. Thus, X-ray crystallite size determinations can be used as a measure of support effectiveness. Consequently, crystallite size determinations have been used routinely in catalyst preparation studies. It must be remembered, however, that X-ray crystallite size measurements tend to error on the high side since the smallest crystallites are not detected.

An analysis of crystallite size data from FC-20, FC-30, and FC-50 carbons indicates that platinum utilization is dependent on crystallite size. This is illustrated in Figure C-2, which is a plot of utilization at 0.40 volts polarized versus crystallite size. These data indicate that differences in carbon type and carbon surface area can affect the response for a given crystallite size. Notice that the lower surface area FC-30 carbon gave better utilizations, at equivalent crystallite size, than the two higher surface area materials (FC-20, FC-50 carbon). The enhanced utilization obtained with FC-30 carbon may be associated with an interaction of the platinum with the support as indicated by a shift in the X-ray peaks. This shift is consistent with alloy formation between platinum and the iron present in the ash of the carbon.

The fact that the FC-20 (450 m^2/gm) and FC-50 carbon (700 m^2/gm) fall on the same curve is further indication that surface area per se is not the controlling factor. Furthermore, these data indicate that crystallite size below 50 Å will be required to obtain the 80 ma/mg initial target. However, the steep rise in utilization below 60 Å is quite encouraging.

Figure C-2

Effect of Crystallite Size
on Futane Utilization Pt/C

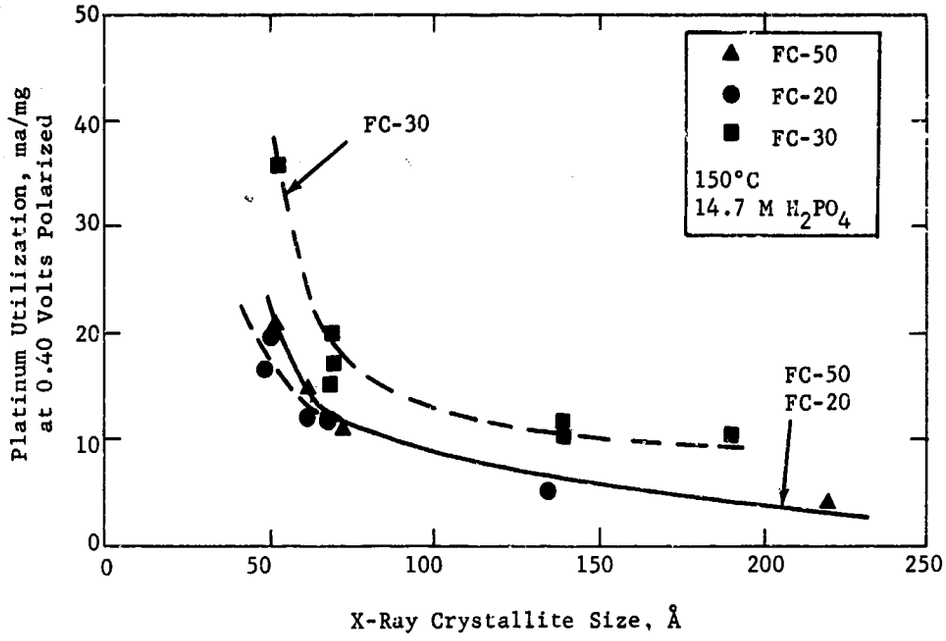

Phase 2 - Structure Factors

Previous studies have shown that physical factors, unrelated to the chemical make up of the catalyst, can markedly affect catalyst effectiveness (6). Problems associated with the state of subdivision of the catalyst and its effect on finished electrode structure can markedly alter platinum utilization. Consequently, the relation of catalyst structure to electrode fabrication was briefly considered. Studies were conducted to evaluate the effect of catalyst particle size and electrode thickness on utilization to confirm the previous finding with new carbon supported catalysts with higher platinization levels. In addition, the use of an alternate Teflon source was also evaluated.

Part a - Effect of Grinding

An examination of the effect of grinding before and after catalyst preparation was conducted to determine if the state of subdivision of the carbon could affect utilization. Various grinding procedures were evolved including mechanical mortar grinding, ballmilling and colloid milling (hydraulic grinding). The results shown in Table C-7 and Appendix C-1 indicate that effective grinding prior to preparation can result in up to a fourfold improvement in platinum utilization.

Table C-7

Effect of Grinding on
Platinum Catalyst Performance - Butane

(5-6% Pt on FC-20 Carbon - 10% SiO_2)

Grinding Method	Limiting Current, ma/cm^2	
	Before Preparation	After Preparation
Mortar	5	--
Ballmill	12	17
Colloid Mill	23	--

Surprisingly, ballmilling after final activation also showed some benefit over ballmilling prior to platinization.

While the colloid mill procedure was most effective, it was also the most difficult to control and reproduce. Accordingly, ballmilling after catalyst preparation was chosen as the preferred grinding method for all other comparative studies. Performance improvements were obtained with both FC-20 carbon and FC-50 carbon supported catalysts when the materials were ballmilled after catalust preparation. Data indicated (Table C-8) that performance improvement became independent of milling time in the 2-24 hour range, though shorter ballmilling was less effective. Prolonged ballmilling for 168 hours also gave a decreased performance.

Table C-8

Effect of Ballmilling
Time on Platinum Performance

(Ballmilled after Catalyst Preparation)

FC-50 Carbon Support

Time, hr Ballmill After Preparation	Limiting Current, ma/cm^2
1/2	20
2	40
4	45
8	40
24	45
168	20

Part b - Teflon Emulsion Studies

For reasons of interface control, the Teflon emulsion required for the sintered carbon Teflon electrodes can contain no surfactant. Until recently this has resulted in our use of Dupont's surfactant-free Teflon 41 BX. Because of low demand for this latter product (due to the manufacture of a new product), some recent batches have been of inferior quality. Because of the reproducibility problems introduced by these batches, the use of Teflon 42 BX was evaluated as a potential substitute. According to Dupont, this material should prove to be of more consistent quality.

Tests indicate that Teflon 42 BX sinters at a lower temperature than the 41 BX material used previously. Studies showed that at 22 wt % Teflon the electrode performance was practically independent of temperature in the 302 to 330°C range. However, at lower Teflon contents, sintering at 330°C was superior to 315°C. Hence, the following sintering conditions were chosen for Teflon 42 BX: one minute at 330°C, 2200 psi independent of Teflon content. This set of conditions was used for most of the supported carbon electrodes discussed in this report.

Part c - Effect of Electrode Thickness

Previous studies (7) have indicated that the highest platinum utilization is achieved with very thin electrodes. These structures require high platinization levels in order to attain significant current levels. However, as platinization is increased, catalyst utilization decreases. Accordingly, a study was initiated to prepare an effective platinum on carbon catalyst with higher platinization levels.

Use of a double adsorption procedure (Phase 1) was effective in preventing appreciable platinum crystallite growth. As indicated earlier, ammonium chloroplatinate is adsorbed on FC-20 carbon, then reduced at 150°C and a second adsorption is carried out before the reduction and final activation steps. An 11% Pt on ozonized (0.1 gm O_3/gmC)FC-20 carbon catalyst prepared by this procedure showed improved butane utilization in going from a thick 23 mil electrode to thin 10-15 mil structures. This is illustraced in Table C-9.

Table C-9

Effect of Electrode Thickness on
Platinum Utilization - 11% Platinization Level

(Butane, 14.7 M H_3PO_4, 150°C)

Platinum Loading, mg/cm^2	Electrode Thickness, mils	Limiting Current Density at 0.45 Volts Polarized, ma/cm^2	Platinum Utilization, ma/mg
4.7	23	85	18
3.2	15	80	25
1.6	10	40	25

Although the utilization was somewhat lower than that obtained with a single impregnation, a current density of 80 ma/cm^2 was obtained at 3 2 mg Pt/cm^2 loading.

By contrast a 4.5% Pt on FC-50C catalyst prepared by single adsorption showed debit only at high electrode thickness as shown in Table C-10.

Table C-10

Effect of Electrode Thickness on
Utilization of a 4.5% Pt Catalyst

Electrode Thickness, mils	Pt Loading, mg/cm^2	Highest Limiting Current, ma/cm^2 (1)	Pt Utilization, ma/mg
9	0.47	15	32
22	1.9	60	32
34	2.8	55	20

(1) Polarization approximately 0.45 volts.

Thus, the effect of electrode structure appears to be highly dependent on platinization level.

Part d - Electrode Fabrication

Previous electrode structure studies indicated that it was possible to partially separate the wetproofing and electrode fabrication steps. These exploratory experiments indicated that controlled coagulation from a dilute dispersion of catalyst plus Teflon emulsion could result in more effective Teflon utilizations. Consequently, an alternate electrode fabrication procedure was briefly examined in conjunction with a study of electrode drying effects. A 6% Pt-10Ir catalyst on FC-30 carbon was used as the model material. In this procedure a slurry of catalyst and Teflon 42 BX emulsion in water was heated with stirring until coagulation occurred. Sintering of the electrodes was carried out with increasing degrees of wetness, as a means of increasing electrode porosity. This technique requires slow closing of the sintering press to prevent the wet electrodes from being blown apart. The data, shown in Table C-11, indicates an advantage for the wet sintering procedure using slurry type electrodes.

Table C-11

Effect of Electrode Drying on Performance

6% Pt-10Ir on FC-30 Carbon(1)

Drying Time, min	Performance, ma/cm^2 at 0.40 volts Polarized
-15(2)	32
0	27
15	23
30	15
60	12

(1) Electrodes prepared from catalyst-Teflon hot slurry.
(2) Sintered without initial pressing between filter paper; hence, "negative" drying time.

Electrodes prepared by the standard gelation procedure did not show a similar benefit from increased drying. Using this standard technique, the highest performance at 0.40 volts polarized was 23 ma/cm^2 and was obtained after 1/2 hour of drying.

Repeat tests with older batches of Teflon 42 BX emulsion gave poorer performance indicating that Teflon particle size distributions may be a critical factor when applying this slurry technique. Furthermore, the importance of the carbon support has not been fully evaluated. Initial experiments with FC-50 carbon indicates that this material may not be adapted to the slurry technique due to problems with Teflon-carbon coagulation.

The best slurry electrode showed a further improvement in performance after washing and drying. A limiting current of 60 ma/cm^2 was achieved. Careful examination of a second electrode after washing showed that some white crystalline solid appeared on the surface. It is conceivable, therefore, that this improved performance is a result of washing out an impurity.

Phase 3 - Conclusions

The use of carbon supports with or without other co-supports continues to show promise of significant improvements in platinum utilization in the future. Studies of various platinization techniques including coprecipitation, indicates that adsorption from aqueous ammonium chloroplatinate provides materials with highest utilization and smallest crystallite size. However, the limited adsorption capacity (at the proper pore diameter) continues to reduce platinum utilization and limit attainable platinization levels. Attempts to increase this platinization level through alteration in adsorption temperature did not uncover a more favorable isotherm. However, a newly developed ozone treatment has improved utilization by deactivating ineffective adsorption sites. This technique, coupled with multiple adsorptions and low temperature hydrogen reductions has allowed us to reach an 11% platinization level with only a small loss in utilization. This type of system has attained 80 ma/cm^2 on butane at 3.2 mg/cm^2 loading. Furthermore, analysis of X-ray crystallite data indicates that platinum utilization increases with decreasing crystallite size.

The structure of the carbon co-support system has also been shown to affect utilization. Data indicates that both sodium tungsten bronze and silica can act as effective carbon co-supports with carbon yielding about the same platinum utilization improvement. In addition, a new co-support system based upon the alumino-silicate molecular sieves is under study. Although, initial performance was poor, its potential for producing small platinum sites warrants further investigation.

Electrode structure factors relating to catalyst particle size, Teflon emulsion, electrode thickness and electrode fabrication were found to also affect performance. In the course of these studies, a new electrode fabrication technique (slurry coagulation) was developed which allows independent wetproofing and fabrication. This will be explored further in the future.

2.4 Task D, New Electrolytes

As previously shown, the activity of hydrocarbon electrodes is limited by a chemical rather than diffusion controlled mechanism. One possible approach, improved catalysis, has been discussed. An alternative is highertemperature operation. Since temperature increases materials and start-up problems as well as limiting the choice of power package size to a relatively high power, temperature cannot be indiscriminately raised. It is believed that operation at the lower end of the intermediate temperature fuel cell range, approximately 150-300°C, will provide maximum benefits with relatively minor increases in engineering problems. For example, power systems as small as 300 watts would be thermally self-sustaining and start-up could be readily accomplished by external heating.

Previous studies have shown that substantial improvements in electrode activity can be obtained by using an intermediate temperature electrolyte such as pyrophosphoric acid (7,8). The extreme corrosiveness of this electrolyte necessitated a search for other electrolytes that could operate in the same temperature range. Molten alkali metal bisulfates were shown to have many properties required of a fuel cell electrolyte. However, this electrolyte was eliminated as a potential fuel cell electrolyte because of its adverse electrochemical oxidation-reduction properties (8).

Phase 1 - Mixed Alkali Metal Dihydrogen Phosphate Melts

Molten alkali metal dihydrogen phosphates were chosen as the next class of intermediate temperature electrolyte for investigation. These systems have a number of advantages. For example, in the contemplated temperature range, molten phosphates do not give off volatile phosphorous oxides (47). Water is lost but can be readily balanced in a total system. By contrast, many molten electrolytes have volatile dissociation products which must be supplied to the cathode to reduce concentration polarization and to retain electrolyte invariance (48,49). Molten bisulfates, for example, slowly lose SO_3 (50,8). Also, other electrolytes, e.g., carbonates require operating temperatures at which the salts are slowly lost by vaporization (51). Such is not the case for phosphates.

Molten phosphates have a very important additional advantage over bisulfate melts in that the oxidizing power of phosphates are negligible below 300°C (52). This means that unwanted electrochemical redox reactions leading to mixed potentials would not be a problem with this electrolyte.

Part a - Synthesis of the Mixed Alkali Metal Phosphate Melts

The studies on phosphate melts were primarily carried out using a melt made from a mixture of KH_2PO_4 and $NaH_2PO_4 \cdot H_2O$. The melt most frequently used was one having as its initial components, 25 wt % $NaH_2PO_4 \cdot H_2O$ and 75 wt % KH_2PO_4. This mixture is heated until a clear colorless liquid is obtained. Repeated trials have shown that by this simple procedure, a low melting phosphate salt can be reproducibly prepared. The initial mixture undergoes about a 7% weight loss on heating. This is due to the loss of water of hydration and by condensation reactions to form higher phosphates. The weight losses of some representative samples are shown in Appendix D-1.

Phosphate mixtures of higher sodium content produced solids having higher melting points. The melts remained liquid below their melting point, resolidifying to a clear transparent solid below 100°C. Table D-1 shows some of the properties of these systems.

Table D-1

Properties of Mixed Alkali Phosphate Melts

Mixture	Initial Components, wt %	Approximate Melting Pt, °C	After Melting
A	$NaH_2PO_4 \cdot H_2O$, 25 KH_2PO_4, 75	200	Viscous liquid below 100°C.
B	$NaH_2PO_4 \cdot H_2O$, 50 KH_2PO_4, 50	200	Viscous liquid at 100°C.
C	$NaH_2PO_4 \cdot H_2O$, 75 KH_2PO_4, 25	290	Very viscous liquid at 200°C.
D	Mixture A, 50 K_2HPO_4, 50	320	

Other mixed alkali metal phosphate melts were composited, but the bulk of the work was performed using mixture A in Table D-1.

Part b - Stability of the Mixed Alkali Metal Phosphate Melts

Phosphate salts at moderately high temperatures lose sufficient water and are converted to metaphosphates. The metaphosphates have much higher melting points than the starting compounds. Stability tests were performed to determine if this also occurs with the mixed alkali metal phosphate melts under projected fuel cell conditions. The particular melt under investigation was composited from a mixture of 25 wt % $NaH_2PO_4 \cdot H_2O$, 75 wt % KH_2PO_4, hereafter called Mixture A as in Table D-1. No other compositions were investigated.

The melt was tested for stability by maintaining samples at 240, 260, and 300°C for ten days. At each temperature a condenser was used to minimize water losses. In addition, at the two lower temperatures, the melt samples were exposed directly to the atmosphere, with no provisions taken to prevent water losses. The results are shown in Table D-2.

Table D-2

Results of Ten Day Stability
Tests of the Molten Phosphates

Sample	Temp, °C	Condenser Used	Result After 10 Days on Temp
1	240	Yes	Clear melt
2	"	No	" "
3	260	Yes	" "
4	260	No	" "
5	300	Yes	Onset of cloudiness after 30 hours

These results indicate that the mixed alkali metal phosphate melts are probably stable below 260°C. At 300°C, the melt gradually became semi-solid. Attempts were made to equilibrate the melt at 300°C with water by passing humidified nitrogen over but not through the melt. This did not prevent the formation of white solids, which were probably insoluble metaphosphates.

Part c - Carbon Dioxide Rejecting
Properties of Molten Phosphates

In aqueous medium, no electrolyte system can be carbon dioxide rejecting if it contains a weaker acid than bicarbonate ion. The prediction of the carbon dioxide rejecting properties of a non-aqueous electrolyte, or of an electrolyte in a non-aqueous medium is rendered more difficult because of the effect of the medium on the acid strengths. In the case of an acid dissolved in two solvents of equal acid-base strength, but different dielectric constants, the difference in the ionization constants of the acid in the two solvents is dependent on the acid charge types involved and the difference in the dielectric constant. From simple electrostatics, the change in ionization constants may be estimated.

By considering the phosphate melt both as solvent and electrolyte, and assuming that the relative acid-base strengths of water and the melt are equal, it is possible to predict the carbon dioxide rejecting properties of the melt. The dissociation constants of negatively charged acids of the type HB^{-1}/B^{-2} and HB^{-2}/B^{-3}, HCo_3^{-1}/Co_3^{-2}, $H_2PO_4^{-1}/HPO_4^{-2}$, $H_2P_2O_7^{-2}/HP_2O_7$ are markedly influenced by a change in dielectric constant. The change in dissociation constant due solely to a change in dielectric constant D is given by the relation (53).

$$\Delta (pKa) = 2K\Delta \left(\frac{1}{D}\right) \text{ for the } HB^{-1}/B^{-2} \text{ system,}$$

where pKa has its usual meaning and k is a constant containing the electronic charge and the ionic radii of the given acid system. For the acid systems listed above, the (k) values are similar so that both $H_2PO_4^{-1}$ and HCO_3^{-1} will undergo the same Δ pKa in the melt. Since the dihydrogen phosphate anion is a stronger acid in water than bicarbonate ion, it follows that it will also be a stronger acid in the melt, and the melt system should, therefore, reject carbon dioxide. The same considerations hold for other species such as $H_2P_2O_7^{-2}$, $HP_2O_7^{-3}$ and similar systems existing in the melt.

Experiments in which powdered cesium carbonate is added to the phosphate melt showed that carbon dioxide is evolved with each charge addition. Furthermore, the potential of a hydrogen electrode in the melt versus that of a reference electrode whose potential is independent of the melt acidity and is between that of a hydrogen and oxygen electrode in the melt, increases when cesium carbonate is added. This is exactly analogous to measuring the potential difference between a hydrogen electrode and a calomel in aqueous medium when a basic material is added. Since carbonate acts as a base to the melt acids, the melt acids are stronger than bicarbonate ion. The melt is therefore carbon dioxide rejecting. In this respect, the melt system is very similar to aqueous electrolyte systems.

Part d - Reference Electrodes for the Phosphate Melts

To facilitate testing of the mixed alkali metal phosphate melts, it was necessary to develop a convenient reference electrode system. The system chosen was metallic silver in contact with a silver ion containing phosphate melt. This was chosen because silver has only one stable valence state, the metal has no observable tendency to dissolve in molten silver salts, and generally is highly reversible to its ions (5). A dilute solution of silver phosphate in the phosphate melt was used to make the electrolyte in the reference electrode as similar as possible to the electrolyte system under study. This minimizes the liquid junction potential. Furthermore, the problem of flow due to the hydrostatic head at the liquid-liquid junction is reduced by having the two electrolytes as alike as possible.

The initial components making up the reference electrode electrolyte are KH_2PO_4, 72.75 wt %, $NaH_2PO_4 \cdot H_2O$, 24.25 wt %, and Ag_3PO_4, 3 wt %. This mixture is heated until a light yellow melt is obtained. The reference electrode, a silver wire immersed in this melt at 250°C, was found to be quite reliable. The potential difference between this electrode and a hydrogen electrode in the phosphate melt at 250°C is reproducible to within $\pm$ 10 mv. The potential difference is achieved rapidly after the admission of hydrogen to the platinum catalyst and did not exhibit any instability. Based on the hydrogen-reference electrode measurements, the oxygen-reference electrode voltage measurements indicate that the oxygen electrode was practically at theoretical thermodynamic potential. This is quite similar to the behavior of oxygen electrodes in pyrophosphoric acid at the same temperature (7).

Part e - Conductivity of the Mixed Alkali Metal Phosphate Melts

Resistance measurements of the phosphate melts were made in a standard conductivity cell with an AC bridge from 200 to 280°C. The calculated resistivities were based on the assumption that the cell constant (1.0 at 25°C) of the cell does not vary appreciably with temperature. No differences were observed between the values obtained at 60 or 1000 cps. Figure D-1 illustrates the results with the phosphate melt, with the specific resistance falling from 77 ohm cm at 225°C to 16 ohm cm at 275°C. The resistivity of this melt at 275°C is somewhat higher than desired for a fuel cell electrolyte, although higher electrode activity should more than offset any disadvantage.

Figure D-1

Conductance of Mixed
Alkali Metal Phosphate Melt

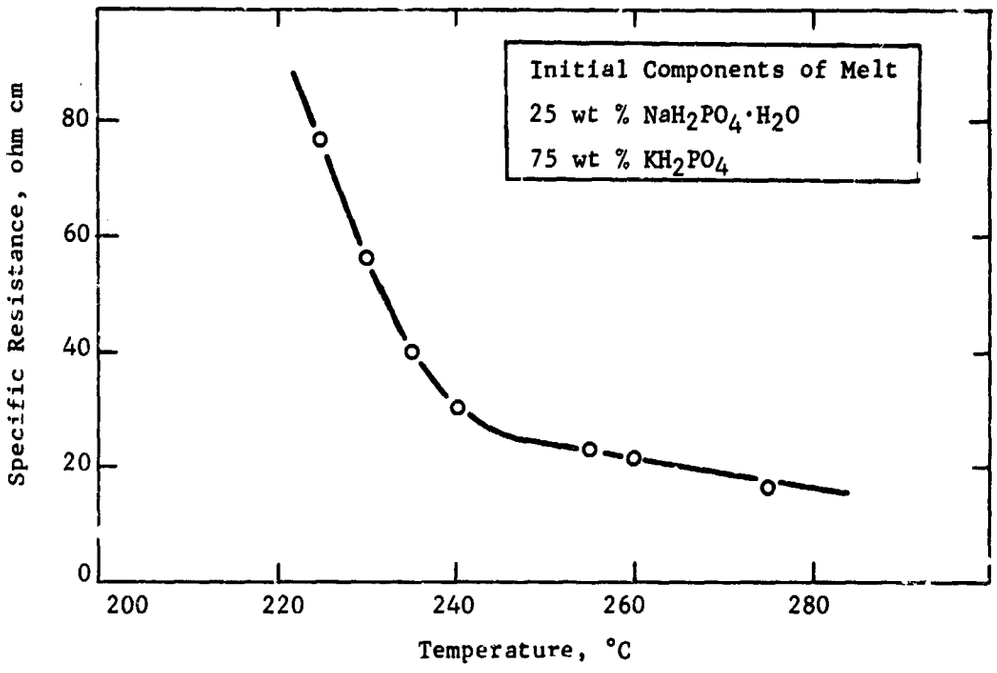

Attempts were made to modify the melt properties so that ionic conductance could be increased. Phosphate melts consist of polymeric anions known as polyphosphates. Depolymerization to lower "anionic molecular" weight melt components would result in increased conductance. This would be due both to the decreased viscosity and the increased number of charge carriers. Depolymerization can be accomplished by the cleavage of the (P-O-P) bond, for example, with the simultaneous acceptance of an oxygen ion from a basic fluxing agent (55,56). A polyphosphate anion $[H_2P_nO_{3n+1}]^{-n}$ where n = 1,2,3, can be cleaved to smaller anions as shown below

$$H_2P_nO_{3n+1}^{-n} + ZO_4^{-2} \longrightarrow \begin{cases} HP_yO_{3y+1}^{-(y+1)} + HP_mO_{3m+1}^{-(m+1)} \\ + ZO_3 \end{cases}$$

where ZO_4^{-2} is a general basic fluxing agent and n=y+m.

Fluoride ion is also a potential depolymerizing agent since in addition to being an anionic base, it is unable to serve as a bridging group between tetrahedra making up the polymeric anionic aggregate.

Attempts were made to increase the phosphate melt conductivity by additions of calcium oxide, cupric oxide, cobalt oxide, nickel oxide, zinc oxide, cesium carbonate, and cesium fluoride. Of the oxide ion fluxing agents only zinc oxide and cesium carbonate exhibited appreciable solubility in the melt. Cesium fluoride also exhibited appreciable solubility. As shown in Figure D-2, these agents lowered the electrolytic resistance by substantial amounts in the temperature range of 210-230°C. The resultant resistances are still too high in this range. At 240-280°C, only small improvements are obtained.

Figure D-2

Conductance of Phosphate
Melt Containing Depolymerizing Agents

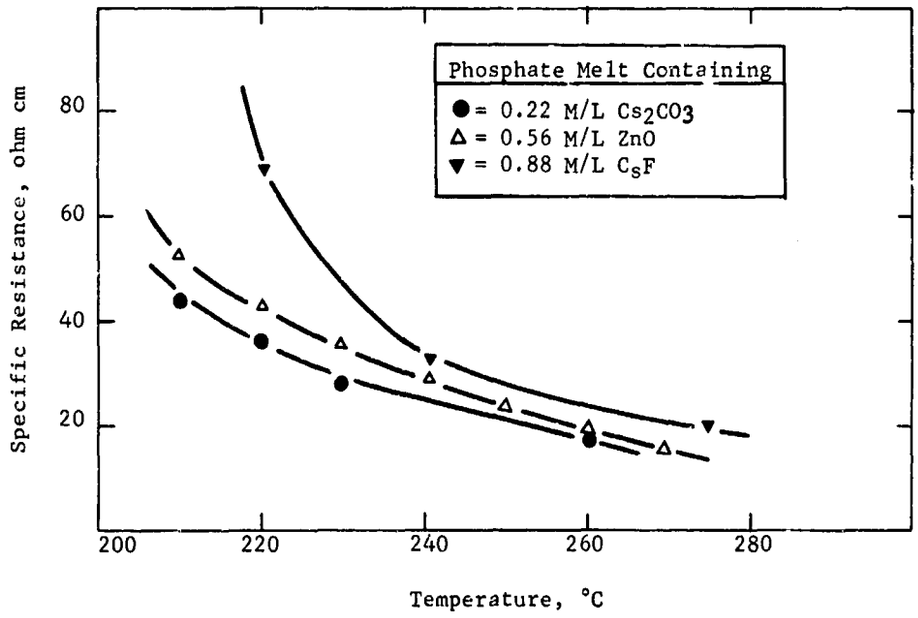

If the initial phosphate melt does not contain many higher polymeric anions, then the addition of the fluxing agents would not be expected to cause large increases in ionic conductance due to depolymerization. The only result would be to increase the conductance because of the increase in the number of charge carriers. This increase will not be appreciable if the ionic melt in which the salts are dissolved is rather viscous (57).

Part f - Buffer Behavior of the Mixed Alkali Metal Phosphate Melt

The ability of the phosphate melt to minimize ionic concentration polarization was tested at 250°C. The electrode used for testing the buffering ability of the electrolyte was the standard sintered platinum-Teflon type. At the anode, hydrogen, which would not be expected to be activation polarized was used as the test fuel. In addition to dry hydrogen, hydrogen of varying water content were used to determine if water had any effect on anodic buffering capacity. Figure D-3 shows that the mixed phosphate melt has adequate anodic buffering. Unlike pyrophosphoric acid, however, there is a finite amount of concentration polarization (7). It is doubtful that water has any influence on the anodic buffering capacity. The detailed data are given in Appendix D-2.

Figure D-3

Anodic Buffer Action of the Mixed Phosphate Melt

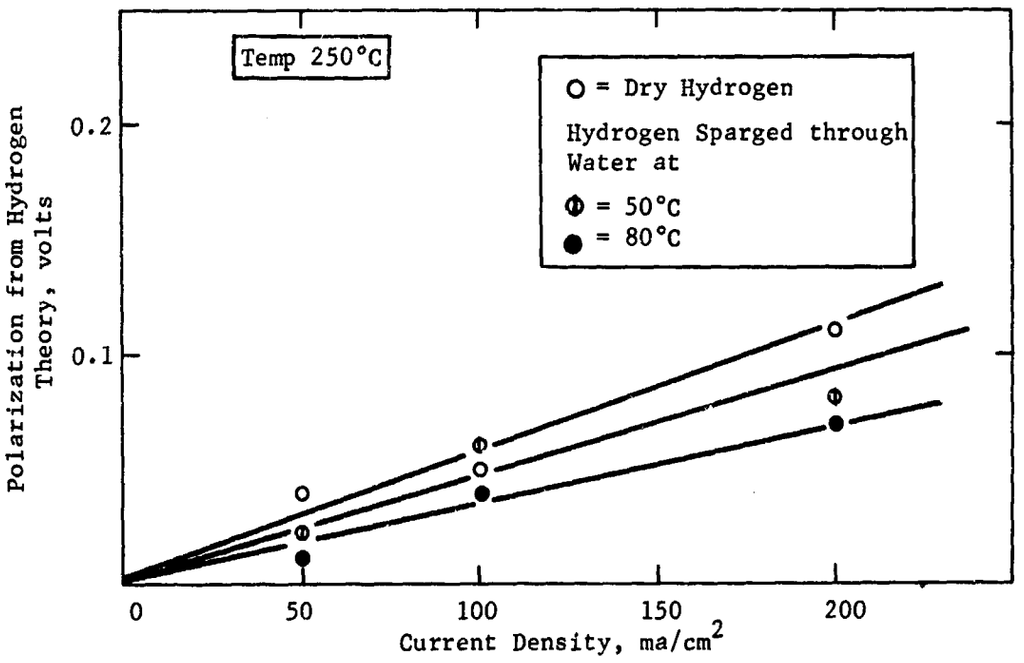

Cathodic ionic concentration was measured by evolving hydrogen from the platinum-Teflon structure, while admitting hydrogen to the electrode. The possible influence of water was tested as it was in the anodic buffering study. The results shown in Figure D-4, indicate that the phosphate melt has adequate cathodic buffering capacity, but that it allows a finite concentration polarization. The detailed data are given in Appendix D-3.

Figure D-4

Cathodic Buffer Action
of the Mixed Phosphate Melt

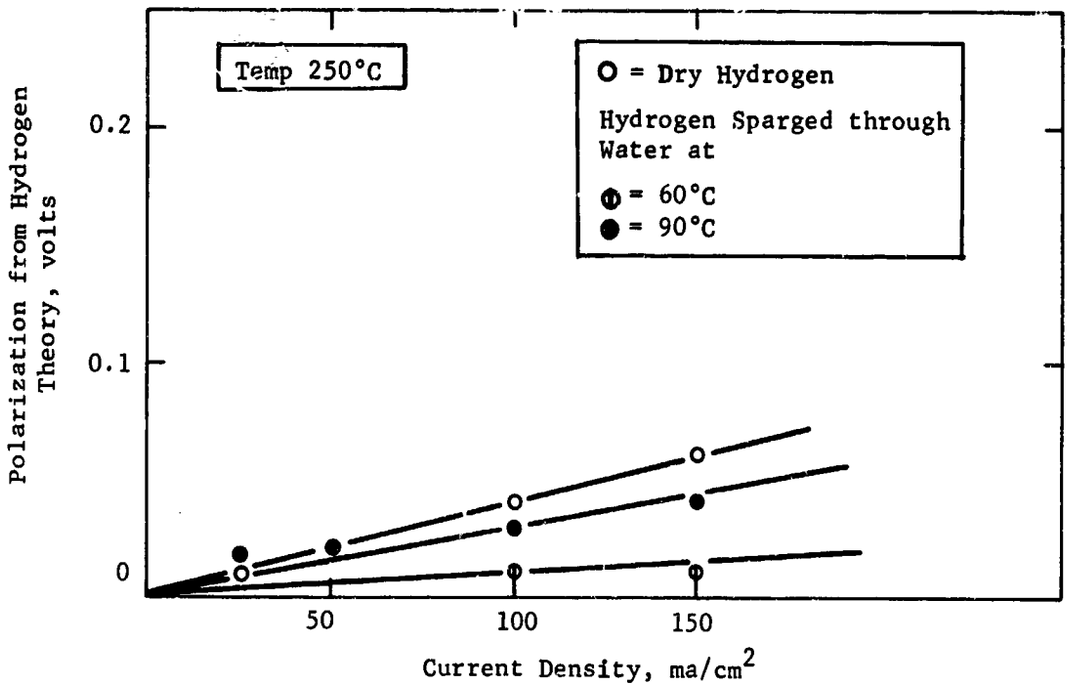

Addition of water apparently has little if any influence on the cathodic buffering capacity.

The ability of this melt to act both as an anodic and cathodic buffer medium would not be expected on the basis of the buffering properties in aqueous solutions of primary phosphate salts such as (KH_2PO_4). An aqueous solution of KH_2PO_4 results from titrating a phosphoric acid solution with potassium hydroxide to its first end point. This is a region of minimum buffering capacity. The existence of ions in the phosphate melt is a sufficient condition for conductance but not for buffering ability. Apparently there exists in the melt acidic and basic ionic components in sufficient quantity and having adequate mobility to confer buffer capacity to the melt.

Part g - Hydrocarbon Activity in
the Mixed Phosphate Melt

Tests of hydrocarbon activity in the phosphate melt were carried out with butane at 250°C. The electrodes were sintered platinum-Teflon structures containing 50 mg/cm^2 of catalyst. Butane was sparged through water at 80°C because previous work in molten pyrophosphoric acid and potassium bisulfate electrolytes showed that humidification was necessary for maximum hydrocarbon activity (7,8). Although the data were scattered, high current densities at reasonable polarizations were obtained. This is shown in Figure D-5, the detailed data given in Appendix D-4.

Figure D-5

Butane Activity in
Mixed Phosphate Melt at 250°C

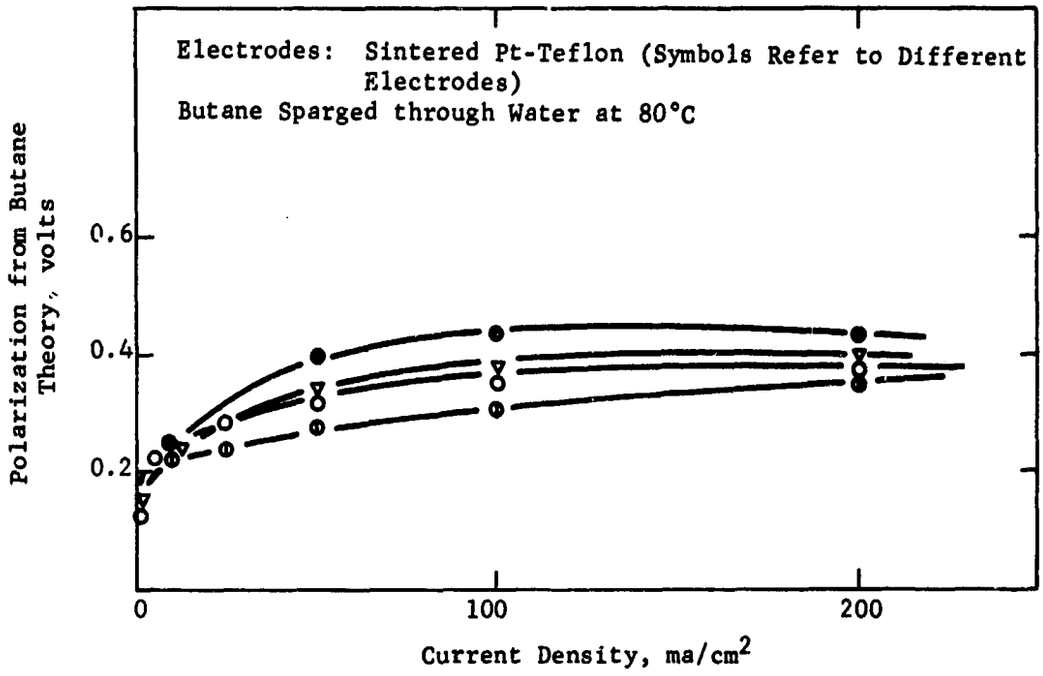

The effect of water addition to the fuel was not investigated in detail. Performance using butane of a lower water content, however, was poorer as shown in Figure D-6. It is probable that the hydrocarbon activity dependence on fuel water content is the same with the phosphate melt as with pyrophosphoric acid and potassium bisulfate melts.

Figure D-6

Poorer Activity Obtained Using
Lower Water Content Butane Feeds

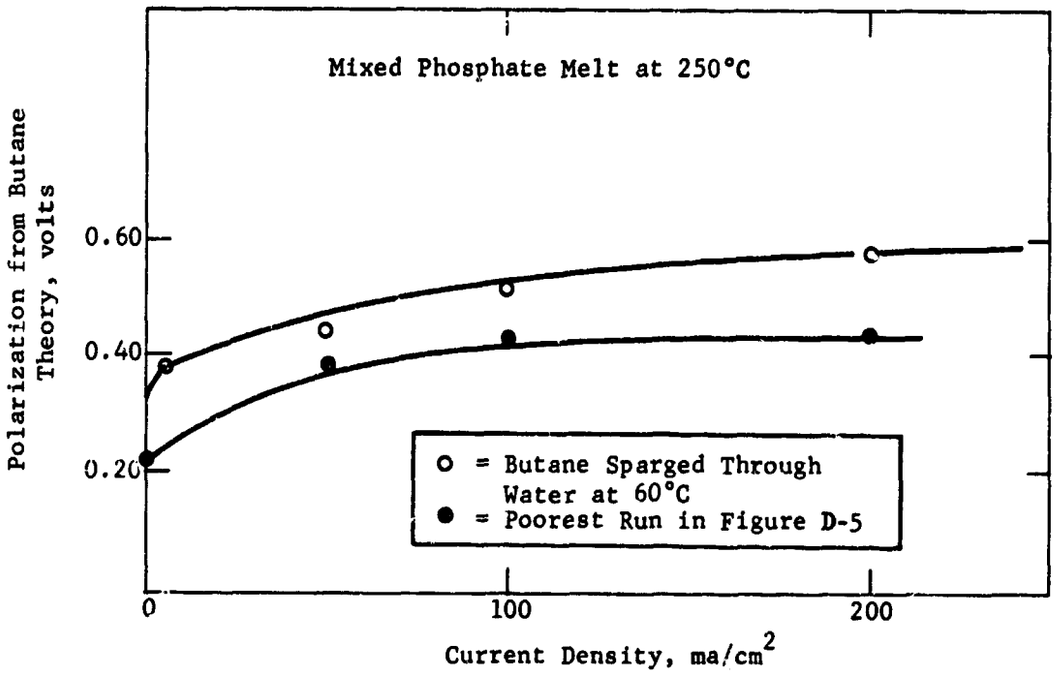

In the butane performance tests where water is added, polarization decreased with increasing current density in the range above 200 ma/cm^2. This may be attributed to the vigorous stirring action of carbon dioxide evolved at these current densities. Due to this evolution, it is possible that the ionic concentration polarization is less with butane above 200 ma/cm^2 than with hydrogen at the same current. Another possible source for the observed polarization decrease could be local heating at the electrode due to the high current density. This improvement at the 200 ma/cm^2 level and beyond was not observed when the fuel was humidified. However, in this case the fuel temperature may have been low and local cooling may have occurred. The inherently lower anodic activity at these conditions may more than compensate improvements due to reduced concentration polarization.

These initial results are very significant in that they demonstrate that saturated hydrocarbons can support high current densities at acceptable polarization in the phosphate melt. This result was not necessarily anticipated. Previous experience has shown that in aqueous electrolytes, saturated hydrocarbons are not appreciably absorbed on platinum catalyst except in low pH solutions. Substantial hydrocarbon activities have been obtained in pyrophosphoric acid and potassium bisulfate melts, but these are strong acid melts. The mixed phosphate melt is not a strong acid melt. Aqueous solutions of the solidified melt have a pH between 4 and 5. It is possible the factors responsible for the low reactivity of saturated hydrocarbons in aqueous media at intermediate and high pH may not be operative in non-aqueous media.

Part h - Oxygen Performance in the Mixed Phosphate Melt

The performance of oxygen in the phosphate melt at 250°C was determined using the sintered platinum-Teflon electrode. Performance runs were carried out with dry oxygen, and with pre-humidified oxygen. The results are shown in Figure D-7, the detailed data given in Appendix D-5.

Figure D-7

Oxygen Performance in the Phosphate Melt

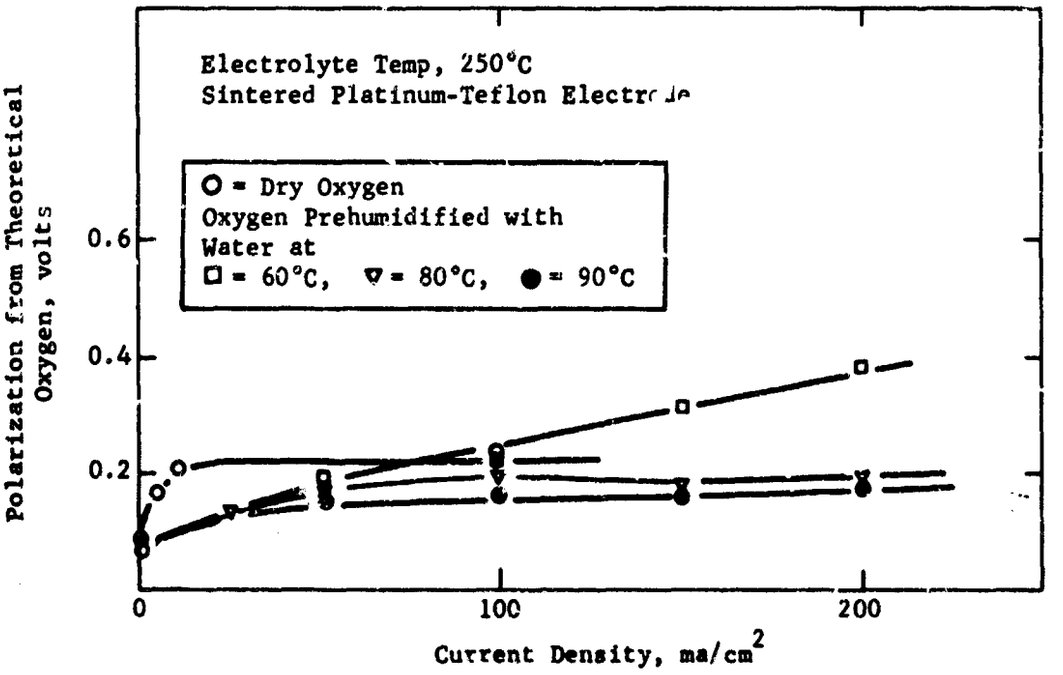

There are two features of the oxygen behavior in the phosphate melt that bear marked resemblance to that exhibited in pyrophosphoric acid. These are the low polarizations at open circuit and under load conditions. The polarizations at 100 ma/cm^2 in the melt are about the same as the open circuit polarizations exhibited at the same electrodes in lower temperature systems such as phosphoric and sulfuric acid. One major difference is that pre-humidification of the oxygen feed increases activity, particularly at the higher current densities. A possible explanation is that water addition increases the oxygen solubility in the melt. In pyrophosphoric acid, pre-humidification of the oxygen feed had no effect on activity.

Part i - Corrosion Properties of
the Mixed Phosphate Melts

Phosphate melts do not appear to have the corrosiveness of pyrophosphoric acid. A tantalum screen in pyrophosphoric acid at 250°C is completely corroded in about ten minutes. By contrast, at temperatures ranging from 250-300°C, a tantalum screen kept in the mixed phosphate melt for four hours did not show any signs of corrosion.

A nickel-cobalt alloy contacting the phosphate melt at 250°C for 4.5 hours under a hydrogen blanket did not corrode. The dissolved melt gave negative tests for nickel and cobalt ion. The alloy did not suffer any loss of electronic conductivity as a result of contact with the melt.

Pyrex glass which leaches quite rapidly when contacted with hot pyrophosphoric acid, is not attacked by the mixed phosphate melt.

This lack of corrosive properties is encouraging, especially when the operating temperature of the electrolyte is considered. Further work will examine the stability of other substrates in this melt.

Phase 2 - Conclusions

Mixed alkali metal phosphate melts are good buffers, are carbon dioxide rejecting and appear to be stable at 250°C. The electrolytic resistivity of the melt is higher than desired, but could be tolerated. Butane activity on massive platinum electrodes in the melt is comparable to that obtained in phosphoric acid at 150°C on the same structure. Oxygen activity on high platinum content electrodes in this medium is substantially higher than that in phosphoric acid provided the oxygen feed stream is prehumidified.

The results obtained using the phosphate melts are similar to what was obtained using pyrophosphoric acid, although activities in the acid are greater. Because they are much less corrosive, phosphate melts are more promising as intermediate temperature fuel cell electrolytes.

SECTION 3

REFERENCES

(1) Heath, C. E., Tarmy, B. L., et al, Soluble Carbonaceous Fuel-Air Fuel Cell, Report No. 1, Contract DA 36-039 SC-89156, 1 Jan 1962 - 30 June 1962.

(2) Tarmy, B. L., et al, Soluble Carbonaceous Fuel-Air Fuel Cell, Report No. 2, Contract DA 36-039 SC-89156, 1 Jan 1962 - 31 Dec 1962.

(3) Tarmy, B. L., et al, Soluble Carbonaceous Fuel-Air Fuel Cell, Report No. 3, Contract DA 36-039 AMC-00134(E), 1 Jan 1963 - 30 June 1963.

(4) Tarmy, B. L., et al, Soluble Carbonaceous Fuel-Air Fuel Cell, Report No. 4, Contract DA 36-039 AMC-00134(E), 1 Jan 1963 - 31 Dec 1963.

(5) Heath, C. E., Holt, E. L., Horowitz, H. H., Levine, D. G., Tarmy, B. L., et al, Hydrocarbon-Air Fuel Cell, Report No. 5, Contract DA 36-039 AMC-03743(E), 1 Jan 1964 - 30 June 1964.

(6) Heath, C. E., Holt, E. L., Horowitz, H. H., Levine, D. G., Tarmy, B. L., et al, Hydrocarbon-Air Fuel Cell, Report No. 6, Contract DA 36-039 AMC-03743(E), 1 July 1964 - 31 Dec 1964.

(7) Epperly, W. R., Holt, E. L., Horowitz, H. H., Levine, D. G., et al, Hydrocarbon-Air Fuel Cell, Report No. 7, Contract DA 36-039 AMC-03743(E), 1 Jan 1965 - 30 June 1965.

(8) Heath, C. E., et al, Hydrocarbon-Air Fuel Cell, Report No. 8, Contract No. DA 36-039 AMC-03743(E), 1 July 1965 - 31 Dec 1965.

(9) Giner, J., Electrochimica Acta 8,857 (1963).

(10) Anderson, S., Wadsley, A. D., Acta Cryst. 15, 201 (1962).

(11) Wadsley, A. D., in Chapter 3 of Non-Stoichiometric Compounds, Madelcorn, L., Ed., Academic Press, 1964.

(12) Sienko, M. J., J. Am. Chem. Soc. 81, 5556 (1959).

(13) Sienko, M. J., Chapter 21 in Non-Stoichiometric Compounds, Advances in Chemistry, Series No. 39, American Chemical Society, 1963.

(14) Shanks, H. R., Sidles, P. H., Danielson, G. C., loc. cit., Chapter 22.

(15) ASTM X-ray cards 5-0386 and 5-0387.

(16) ASTM X-ray cards 5-0392 and 5-0393.

(17) Gebert, E., Ackermann, R. J., Inorganic Chemistry 5,136 (1966).

(18) Keeling, R. O., Jr., Acta Cryst 10,209 (1957).

(19) Ribnick, A. S., Post, B., Banks, E., Chapter 23 in Non-Stoichiometric Compounds, loc. cit.

(20) Wadsley, A. D., Reviews of Pure and Applied Chemistry 5, 165 (1955).

(21) Glemser, O., Naumann, C., Z. anorg. allgem. chem. 265, 288 (1951).

(22) Benson, J. E., Kohn, H. W., Boudart, M., J. Catalysis 5, 307 (1966).

(23) Niedrach, L. W., Weinstock, I. B., J. Electrochem. Tech. 3, 270 (1965).

(24) Pourbaix, M., Atlas d'Equilibres Electrochimiques, Gauthier-Villars and Co., Paris, 1963.

(25) Hagg, G., Z. Physik. Chem. B 29, 192 (1935).

(26) Ornatskala, Z. I., Zhur. Tekhn. Fiz. 27, 130 (1957).

(27) Brown, B. W., Banks, E., Phys. Rev. 84, 609 (1951).

(28) Ostertag, W., Rare Earth Tungsten Bronzes, Air Force Materials Laboratory Report No. AFML-TR-65-120, July, 1965.

(29) Ostertag, W., Inorganic Chemistry 5,758 (1966).

(30) Shropshire, J. A., Horowitz, H. H., J. Electrochem. Soc. 113, 490 (1966).

(31) Weininger, J. L., Breiter, M. W., J. Electrochem., Soc. 111,707 (1964).

(32) Past, W. E., Jofa, S. A., Zhur. Fiz. Khim. 33, 1230 (1959).

(33) Bond, G. C., Catalysis by Metals, Academic Press, 1962.

(34) Gileadi, E., J. Electroanal. Chem. 11, 137 (1966).

(35) Shropshire, J. A., J. Electrochem. Soc. 112, 465 (1965).

(36) Gileadi, E., Rubin, B. T., Bockris, J. O'M., J. Phys. Chem. 69, 3335 (1965).

(37) Langer, S. H., Landi, H. P., J. Am. Chem. Soc. 85,3043 (1963).

(38) Wood, B. J., Wise, H., J. Catalysis 5, 135 (1966).

(39) Hume-Rothery, W., Atomic Theory for Students of Metallurgy, Institute of Metals, 1960.

(40) Vol'kenshtein, F. F., The Electronic Theory of Catalysis on Semi Conductors, MacMillan Co., New York, 1963.

(41) Vol'kenshtein, F. F., Kinetica i Kataliz 1, 32 (1960).

(42) Vol'kenshtein, F. F., Peshev, O., Kinetica i Kataliz 6, 95 (1965).

(43) Bozworth, R. M., Ferromagnetism, D. Van Nostram Co., Inc., (1953).

(44) Lyabarskii, G. D., Evzerithin, E. I., Slinkin, A. A., Kinetica i Kataliz 5,311 (1964).

(45) Lybarskii, G. D., et al, Kinetica i Kataliz 1,385 (1960).

(46) Dubinin, M. M., Zaverina, E. D., Dokl. Akad. Navk SSSR 84,93 (1952).

(47) Brown, E. H., Whitt, C. D., Ind. Eng. Chem. 44,615 (1952).

(48) Young, G. J., Fuel Cells, Reinhold, New York, (1960), p. 82.

(49) Broers, G. H. J., "High Temperature Galvanic Fuel Cells," Ph.D. Thesis, University of Amsterdam, 1958.

(50) Walrafen, G. E., J. Chem. Phys. 37,662, 1962.

(51) Broers, G. H. J., Schenke, M., in Hydrocarbon Fuel Cell Technology, Academic Press, New York (1965).

(52) Van Wazer, J. R., Phosphorus and its Compounds I, 780 Interscience Publishers, New York.

(53) Elving, P. J., Spritzer, M., Talanta 12,1243 (1965).

(54) Ives, D., Reference Electrodes-Theory and Practice, (Janz, G. Ed.), Academic Press, New York, (1961).

(55) Audrieth, L. F., Kleinberg, J., Non-Aqueous Solvents, Chapter 14, John Wiley and Sons Inc., New York, 1952.

(56) Kriedl, N. J., Weyl, W. A., J. Am. Ceram. Soc. 24,372 (1941).

(57) Milazzo, G., Electrochemistry, p. 92, Elsevier Publishing Co., 1963.

(58) Brown, C. A., Brown H. C., J. Am. Chem. Soc. 84,2829 (1962).

(59) Kuo, K., J. Of Metals (Trans AIME) 5,745 (1953).

(60) Kiessling, R., J. Of Metals (Trans AIME) 5,745 (1953).

(61) Rautala, P., Norton, J. T., J. Of Metals 4,1045 (1952).

(62) Kuo, K., Acta Metallurgica 1,611 (1953).

(63) Sachs, K., Nature 169,411 (1952).

(64) Borusevick, L. K., Gradyshevskii, E. I., Deforov, T. F., Popova, N. M., Zh. Strukt. Khim. 6,313 (1965).

(65) Kuo, K., Acta Metallurgica 1,301 (1953).

(66) Reiffenstein, E., Nowotny, H., Benesvosky, F., Monasch Chemie 96,1543 (1965).

(67) Kiessling, R., Symposium on Reactivity of Solids, Gothenberg, 1954, p. 1065.

(68) Arkharov, V. J., Kiselev, S. T., Izvest Akad Nauk SSSR Otdelenie Tekniceskikh Nauk 136 (1949) Structure Reports 12 p. 47.

APPENDIX A-1

ADSORPTION OF IODIDE AND BUTANE ON PLATINUM

For these experiments a flag electrode covered with powdered platinum black was used. The electrolyte was 3.7 M sulfuric acid; the temperature was 80°C. For iodide adsorptions the electrode was submerged in the electrolyte. For butane adsorptions the electrode was held in the butane gas phase with its lower edge just touching the electrolyte. All voltage scans were carried out with the electrode totally submerged. Table A-1 shows the growth of the iodine oxidation peak and the decrease in hydrogen peaks as iodine was adsorbed at open circuit under nitrogen. Scans were run from -0.10 volts to +1.35 volts versus S.C.E. after adsorption of iodide, and were repeated until the iodide wave was no longer apparent. Fresh electrolyte was used for each run and 0.25 cc of .01 M KI was added.

Table A-1

Iodide Adsorptions

Adsorption Time, min	Q_H, Coulombs(1) No I	With I	Difference	Q_o(1) Coulombs	Q_I(1) Coulombs	$Q_I/\Delta Q_H$
30	716.5	584.5	133	1857	419	3.15
60	721	546.5	174.5	1809	557	3.20
90(2)	712.5	595	117.5	1834	423	3.60
120	728	486.5	242	1852.5	752	3.11

(1) Q_H = integrated coulombs in both hydrogen peaks; Q_o = coulombs in oxide reduction peak; Q_I = coulombs in iodine oxidation peak.

(2) Q_H with iodine, ΔQ_H, Q_I and $Q_I/\Delta H$ all seem to be out line with other values for this run.

In a second series of runs 0.25 cc of .01 M KI was added to the electrolyte and was allowed to adsorb for one to two hours. Butane adsorptions were carried out for varying periods of time at +0.05 volts versus S.C.E. Butane scans were run from +0.05 to +0.95 volts versus S.C.E. to avoid butane desorption at lower potentials and iodine oxidation at higher potentials. In one series of runs scans were run from -0.10 to +0.95 volts from S.C.E. to measure hydrogen coverage between butane adsorptions. Finally at the end of each series a full scan was run from -0.10 to +1.35 volts versus S.C.E. to determine the iodine coverage and, following its removal, the total hydrogen coverage. Table A-2 presents this data along with coverage values calculated from the data and parameters related to the shape of the oxidation wave.

Table A-2

Butane Adsorption and Oxidation in Presence and Absence of Adsorbed Iodine

cc .01 M KI Added	Butane Adsorption Time, min	Butane Adsorbed, Coulombs	Oxide Red'n Coulombs	Iodine Oxid'n Coulombs	Pt H Coulombs	Fraction Pt Sites Available(1)	Butane Coverage Uncorr.	Butane Coverage Corr.(2)	Potential Max I volts vs S.C.E.	Max I, ma Uncorr.	Max I, ma Corr.(2)	I at 0.45 v vs S.C.E. Uncorr.	I at 0.45 v vs S.C.E. Corr.(2)
0	1	917	2021	0	--	1.00	0.322	0.322	0.419	87	87	85	85
0	5	2123	1973	0	--	1.00	0.747	0.747	0.469	163	163	160	160
0	30	2845(5)	2068	0	--	1.00	1.000	1.000	0.544	227	227	150	150
0.25	1	1771			--	0.671	0.623	0.93	0.581	142	212	80	119
0.25	5	1481			--	0.671	0.521	0.78	0.496	113	164	104	155
0.25	5	1455	2029	753	--	0.671	0.511	0.76	0.496	107	160	100	149
0.25	15	1834			--	0.671	0.645	0.96	0.551	142	212	95	142
0.25	30	1852			--	0.671	0.651	0.97	0.586	154	230	74	110
0.25	0	0			447(3)	0.538	0	0	--	0	0	0	0
0.25	1	1495			385	0.538	0.525	0.976	0.577	125	232	62	115
0.25	5	1214	2005	1058	388	0.538	0.427	0.79	0.509	90	167	82	152
0.25	15	1385			385	0.538	0.487	0.905	0.564	111	206	68	126
0.25	30	1449			378	0.538	0.509	0.945	0.586	122	227	58	108
0	0	0	--	--	712(4)	--	--	--	--	--	--	--	--

(1) Calculated as 1 - Iodide Peak/3.18/720 (3.18 = avg value of $Q_I/\Delta Q_H$; 720 = avg value of $Q_{..}$ from Table A-1 and below).
(2) Obtained by dividing uncorrected value by fraction of sites available for butane adsorption.
(3) Note that after initial value Pt H coverage is constant, indicating that no more iodine is adsorbing. Average value of $Q_I/\Delta Q_H$ from these numbers is 3.18, agreeing with Table A-1.
(4) Taken at end of experiment, in agreement with Table A-1.
(5) Considered to be saturation butane coverage.

APPENDIX A-2

BUTANE ADSORPTION ON IODIDE TREATED FLAG ELECTRODE

3.7 M H_2SO_4, 80°C

cc .01 M KI Added	Butane Ads Time, min(1)	Millicoulombs in Butane Peak(2)
0	0.5	1392, 400
0	1.0	1190, 545
0	2	912, 859
0	5	1614, 1478
0	15	2475, 2404
0	30	2774
0.30(3)	0.5	357
0.30	1.0	556, 492
0.30	2.0	753, 802, 753
0.30	5	1364, 1350
0.30	15	2087
0.30	30	2398

(1) Electrode in vapor phase, bottom touching electrolyte during adsorption.

(2) Determined by integration of voltage scan from 0.05 to 0.95 volts versus S.C.E. 31.1 sec/1/2 cycle, electrode totally submerged. Replicate runs. Note irreproducibility of first two points. High values are off curve.

(3) Iodide coverage very low, 6%, for unexplained reason. Scan from -0.12 to +1.33 volts versus S.C.E., 50 sec/1/2 cycle,yields: total H peaks 698 mc, 0 peaks 2060 mc, I^- peak = 130 mc,I coverage = 130 ÷ 3.18/698 = 5.9%.

APPENDIX A-3

BUTANE ADSORPTIONS IN FLOWING ELECTROLYTE UNIT

Comparative adsorption rate measurements were made simply by flowing butane or argon saturated electrolyte, 3.7 M H_2SO_4 at 80°C, through the catalyst and running continuous scans. For unknown reasons, the scan shape varied with the flow rate as well as the nature of the gas. Base lines for measurement of fuel peaks were hard to establish. Therefore, measurements were made under varying flow conditions and scan lengths, and the entire anodic and cathodic coulombs were measured as shown in Table A-3. From some of these values, relative rates of butane adsorption were obtained by difference as shown in Table A-4.

Table A-3

Flowing Electrolyte System Measurements

3.7 M H_2SO_4, 80°C, Sintered Au Disk

Gas	Flow Rate(1)	Q Anodic - Q Cathodic, m.c. Long Scan(2)	Q Anodic - Q Cathodic, m.c. Short Scan(3)
Argon	0	-36	-45
	Grav.	236	47
	Max.	353	123
Butane	0	27,40	--
	Max.	1080	910,892
Butane + KI (I)	0	--	98
	Max.	--	407
Butane + KI (II)	0	--	122
	Max.	--	476

(1) Grav. (gravity) flow, approx. 10 cc per min. Maximum flow achieved by sucking with circulating Mace pump estimated at 15 to 20 cc/min.

(2) 0.05 to 1.3 volts versus S.C.E.

(3) 0.05 to 0.9 volts versus S.C.E.

Table A-4

Calculated Relative Adsorption Rates

	Control Run	Run I	Run II
Corrected Butane Peak, mc(1)	775	284	353
Iodide Peak, mc	0	1130	675
Oxide Peak, mc	1372	1372	1445
Calc. Total H, mc (Oxide x 0.355)	488	488	513
Calc. ΔH, mc Iodide $\div$ 3.18	0	356	213
Fraction Sites Uncovered by I	1.0	0.27	0.59
Relative Butane Adsorption Rate	1.0	0.37	0.47

(1) Taken from short scan values at maximum flow rates, correcting for argon blank under same conditions.

APPENDIX B-1

PREPARATION OF TRANSITION AND POST-TRANSITION METAL TUNGSTEN BRONZES

Stoichiometric Composition of Mix	Components of Mix	Preparation Conditions, N.B. Ref.	Characterization of Products
$In_{0.2}WO_3$	In_2O_3, W WO_3	4239-50-2 Fired in an evacuated quartz tube at 982°C in a Leco furnace.	Highly conductive blue pellets impure cubic structure with a = 10.1 A possible.
$Ti_{0.2}WO_3$	Ti_2, W, WO_3	4239-37 As above.	Highly conductive blue pellets.
$Mn_{0.2}WO_3$	MnO_2, W, WO_3	4239-41 As above.	As above.
$Fe_{0.2}WO_3$	Fe_2O_3, W, WO_3	4239-20 As above.	As above.
$Co_{0.2}WO_3$	CoO, W, WO_3	4239-31	As above.
$Zn_{0.2}WO_3$	ZnO, W, WO_3	4239-32 As above.	Highly conductive blue pellet.
$Zr_{0.2}WO_3$	ZrO_2, W, WO_3	4239-39 As above.	As above.
$Nb_{0.2}WO_3$	Nb_2O_5, W, WO_3	4239-42 As above.	As above. There is possible impure cubic structure with a = 10.4 Å
$Mo_{0.2}WO_3$	MoO_2, W, WO_3	4239-40 As above	Purple pellets, highly conductive
$Sn_{0.2}WO_3$	SnO_2, W, WO_3	4239-38	Highly conductive blue pellets

APPENDIX B-1 (CONT'D)

PREPARATION OF TRANSITION AND POST-TRANSITION METAL TUNGSTEN BRONZES

Stoichiometric Composition of Mix	Components of Mix	Preparation Conditions, N.B. Ref.	Characterization of Products
$Hg_{0.2}WO_3$	HgO, W, WO_3	4239-12 Fired in an evacuated quartz tube at 600°C for 24 hours.	No reaction occurred.
$Tl_{0.2}WO_3$	Tl_2O_3, W, WO_3	4239-16 Fired in an evacuated quartz tube in the Leco furnace at 982°C for 24 hours.	Bronze structure formed a = 3.65 Å c = 6.4 Å
$Tl_{0.2}WO_3$	Tl_2O_3, W, WO_2	4239-16 As above.	As above.
$Tl_{0.35}WO_3$	Tl_2O_3, W, WO_3	4239-30 As above.	As above.
$Bi_{0.2}WO_3$	Bi_2O_3, W, WO_3	4239-19 As above.	Black pellet with unreacted starting materials also present.
$Mn_{0.2}WO_3$	Mn, WO_3	4239-47 As above.	Highly conductive blue pellet X-ray the same as product from MnO_2, W, WO_3

APPENDIX B-2

SOME RESULTS ON TRANSITION AND POST TRANSITION METAL TUNGSTEN BRONZES AS CATHODES

$Tl_{0.2}WO_3$ O_2 as Fuel NB 4349-18

Volts Polarized Vs Standard Oxygen Potential	ma/cm^2
0.640	0.0 (open circuit)
0.895	1.0
0.935	3.0
0.995	6.0
1.00	1.0
1.04	2.0
1.08	4.0
0.685	0
0.895	1.0
0.937	3.0
0.995	6.0
1.00	10.0
1.04	2.0
1.08	4.0

The change in open circuit indicates that the reactions occurring caused a change in the electrode. Oxidation is suspected.

APPENDIX B-3

X-RAY CRYSTALLOGRAPHY LINES FOR TUNGSTEN OXIDES AND NICKEL TUNGSTEN BRONZES

Material	$Ni_{0.2}WO_3$ From NiO W and WO_3 not Active as a Catalyst	$Ni_{0.237}WO_3$ From NiO,W and WO_3 an Active Catalyst	$Ni_{0.2}WO_3$ From Ni,W and WO_3 an Inactive Catalyst but a cubic structure	$WO_{2.96}$	$NiWO_4$ Prepared From Ni_2O_3, Wl and WO_3	$WO_{2.73}$	$WO_{2.9}$
X-ray	12.5	12.8	12.8			12.9	
Lines	9.2						
Found	8.3	8.35	8.6			8.27	
ld Spacings	6.65	6.55				6.54	
	6.15	6.15	6.2			6.11	
	5.70	5.70	5.7		5.72		
	5.20	5.25				5.22	
	4.58	4.62	4.63		4.63	4.39	
	4.40	4.45		4.47		4.54	4.28
						4.43	
	3.91	3.91		3.86		4.37	3.89
	3.82	3.81	3.82	3.82			
	3.76	3.74	3.75	3.76	3.73	3.78	3.77
	3.64	3.66	3.66	3.65		3.73	3.70
						3.63	
	3.57	3.58	3.58	3.49	3.59	3.48	3.64
			3.49			3.44	
			3.31	3.33		3.39	
	3.27	3.26	3.26			3.31	
						3.25	
	3.17	3.18	3.18	3.20		3.17	
				3.10			
	3.07	3.06		3.07		3.05	
	3.03	3.03				3.02	
	2.94	2.95				2.958	
						2.937	
	2.92	2.92		2.91		2.91	
	2.88	2.89	2.895		2.90		
	2.825	2.835	2.84	2.85	2.845	2.87	2.82
				2.77		2.80	
	2.74	2.76	2.73	2.72		2.76	2.73
	2.655	2.66	2.70*				2.71
				2.67		2.65	
	2.62	2.63	2.63	2.64			2.64
	2.528	2.535	2.535	2.58			
	2.455	2.46	2.46	2.50	2.465	2.46	
	2.44	2.435		2.43	2.42	2.42	
	2.42	2.418	2.418				
	2.31	2.315	2.315	2.29	2.307		
			2.213				

APPENDIX B-3 (CONT'D)

Material	$Ni_{0.2}WO_3$ From Ni0 W and WO_3 not Active as a Catalyst	$Ni_{0.237}WO_3$ From NiO,W and WO_3 an Active Catalyst	$Ni_{0.2}WO_3$ From Ni,W and WO_3 an Inactive Catalyst but a cubic structure	$WO_{2.96}$	$NiWO_4$ Prepared From Ni_2O_3, Wl and WO_3	$WO_{2.73}$	$WO_{2.9}$
	2.22	2.23	2.20*	2.22	2.258		2.71
	2.165	2.17	2.17	2.19	2.17		
	2.075	2.075		2.14	2.134		
	2.023	2.025	2.025		2.025		
	2.01	2.01		2.01			
	1.958	1.96					
				1.98			
	1.90	1.925	1.92	1.96	1.96		1.96
	1.89	1.893	1.895*		1.893		1.898
	1.868	1.87					1.884
	1.86	1.858	1.818	1.833			
	1.775	1.78	1.78	1.802			
	1.745	1.748	1.752		1.767		1.741
	1.70	1.708	1.708*	1.719	1.747		
				1.714	1.723		1.720
	1.678	1.68	lines with		1.681		
	1.652	1.655	Asterick Fita	1.700		1.700	
				1.679			
	1.635	1.638	Cubic	1.6649			
				1.62			

APPENDIX B-4

HYDROGEN ACTIVITY OF NICKEL TUNGSTEN BRONZES

(Sintered Teflon Emulsion Electrode, 200 mg Catalyst/cm^2)
3.7 M H_2SO_4 90°C. - 5 cm^2 Electrode

Sample No.	Preparative Procedure	Gas	ma	Volts Polarized From Hydrogen
1	$Ni_{0.237}WO_3$ prepared from N, O, W, and WO_3 by heating at 800°C. for 72 hrs.	N_2	-0.4	0.14
		H_2	+1.4	0.14
		H_2	1.9	0.34
		H_2	2.0	0.54
		H_2	2.15	0.74
		H_2	4.0	0.94
		N_2	.05	0.94
2	Prepared and tested as Sample 1.	N_2	0.03	0.94
		H_2	1.0	0.94
3	Prepared by sintering at 975°C. for 144 hrs. Same test conditions.	N_2	0.03	0.94
		H_2	1.0	0.94
4	Prepared and studied as Sample 1.	N_2	0.00	0.4
		H_2	1.25	0.4
		N_2	0.02	0.94
		H_2	1.5	0.94
		O_2(1)	0.9	0.4
		O_2	0.0	0.8
4A	Same as 4 but a different electrode.	N_2	0.04	0.4
		H_2	0.04	0.4
		N_2	0.02	0.94
		H_2	1.0	0.94
5	Prepared and studied in the same way as Sample 1.	N_2	-0.05	0.34
		H_2	+19.0	0.34
		N_2	+0.03	0.54
		H_2	23.0	0.54

(1) From theoretical O_2.

APPENDIX B-5

NICKEL TUNGSTEN BRONZE PREPARATIONS

Stoichiometric Composition of Mix	Components of Mix	Preparation Conditions	Notebook Reference	Characterization of Product	Catalytic Activity	Notebook Reference	Other Information
$Ni_{0.2}WO_3$	NiO, W, WO_3	Heated in Leco at 982°C in an evacuated quartz tube pellets were wrapped in Pt foil	4239-26	3 pellets were formed. A blue had a sp. cond. of 0.69 mho/cm, a purple with sp. cond. of 33 mho/cm and a black pellet sp. cond. > 100.	None showed any electrochemical activity. Black pellet was 70 mv polarized at open circuit, others had higher polarization.	4239-22,24,25	No hydrogenation activity was found in Brown[2] hydrogenator 3346-A11-1. No cubic structure found by X-ray.
$Ni_{0.2}WO_3$	Ni, WO_3	As above.	4239-44-1	Specific conductance > 10 mho/cm	No activity	4349-A33	No hydrogenation in Brown[2] hydrogenator. Notebook 4870-12.
$Ni_{0.2}WO_3$	Ni_2O_3, W, WO_3	As above but without wrapping in platinum foil.	4239-44-4-1	Blue pellets of high conductivity.	Insufficient sample		A cubic structure may be present.
Ni, WO_3	Ni, WO_3	Fired in a muffle furnace in an evacuated quartz tube at 800°C for 72 hours then fired in the Leco at 982°C for 24 hours.	4239-45-3	Blue pellets of high conductivity	Activity on hydrogen	660224-1	No hydrogenation activity.
Ni, WO_3	Ni, WO_3	Fired in the Leco furnace at 982°C in an evacuated quartz tube.	4239-47-5A	Blue pellets of high conductivity	Activity on hydrogen	4349-A45	No hydrogenation activity.
$Ni_{0.4}WO_3$	Ni, WO_3	As above	4239-47-4A	Blue pellets of high conductivity	No activity, considerable corrosion	4870-24-26	No hydrogenation activity.
$Ni_{0.237}WO_3$	NiO, W, WO_3	Fired in a muffle furnace in an evacuated quartz tube at 800°C for 70 hours.	4239-43-19-1	Blue pellets of high conductivity	Activity on hydrogen, perhaps on ethylene	3346-A11 and 13,4870-48,49	No hydrogenation activity.
$Ni_{0.237}WO_3$	NiO, W, WO_3	Fired at 800°C in an evacuated quartz tube in a muffle furnace.	660091-21-1	Blue pellets of high conductivity	Activity on hydrogen	3346-A19	
$Ni_{0.237}WO_3$	NiO, W, WO_3	Fired at 982°C in an evacuated quartz tube in the Leco furnace.	660091-21-2	Blue pellets of high conductivity	Activity on hydrogen	3346-A24	
$Ni_{0.237}WO_3$	NiO, W, WO_3	Fired at 800°C in an evacuated quartz tube for 72 hours. Reactants were ground together before firing.	660091-23	Blue pellets of high conductivity	Activity on hydrogen	3346-A30	
$Ni_{0.237}WO_3$	NiO, W, WO_3	As above but reactants were not ground together before firing.	660091-35	Blue Pellets of high conductivity	Activity on hydrogen	66-0224-5	

APPENDIX B-6

REPORTED ETA CARBIDES

Compound	Lattice Constant, a (Å)	Ref
Mn_3W_3C	11.14	49
Mn_3Mo_3C	1..13	59
Cr_3Nb_3C	11.49	59
V_3Zr_3C	12.12	59
$(CrFe)_3Ta_3C$	11.40	59
$(CrCo)_3Ta_3C$	11.40	59
$(CrNi)_3Ta_3C$	11.40	59
Co_2W_4C	11.210	60
Co_3W_3C	10.96	61
$Co_2W_4C(Co_3W_6C_2)$	11.25	61
$Ni_2(TiTa)_4C$	11.52	62
$Co_2(TiTa)_4C$	11.51	62
$Ni_2(TiNb)_4C$	11.58	62
Co_3Nb_3C	11.633	64
Co_3Ta_3C	11.63	64
V_3Zr_3C	12.12	65
Cr_3Nb_3C	11.49	65
Mn_3Mo_3C	11.13	65
Mn_3W_3C	11.05	65
Fe_2Mo_4C	11.26	65

APPENDIX B-6 (CONTINUED)

Compound	Lattice Constant, a (Å)	Ref
Co_2Mo_4C	11.25	65
Ni_2Mo_4C	11.25	65
$(CrFe)_3Ta_3C$	11.40	65
$(CrCo)_3Ta_3C$	11.40	65
$(CrNi)_3Ta_3C$	11.35-11.44	65
$(CrCu)_3Ta_3C$	11.52	65
$(VFe)_3Ta_3C$	11.54	65
$(V\ Co)_3Ta_3C$	11.56	65
$(VNi)_3Ta_3C$	11.56	65
$(VNi)_3Nb_3C$	11.50	65
VAl_2Nb_3C	11.7	66
VAl_2Ta_3C	11.6	66
$CrAl_2Nb_3C$	11.7	66
$CrAl_2Ta_3C$	11.6	66
$MnAl_2Nb_3C$	11.6_9	66
$MnAl_2Ta_3C$	11.6_1	66
$FeAl_2Nb_3C$	11.6_3	66
$FeAl_2Ta_3C$	11.5_7	66
$CoAl_2Ta_3C$	11.6_2	66
$CoAl_2Nb_3C$	11.5_6	66
$NiAl_2Nb_3C$	11.64, 11.50	66
$NiAl_2Ta_3C$	11.59, 11.45	66

APPENDIX B-6 (CONTINUED)

Compound	Lattice Constant, a (Å)	Ref
$CuAl_2Nb_3C$	11.69, 11.55	66
$CuAl_2Ta_3C$	11.66, 11.51	66
$ZnAl_2Nb_3C$	11.6_3	66
Co_3W_3C	11.090	67
Co_2W_4C	11.210	67
$(Ni_{0.58}Co_{0.30}Si_{0.12})_3$ $(Mo_{0.49}W_{0.07}Cr_{0.44})_3C_{0.95}N_{0.5}$	10.95	63
Fe_3W_3C	10.63	68

APPENDIX B-7

PREPARATION OF ETA PHASE CARBIDES

Item No.	Compound Desired	Notebook Reference	Firing Composition	Firing Conditions	Compound Obtained	Catalysis Tests	Notebook Reference	Other
1	Ni_3W_3C	4239-21	Ni, W, C	Quartz tube furnace to max power obtainable for a short period.	WC	None		Distilled Ni?
2	Mn_3W_3C	4239-22	Mn, W, C	Quartz tube furnace heated till a metal mirror formed.	Not known, but no eta phase.	None		Distilled Mn?
3	Ni_3W_3C	4239-18-5	Ni, W, C	Quartz tube furnace, temperature could not be monitored.	W, WC	Galvanostatic showed activity. No hydrogenation activity.	4349-29 4870-44	--
4	$Ni_{1.5}Cr_{1.5}Ta_3C$	4239-18-6	Ni, Cr, Ta, C	Quartz tube furnace temperature could not be monitored.	TaC, $(NiCr)_2Ta_6C_4$ is possible	None		
5	Ni_3W_3C	4239-18-4	Ni, W, C	4 weeks in an evacuated quartz tube in muffle at 825°C.	WC Ni_3W_3C $Ni_3W_6C_4$ Ni_3W_3C WC Ni_2W_4C	Galvanostat showed no activity in acid. In KOH some activity was found. No hydrogenation activity. Potentiostat showed activity.	4349-48 4349-50 4870-4 4870-15	
Sample was heated in 30% H_2SO_4 for 3 hours, nickel came off 4239-43-16.								
6	$Cr_{1.5}Co_{1.5}Ta_3C$	4239-43-17	Cr, Co, Ta, C	Quartz tube furnace for 1 hr. at ~1200°C	TaC	No hydrogenation activity.	660091-38	
7	Mn_3W_3C	4239-43-18	Mn, W, C	Quartz tube furnace 1 hr. at ~1200°C	Mn_2W_4C + W Mn_3W_3C Lattice constant 11.20 Å	Galvanostatic testing of acid washed sample high corrosion current. Mn found in electrolyte as major in acid. Potentiostat - no activity.	4349-41 4870-23	No hydrogenation activity 4870-43
Sample was acid washed for 3 hrs. in 30% H_2SO_4, Mn came off.								
8	Mn_3W_3C	4239-46-1	Mn, W, C	Quartz tube furnace 1 hr. at ~1200°C, 50-100 μ.	Mn_2W_4C + W Mn_3W_3C Lattice constant 11.20Å	No activity in acid. No hydrogenation activity. Potentiostat - no activity.	4349-49 4870-5 4870-20	
Sample was acid washed for 3 hrs. in 30% H_2SO_4 at 100°C, Mn came off.								
9	Mn_3Mo_3C	4239-46-2	Mn, Mo, C	Quartz tube furnace, 1 hr. at ~1200°C, 50-100 μ	Mn_3Mo_3C Mn_3Mo_3C or Mn_2W_4C Some Mo_2C	Potentiostat showed no activity. No hydrogenation activity.	4870-30 3346-A252	
Washed in 30% H_2SO_4 for 3 hrs. at 100°C								
10	Mn_4W_3C	4239-46-3	Mn, W, C	Quartz tube furnace, 1 hr. at ~1200°C	Mn_2W_4C Phase " Lattice constant 11.2 Å W	Galvanostat showed corrosion current Potentiostat showed no activity.	3346-A3 4870-27	
Washed in 30% H_2SO_4 for 3 hours at 100°C								
11	Mn_3Ta_3C	4239-48-1	Mn, Ta, C	Quartz tube furnace, 1 hr. at ~1200°C.	TaC Some unknown.	No hydrogenation.	660091-38	
12	Mn_3Nb_3C	4239-48-2	Mn, Nb_2O_5C	Quartz tube furnace, 1 hr. at ~1200°C, 50-150 μ	Cubic Phase a = 14.6 Å " but no eta phase.	Potentiostat showed no activity. No hydrogenation activity.	4870-42	
Washed in 30% H_2SO_4 for 3 hours at 100°C								
13	Mn_3Nb_3C	4239-48-4	Mn, Nb, C	Water cooled bell jar, 1 hr. at 1260°C	NbC No η phase.			
Washed in 30% H_2SO_4 for 6 hours at 100°C								
14	Mn_3Zr_3C	4239-48-3	Mn, ZrO_2, C	Water cooled bell jar, 75 min at 1200°C at less than 10^{-4} torr.	Unreacted ZrO_2	No hydrogenation	4870-43 3346-A-16	
Washed in 30% H_2SO_4								
15	Mn_3W_3C	4239-49-1	Mn, W, C	4 week sinter in muffle furnace in an evacuated quartz tube	Mn_3W_3C Lattice constant 11.21 A, W metal	No hydrogenation activity	660091-A38	
16	Mn_2W_4C	4239-49-2	Mn, W, C	Water cooled bell jar, 50 min, 1320°C, 50-200 μ	No η phase W metal			
Washed in 30% H_2SO_4 for 6 hours at 100°C								
17	$Ni_{1.5}Mn_{1.5}Ta_3C$	4239-49-4	Ni, Mn, TaC	Fired in water cooled bell jar until Mn vapor came off profusely.	Ta_2C	No hydrogenation activity	60091-38	

APPENDIX B-7 (CONT'D)

PREPARATION OF ETA PHASE CARBIDES

Item No.	Compound Desired	Notebook Reference	Firing Composition	Firing Conditions	Compound Obtained	Catalysis Tests	Notebook Reference	Other
18	Ni_3W_3C	4239-49-5	Ni, W, C	Water cooled bell jar, 40 min at max temp of 1480°C at 100 μ	Ni_2W_4C Some Ni_3W_3C Lattice constant 11.20 and 10.94	Potentiostat showed no activity	4870-36	
19	Nb_3Al_3C	4239-49-6	Nb, Al, C	Water cooled bell jar, 75 min at $< 10^{-4}$ torr	Nb_3Al_3C a ~14.1A	No activity	4870-41	
Washed in 30% KOH Washed in 30% H_2SO_4 at 100°C 6 hrs								
20	Nb_3Al_2MnC	4239-49-7	Nb, Al, MnC	Water cooled bell jar, 75 min at $< 10^{-4}$ torr	Nb_3Al_2MnC a ~11.1A	No hydrogenation	3346-A18-3	Washing written up in 660091-20
Washed in Cold KOH (30%) Washed in 30% H_2SO_4 for 6 hours at 110°C					"	No hydrogenation No potentiostatic activity in acid or base.	660091-38 3346-A25	
21	Ni_3W_3C	660091-1	Ni, W, C	4 weeks in evacuated quartz tubes in muffle at 800-850°C	Ni_2W_4C, a = 11.4 Ni_3W_3C in acid washed sample. Unwashed doesn't show these WC possible.			
Washed in 30% H_2SO_4 for 6 hours at 100°C								
22	Co_3W_3C	660091-2	Co, W, C	Water cooled bell jar, 90 min at 1390-1430°C at $< 5 \times 10^{-4}$ torr	Co_3W_3C a = 10.94 Co_2W_4C a = 11.26 W	No hydrogenation activity	660091-38	
23	Ni_3Mo_3C	660091-3	Ni, Mo, C	Water cooled bell jar 90 min at 1450-1570°C at ~5×10^{-5} torr	Ni_2Mo_4C recovered as a lump - Ni_3Mo Mo_3C, a = 10.96 Ni_2Mo_4C Lattice constant 11.25	No potentiostatic activity	3346-A12	Ground up some in spex grinder. X-ray showed very serious WC contamination. Qual emission in acid showed major Ni, trace Mo
Washed in 30% H_2SO_4 for 6 hours at 100°C								
24	Fe_3W_3C	660091-4	Fe, W, C	Water cooled bell jar, 60 min at 1430°C at 50 μ Sample was difficult to degas and a corona was seen that increased in intensity with temp and power.	Cubic form with poor lattice structure a ~12.3	No Hydrogenation activity	3346-A17-3	
Washed in 30% H_2SO_4 for 6 hours at 100°C					Cubic form with lattice constant a ~11.4 Fe_2W_4C?			Lattice constant is a little large for Fe_2W_4C.
25	Co_3Mo_3C	660091-5	Co, Mo, C	Water cooled bell jar, 1320°C on pyrometer for 13 hrs.	Probably Co_7Mo_6			
Washed in 30% H_2SO_4 for 6 hours at 100°C								
26	$Ni_{3.5}W_3C$	660091-6-1	Ni, W, C	Water cooled bell jar, 60 min at 1450-1570°C, 25 u	WC Ni_3W_3C a = 10.94 Ni_2W_4C Lattice constant 11.25A	Potentiostat showed no activity	4870-38	
27	$Ni_{3.5}W_3C$	660091-6-2	Ni, W, C	Water cooled bell jar, 100 min from 21° to 1400°C 7 hrs. at 1410°C at 7 x 10^{-5} torr	Ni_3W_3C Super lattice Lattice constant 10.92, some Ni_2W_4C			Hard pellets were recovered broken up by ultrasonic.
Washed in 30% H_2SO_4 for 6 hours at 100°C								
28	$Ni_{1.5}Co_{1.5}Ta_3C$	660091-7	Ni, Co, Ta, C	Water cooled bell jar, 75 min at 1400-1450°C and at 1510°C for 10 min	$Ni_{1.5}Co_{1.5}Ta_3C$ a = 11.44 A			
Washed in 30% H_2SO_4 for 6 hours at 100°C								

APPENDIX B-7 (CONT'D)

PREPARATION OF ETA PHASE CARBIDES

Item No.	Compound Desired	Notebook Reference	Firing Composition	Firing Conditions	Compound Obtained	Catalysis Tests	Notebook Reference	Other
29	$Ni_{1.5}Fe_{1.5}Ta_3C$	660091-8	Ni, Fe, Ta, C	Water cooled bell jar, 2 hrs. at 1390-1420°C 5 hrs. at 1450°C	$Ni_{1.5}Fe_{1.5}Ta_3C$ a = 11.4 Ta C			
30	Cr_3W_3C	660091-12	Cr, W, C	Water cooled bell jar 90 min. at 1570-1630°F under the vapor pressure of the mix. A corona was observed	No cubic structure	No hydrogenation activity	660091-38	Chromium was melted
Acid washed for 6 hrs. in 30% H_2SO_4 at 100°C Acid washing was dark green					No cubic structure			
31	$Ni_{3.0}W_3C$	660091-13	NiO, WO_3, C	Water cooled bell jar 5 hrs. to 1090°C 1-1/2 hrs. at 1290°C 3/4 hrs. at 1320°C	Ni_3W_3C some Ni_2W_4C	No hydrogenation activity	3346-A20	
Washed in 30% H_2SO_4 for 6 hrs. at 100°C					"	Bad corrosion during potentiostat testing		
32	V_3Ta_3C	660091-14	V, Ta, C	Water cooled bell jar 6 hrs. at 1205-1295°C	No η phase formed Ta_2C found			
33	Mn_3Nb_3C	660091-16	Mn, Nb, C	Water cooled bell jar at about 1100°C for 12 hrs. 2 hrs. to get to 1100°C	NbC, Nb_2C η phase possible			
34	Cr_3Nb_3C	660091-17	Nb, Cr, C	Water cooled bell jar 10 hrs. at ~1800°C, pressure less than 5×10^{-5} mm	η phase a = 11.5			
35	V_3Zr_3C	660091-18	V, ZrO_2, C	Water cooled bell jar 4-1/2 hrs. at ~1630 pressure less than 50 μA corona	Unreacted ZrO_2 No evidence for eta phase	No hydrogenation	660091-38	
36	Mn_3Zr_3C	660091-19	Mn, ZrO_2, C	Water cooled bell jar 1-1/2 hrs. to 1200°C 3 hrs. at 1200°C 1400°C for 10-1/2 hrs.	No η phase ZrO_2	No potentiostatic activity	3346-A29	
37	Fe_3W_3C	660091-4-2	Fe, W, C	Water cooled bell jar 12 hrs. at 1500°C at less than 10^{-5} mm	Fe_7W_6W No eta phase			
38	$CuAl_2Nb_3C$	660091-24	Cu, Al, Nb, C	Water cooled bell jar 6 hrs. at 1205-1295°C	$CuAl_2Nb_3C$ + some Nb, NbC Cu_9Al_4			

APPENDIX B-8

VOLTAGE SCANS ON RANEY NICKEL IN BASE

50 mg Raney Ni, Gold Flag Screen Electrode Support
3 M KOH, 80°C

NB Ref.	Scan Range volts vs S.C.E.	Scan Time, sec(1)	Total Millicoulombs Anodic Uncorr.	Anodic Corr.(2)	Cathodic Uncorr.	Cathodic Corr.(2)	Remarks
4610-							
48-1	1.10-0.95	207.7	1554	--	1860	--	C_2H_4 atm.
48-2	1.10-0.95	207.7	1668	--	2107	--	Shoulder at 0.99.
49-1A	1.10-0.85	825	3889	5915	3680	5182	Sharp peak at 0.925.
1B	"	"	3209	4487	3252	4896	No effect of C_2H_4 exposure at 1.00 volts.
2	"	"	1546	1939	2668	4727	Anodic loss due to reduction and possibly
3	"	"	1399	1775	2252	3896	catalyst loss.

							Coulombs in Peaks Anodic	Cathodic
50-2	1.07-0.88	207.7	1575	2093	1400	1617	240	260
50-3	"	825	1888	2727	1710	2662	342	241
50-4	"	1656	--	--	--	--	349	375
50-5	"	1656	1716	2474	1685	3344	289	260
50-6	"	825	--	--	--	--	309	--
50-7	"	825	--	--	--	--	289	--

66-0189							
1-1A	108-0.78	825	1746	2045	1352	1630	Under N_2. Includes large anodic peak at
1-1B	"	"	1549	1738	1173	1515	0.865 volts, which shrinks.
1-1C	"	"	1300	1362	1090	1347	
1-2A	"	"	1554	1879	1312	1712	After 45 min of C_2H_4 at 0.98 volts.
1-2B	"	"	1264	1485	1207	1629	
1-2C	"	"	1110	1407	996	1308	
1-3A	"	"	2360	2859	1402	1704	After 45 min of N_2 at 1.08 volts.
1-3B	"	"	1290	1562	1069	1503	
1-3C	"	"	1080	1400	967	1391	
1-4A	"	"	1628	2005	907	1215	Overnight + 1 hour N_2 at 0.99 volts.
1-5A	"	"	903	1088	774	1175	After 30 min C_2H_4 at 0.99 volts.
1-6A	"	"	1430	1710	1030	1657	After 30 min C_2H_4 at 1.09 volts.
B	"	"	958	1154	825	1022	
1-7A	"	"	1564	1885	999	1791	After N_2 exposure at 1.09 volts.

(1) Per half cycle.
(2) Including end corrections, i.e., parts of anodic scan which are cathodic and conversely. Inclusion of correction tends to over emphasize cathodic scan, which includes H_2 evolution.

APPENDIX B-9

CATALYST PERFORMANCE EVALUATIONS

Electrode Number	Catalyst Number	Catalyst Composition	Catalyst Preparation: Reducing Agent	Catalyst Preparation: Reduction Temp °C	Electrolyte	Operating Temp.	Fuel	Performance: Current Density ma/cm²	Performance: Volts Polarized from Theoretical	Remarks
4774-31-4	4774-30-4	Pd	H_2	175	$KHCO_3/K_2CO_3$(2M)	90°C	H_2	100	0.22	
							C_2H_4	No stable performance		Electrode surface blocked by electrolyte residues.
					3 M KOH	90°C	H_2	40	0.4	
							C_2H_4	<1	>0.4	
4774-31-2	4774-30-2	Pd-50Ag	H_2	175	3 M KOH	90°C	H_2	200	0.34	
							C_2H_4	≤1	>0.6	
4774-44-5	4774-30-5	Ru	H_2	175	3 M KOH	90°C	H_2	42	0.04	
							C_2H_4	No stable performance		
4774-44-12	4774-30-2	Co-50Ru	H_2	425	3 M KOH	90°C	H_2	No stable performance		
							C_2H_4	No stable performance		
0201-7	4774-47-8	Ni	Rad. Anion	27	3 M KOH	90°C	H_2	<3	0.1	Catalyst reduced with lithium biphenyl in tetrahydro furan.
0201-10-15	0201-1-15	$Ni_{95}Ru_5$	H_2	425	3 M KOH	90°C	H_2	<0.1	0.1	
							C_2H_4	No stable performance		
0201-10-7	0201-1-7	$Ni_{50}Ru_{50}$	H_2	425	3 M KOH	90°C	H_2	10	0.1	
							C_2H_4	No stable performance		
0201-23-1	0201-23-1	Ni	Rad. Anion	25	3 M KOH	90°C	H_2	40	0.18	Catalyst deactivated on being polarized to 0.25. Cathodization, or lithium biphenyl activation was unsuccessful in restoring activity.

APPENDIX B-10

EVALUATION OF CATALYTIC ACTIVITY BY CONVENTIONAL OLEFIN HYDROGENATION

In addition to electrochemical tests, a simple technique for establishing the presence of catalytic activity, or, more importantly, the relative activity of a series of catalysts was sought. For this purpose, the use of an automatic hydrogenation device (58) was investigated. This device consists of a hydrogen generator which supplies hydrogen gas on demand to a second flask containing, normally, a solution of an olefin in alcohol and a suspended catalyst. The hydrogen pressure in the system is maintained near atmospheric automatically by compensating for decrease in pressure through addition of sodium borohydride solution into acid contained in the first flask, the addition being controlled by a pressure sensitive mercury valve. The reaction studied was the hydrogenation of an olefin and thus bears no particular relation to a fuel cell anodic oxidation. However, the simplicity of the test, and the fact that active hydrogenation catalysts, such as noble metals, or transition metals, are also well known fuel cell catalysts, prompted an evaluation of this technique for catalyst screening. A further advantage of the technique lies in the freedom of the test from complications due to electrode structure, which can seriously interfere with catalyst evaluation by electrochemical techniques. This test could also be of use in studying regeneration procedures for transition metal catalysts which become seriously deactivated by overpolarization.

For example, during the preparation of some experimental catalysts consisting of cobalt and ruthenium, inadvertent exposure of the catalysts to air apparently caused severe deactivation. These catalysts were subsequently found to be inactive for hexene-1 hydrogenation. Injection of an ethanolic solution of sodium borohydride was successful in these cases in producing activity in the system as shown by the data in Table B-1 and B-5.

Table B-1

Catalyst Activation by Sodium Borohydride

Catalyst	Activity for Hexene-1 Hydrogenation(1) (mm/min/gm)	
	Before Activation	After Activation(2)
Co50/Ru50	0	7.0
Co70/Ru30	0	2.9
Co90/Ru10	0	5.1
Co95/Ru5	0	3.5

(1) H_2 pressure 1 atmosphere, room temperature hydrogenation.

(2) Addition of 2 cc 0.5 M sodium borohydride in ethanol.

A test of cobalt boride, prepared in situ by addition of sodium borohydride solution to a solution of cobalt acetate, did not produce an active catalyst. Thus the appearance of activity is probably a result of reduction of a passivating oxide film which, at room temperature, is stable in the presence of hydrogen and alcohol.

Studies of activation techniques were extended to include a more powerful reducing agent, triisobutyl aluminum. In this study, catalysts containing nickel rather than cobalt were used. The data indicated that for nickel alone, the triisobutyl aluminum reducing agent, used in hydrocarbon solution, was more effective than the sodium borohydride in ethanol. However, for the more active ruthenium containing catalysts, the two agents were essentially equivalent. Cobalt activated by triisobutyl aluminum was much less active than nickel. The results of this study are shown in Table B-2 and B-5.

Table B-2

Comparison of Triisobutyl Aluminum and Sodium Borohydride

Catalyst	Activating[1] Agent	Activity for Hexene-1 Hydrogenation (mm/min/gm)
Co	TIBAL	Very slow
Ni	$NaBH_4$	Very slow
Ni	TIBAL	3.2
Ni50Ru50	$NaBH_4$	9.6
Ni50Ru50	TIBAL	9.6

(1) Reaction conducted in n-heptane solution when triisobutyl aluminum used as activating agent.

These data suggest that ruthenium is relatively easily activated while nickel is not due to a more stable oxide film. Thus the more powerful reducing agent, triisobutyl aluminum, is effective in removing the passivating oxide film from nickel while sodium borohydride is not.

Because of the difficulties associated with catalyst deactivation during preparation, which were readily apparent from the results of hydrogenation experiments, much closer control of catalyst handling conditions were introduced. Minimizing exposure of the catalyst to air resulted in elimination of the necessity for activation procedures. A series of nickel-ruthenium catalysts were prepared which were very active for hexene-1 hydrogenation although not apparently as active as platinum. These data are shown in Table B-3 and B-5.

Table B-3

Activity of Nickel Ruthenium Compared to Platinum

Catalyst	Activity for Hexene-1 Hydrogenation (mm/min/gm)
Pt (50 mg)	19.2
Ni50Ru50 (200 mg)	6.2
Ni70Ru30 (200 mg)	8.3
Ni90Ru10 (200 mg)	5.6
Ni95Ru5 (200 mg)	5.4

Attempts at comparison of platinum and experimental catalyst activity at the same loading, however, revealed a serious drawback in the use of this method for catalyst activity comparisons. The data indicated that the specific rate in millimoles/min/gram was not a constant, but increased rapidly as the amount of catalyst present in the system was decreased, as shown in Table B-4 and B-5.

Table B-4

Catalyst Loading Effects on Specific Activity

Catalyst Loading Ni70/Ru30 (mg)	Observed Rate (mm/min)	Specific Rate (mm/min/gm)
201	1.67	8.3
101	1.58	15.7
50	1.21	24.2
25	0.99	39.6

This finding indicates that the reaction was limited by a physical factor, presumably diffusion, and not by catalyst activity as hoped. Thus, although the test is adequate for the purpose of differentiating between active and inactive catalyst it is not useful in its present form for catalyst activity comparisons, at least for very active catalyst. Several potential methods exist for overcoming this limitation, such as running the reaction at lower temperature, increasing the agitation of the reaction mixture or using a more difficuitly hydrogenated hydrocarbon such as cyclo-octene for example. However, in view of the uncertainty of the presence of any correlation between hydrogenation activity and fuel cell activity, especially for catalysts presumably operating by a two site mechanism, no further work on this technique appeared justified.

This technique may still be of use, however, in studying the important question of nickel activation.

Table B-5

Catalyst Testing by Hydrogenation of 1-Hexene

Notebook Reference	Catalyst Composition Atom %	Reduction Technique	Activation Technique	Catalyst Loading (mg metal)	Support Present	Solvent	Specific Rate (mm/min/gm)	
4774-42	100 Pd	H_2 (177°C)	None	151	Yes	Ethanol	8.1	
4774-39	50Pd-50Ag	"	"	148	"	"	4.7	
4774-9	100 Pt	Commercial	"	50	---	"	21	
4774-10	100 Co	H_2 (482°C)	"	100	Yes	"	0	
4774-10	100 Co		$NaBH_4$	"	"	"	0	In situ activation, $NaBH_4$ in ethanol (0.5 M).
4774-10	50Ni-50Ag	H_2 (482°C)	None	50	No	"	0	
4774-11	70Co-30Ru	"	"	100	"	"	0	
4774-14	95Co-5Ru	"	"	"	"	"	0	
4774-14	"	"	$NaBH_4$	"	"	"	3.5	In situ activation, $NaBH_4$ in ethanol (0.5 M).
4774-15	70Co-30Ru	"	"	"	"	"	2.9	" " "
4774-16	Co_2B	$NaBH_4$	None	"	---	"	0	In situ catalyst preparation.
4774-17	90Co-10Ru	H_2 (482°C)	$NaBH_4$	84	No	"	4.8	In situ activation, $NaBH_4$ in ethanol (0.5 M).
4774-18	50Co-50Ru	"	"	97	"	"	6.9	" " "
4774-19	Ni	"	"	100	"	"	Very Slow	" " "
4774-20	50Ni-50Ag	"	"	88	"	"	0	" " "
4774-21	50Ni-50Ru	"	"	91	"	"	9.6	" " "
4774-22	Ni	"	TIBAL	115	"	n Heptane	3.3	In situ activation, TIBAL in heptane (1 M).
4774-23	50Ni-50Ru	"	"	100	"	"	9.6	" "
4774-24	Co	"	"	86	"	"	1.8	" "
4774-25	"	"	"	131	Yes	"	C	Activation as above, second catalyst prep.
4774-29	Ru	H_2 (177°C)	$NaBH_4$	65	"	Ethanol	Very Slow	In situ activation, $NaBH_4$ in ethanol (0.5 M).
4774-34	50Ni-50Ru	H_2 (482°C)	"	163	"	"	4.5	" " "
4774-37	Ni	"	TIBAL	197	"	n Heptane	Very Slow	In situ activation, TIBAL in n Heptane (1 M).
4774-38	50Ni-50Ru	"	$NaBH_4$	350	"	Ethanol	3.3	In situ activation, $NaBH_4$ in ethanol (0.5 M).
66-0201-1	Ni	Lithium biphenyl	None	210	---	"	5.3	
66-0201-2	Ni	"	"	269	---	"	2.8	Second preparation of this catalyst.
66-0201-3	Ni	H_2 (482°C)	TIBAL	250	Yes	n Heptane	0	Ni dried in inert atmosphere, soaked in heptane solvent of TIBAL (1 mm/cc) overnight at room temperature.

Table B-5 (Cont'd)

Catalyst Testing by Hydrogenation of 1-Hexene

Notebook Reference	Catalyst Composition Atom %	Reduction Technique	Activation Technique	Catalyst Loading (mg metal)	Support Present	Solvent	Specific Rate (mm/min/gm)	
66-0201-4	Ni	H_2 (482°C)	$LiAlH_4$	280	Yes	n Heptane	0	Ni dried inert atmosphere, soaked in tetra hydrofuran/$LiAlH_4$ slurry overnight at room temperature.
66-0201-5	50Ni-50Ru	"	None	100	No	Ethanol	0	
"	"	"	$NaBH_4$	"	"	"	15	In situ activation, $NaBH_4$ in ethanol (.5 M).
66-0201-6	70Ni-30Ru	"	None	"	"	"	0	
"	"	"	$NaBH_4$	"	"	"	13.3	In situ activation, $NaBH_4$ in ethanol (.5 M).
66-0201-9	90Ni-10Ru	"	None	"	"	"	0	
"	"	"	$NaBH_4$	"	"	"	11.8	In situ activation, $NaBH_4$ in ethanol (.5 M).
66-0201-10	95Ni-5Ru	"	None	"	"	"	0	
"	"	"	$NaBH_4$	"	"	"	11.1	In situ activation, $NaBH_4$ in ethanol (.5 M).
66-0201-11	Ni	"	Li-Biphenyl	200	Yes	n Heptane	0	In situ activation, lithium-biphenyl in THF.
66-0201-12	50Ni-50Ru	"	None	205	"	Ethanol	6.2	
66-0201-13	90Ni-10Ru	"	"	201	"	"	5.6	
66-0201-14	70Ni-30Ru	"	"	"	"	"	8.3	Catalyst loading study.
66-0201-15	95Ni-5Ru	"	"	218	"	"	5.4	
66-0201-16	70Ni-30Ru	"	"	102	"	"	15.7	Catalyst loading study.
66-0201-17	70Ni-30Ru	"	"	55	"	"	24.2	"
66-0201-19	70Ni-30Ru	"	"	25	"	"	39.6	"
66-0201-20	70Ni-30Ru	"	"	104	"	"	16.8	Evaluation of effect of H_2O injection.
66-0201-21	70Ni-30Ru	"	"	100	"	"	16.1	Evaluation of effect of aqueous KOH injection.
66-0201-22	Ru	H_2 (177°C)	"	101	"	"	14	
66-0201-25	Ni	Li-Biphenyl	"	103	---	"	16	

APPENDIX B-II

EVALUATION OF HIGH SURFACE AREA ALLOY CATALYSTS

Catalyst Preparation No.	Composition, Atom %	Surface Area, m^2/gm	Crystallite Size, Å	Alloy Magnetic Moment, Bohr Magnetons	Hydrogenation Rate, Millimoles/ Minute/gm (200 mg Charge)	Hydrogen Performance	
						Limiting Current Density, ma/cm^2	Current Density at 0.1 Volts Polarized
66-0087-44-1	Pure Iron	12	--	2.2	Not Evaluated	0	0
66-0087-8-4	30Ni-70Fe			1.8	2.16	34	34
66-0087-44-2	Pure Cobalt	19.7		1.7	No Activity	18	9
66-0087-44-6	65Ni-35Fe	59.5		1.4	1.99	27	26
66-0087-9-1	40Ni-60Co	39.9	71	1.3	2.92	100	96
66-0087-44-4	75Ni-25Co	51.8	53	1.0	3.09	160	118
66-0087-44-5	85Ni-15Fe			1.0	2.74	114	108
66-0087-4[illegible]	89Ni-11Co		58	0.8	2.91	56	48
66-0087-8-5	Pure Nickel	24.8	59	0.6	4.2	44	44
66-0087-9-6	90Ni-10Cu	63.8	--	0.5	3.30	84	80
66-0087-8-3	70Ni-30Cu		--	0.3	3.67 0.17	72 27	64 27
66-0087-9-2	30Ni-60Cu			0.0	No Activity	23	23
66-3087-4-1 High Temperature Hydrolysis	Pure Nickel	53.2	53	0.6	2.62	120	108

APPENDIX C-1

SUPPORTED PLATINUM CATALYSTS

Reference	Catalyst[1]	Carbon Type	Pt Loading, mg/cm²[2]	Run Type[3]	Butane Performance, 14.7 M H_3PO_4, 130°C — Polarization from Theory at Indicated ma/cm², Volts: 0	5	10	15	20	25	30	35	40	45	50	55	60	O_2 Performance Polarization from Theory at Indicated ma/cm², volts: 0	50	100	Comments
4631-1	2.8% Pt on C-10% SiO_2	FC-30C	1.2	A	0.16	0	0.385	0.45	Dead	--	--	--	--	--	--	--	--	--	--	--	
				B	0.13	0.27	--	0.375	0.40	Dead	--	--	--	--	--	--	--	0.23	0.41	0.55	10% CO_2 reburnout of C.
				C	--	--	--	--	0.39	0.44	Dead	--	--	--	--	--	--	--	--	--	
4631-20	2.8% Pt on C-10% SiO_2	"	"	A	0.15	0.26	0.31	0.34	0.375	Dead	--	--	--	--	--	--	--	--	--	--	
				B	0.12	0.24	--	0.32	--	Dead	--	--	--	--	--	--	--	0.29	0.40	0.52	"
				C	--	--	--	--	0.34	Dead	--	--	--	--	--	--	--	--	--	--	
4631-21	2.8% Pt on C-10% SiO_2	"	"	A	0.15	0.32	0.395	0.45	Dead	--	--	--	--	--	--	--	--	--	--	--	
				B	0.135	0.275	0.34	0.43	Dead	--	--	--	--	--	--	--	--	0.23	0.43	0.65	"
				C	--	--	--	0.40	Dead	--	--	--	--	--	--	--	--	--	--	--	
4631-24	2.8% Pt on C-10% SiO_2	"	"	A	0.14	0.29	0.35	0.395	0.40	Dead	--	--	--	--	--	--	--	--	--	--	
				B	0.14	0.25	--	0.335	0.365	0.405	Dead	--	--	--	--	--	--	0.29	0.39	0.47	"
				C	0.13	--	--	--	--	0.38	0.413	Dead	--	--	--	--	--	--	--	--	
4631-32	2.9% Pt on C-10% SiO_2	"	"	A	0.15	0.31	0.37	0.41	0.44	Dead	--	--	--	--	--	--	--	--	--	--	
				B	0.125	0.27	--	0.37	0.405	Dead	--	--	--	--	--	--	--	0.225	0.385	0.49	"
				C	--	--	--	--	--	0.41	Dead	--	--	--	--	--	--	--	--	--	
4631-36	2.8% Pt on C-10% SiO_2	"	"	A	0.14	0.33	0.39	0.45	Dead	--	--	--	--	--	--	--	--	--	--	--	
				B	0.12	0.295	--	0.38	0.41	Dead	--	--	--	--	--	--	--	0.23	0.40	0.535	"
				C	--	--	--	--	0.39	Dead	--	--	--	--	--	--	--	--	--	--	
4631-38	2.8% Pt on C-10% SiO_2	"	"	A	0.12	0.26	0.31	0.345	Dead	--	--	--	--	--	--	--	--	--	--	--	
				B	0.095	0.235	0.32	Dead	--	--	--	--	--	--	--	--	--	0.29	~0.75	--	"
4631-49	2.8% Pt on C-10% SiO_2	"	"	A	0.155	0.30	0.375	0.43	Dead	--	--	--	--	--	--	--	--	--	--	--	
				B	0.15	0.29	0.39	Dead	--	--	--	--	--	--	--	--	--	0.23	>0.75	--	"
4631-61	2.4% Pt on C-10% SiO_2	Spheron-6	1.0	A	0.18	0.37	0.43	Dead	--	--	--	--	--	--	--	--	--	0.25	0.42	0.53	
				B,C	0.17	0.325	0.385	Dead	--	--	--	--	--	--	--	--	--	--	--	--	10% CO_2 burnout of C.
4631-62	0.7% Pt on C-10% SiO_2	"	0.30	A	0.19	Dead	--	--	--	--	--	--	--	--	--	--	--	--	--	--	
				B	0.20	Dead	--	--	--	--	--	--	--	--	--	--	--	0.34	0.53	--	
4631-63	0.5% Pt on C-10% SiO_2	"	0.21	A	0.23	Dead	--	--	--	--	--	--	--	--	--	--	--	--	--	--	
				B	0.30	Dead	--	--	--	--	--	--	--	--	--	--	--	0.40	0.53 @ 25 ma/cm²		Prep in 50% MeOH.
4681-3	2.8% Pt on C-10% SiO_2	FC-30	1.2	A	0.21	0.345	0.40	0.43	Dead	--	--	--	--	--	--	--	--	--	--	--	
				B	0.14	0.265	0.32	0.365	0.41	Dead	--	--	--	--	--	--	--	0.24	0.37	0.50	10% CO_2 reburnout of C.
4681-5	2.8% Pt on C-10% SiO_2	"	"	A	0.155	0.315	0.38	0.42	0.45	Dead	--	--	--	--	--	--	--	--	--	--	
				B	0.15	0.27	0.32	0.37	0.41	Dead	--	--	--	--	--	--	--	0.21	0.365	0.475	"
				C	0.135	--	--	--	--	0.42	Dead	--	--	--	--	--	--	--	--	--	
4681-19	2.5% Pt on C-10% SiO_2	"	1.0	A	0.17	0.28	0.335	0.365	0.385	0.405	Dead	--	--	--	--	--	--	--	--	--	
				B	0.13	0.255	0.30	0.33	0.35	0.38	Dead	--	--	--	--	--	--	0.27	0.38	0.45	20% CO_2 reburnout of C.
				C	0.12	--	--	--	--	--	0.38	Dead	--	--	--	--	--	--	--	--	
4681-22	2.4% Pt on C-10% SiO_2	"	"	A	0.17	0.31	0.37	0.415	Dead	--	--	--	--	--	--	--	--	--	--	--	
				B	0.14	0.28	0.355	Dead	--	--	--	--	--	--	--	--	--	0.23	0.50	0.80	"
4681-25	2.9% Pt on C-10% SiO_2	"	1.2	A	0.125	0.26	0.32	0.36	0.40	Dead	--	--	--	--	--	--	--	--	--	--	
				B	0.125	0.23	--	0.325	--	0.37	Dead	--	--	--	--	--	--	0.30	0.41	0.49	No reburnout.
4681-28	2.5% Pt on C-10% SiO_2	"	1.0	A	0.17	0.33	0.40	0.45	0.42	Dead	--	--	--	--	--	--	--	--	--	--	
				B	0.15	0.28	--	0.365	--	0.40	Dead	--	--	--	--	--	--	0.26	0.35	0.42	20% CO_2 reburnout of C.
				C	0.14	--	--	--	--	--	0.41	Dead	--	--	--	--	--	--	--	--	
4681-30	2.4% Pt on C-10% SiO_2	"	"	A	0.16	0.27	0.33	0.395	0.405	0.44	Dead	--	--	--	--	--	--	--	--	--	
				B	0.12	0.25	--	0.335	--	0.39	Dead	--	--	--	--	--	--	0.25	0.39	0.49	"
4681-38	2.8% Pt on C-10% SiO_2	"	1.2	A	0.135	0.27	0.33	0.37	0.395	0.395	Dead	--	--	--	--	--	--	--	--	--	
				B	0.12	0.24	--	0.31	--	0.355	Dead	--	--	--	--	--	--	0.29	0.40	0.47	10% CO_2 reburnout of C.
				C	0.10	--	--	--	--	--	0.35	0.36	0.38	0.41	Dead	--	--	--	--	--	
4681-40	2.8% Pt on C-10% SiO_2	"	"	A	0.20	0.34	0.41	0.47	0.53	Dead	--	--	--	--	--	--	--	--	--	--	
				B	0.145	0.29	--	0.38	--	0.44	Dead	--	--	--	--	--	--	0.22	0.365	0.46	"
				C	0.14	--	--	--	--	--	0.44	Dead	--	--	--	--	--	--	--	--	
4681-47	2.8% Pt on C-10% SiO_2	"	"	A	0.14	0.28	0.33	0.37	0.39	0.40	Dead	--	--	--	--	--	--	--	--	--	
				B	0.13	0.24	--	0.32	--	0.365	Dead	--	--	--	--	--	--	0.29	0.37	0.45	"
				C	0.10	--	--	--	--	--	0.38	Dead	--	--	--	--	--	--	--	--	

(1) Reduction of Pt salt with carbon monoxide followed by activation step except where indicated.
(2) Sintered carbon Teflon electrode prepared using Teflon 42 BX emulsion (7.5 to 22.5%), except where indicated.
(3) A. Butane performance before oxygen treat.
B. Butane performance after oxygen treat.
C. Butane performance after overpolarization.

APPENDIX C-I (CONT'D)

SUPPORTED PLATINUM CATALYSTS

Reference	Catalyst[1]	Carbon Type	Pt Loading, mg/cm^2[2]	Run Type[3]	Butane Performance, 14.7 M H_3PO_4, 150°C — Polarization from Theory at Indicated ma/cm^2, Volts: 0	5	10	15	20	25	30	35	40	45	50	55	60	O_2 Performance Polarization from Theory at Ind ma/cm^2, volts: 0	50	100	Comments
4682-3	2.8% Pt on C-10% SiO_2	FC-30	1.2	A	0.13	0.26	0.31	0.35	0.38	0.40	0.425	Dead	--	--	--	--	--	--	--	--	10% CO_2 reburnout of C
				B	0.13	0.27	--	0.34	--	0.38	0.395	Dead	--	--	--	--	--	0.28	0.38	0.47	
4682-7	2.8% Pt on C-10% SiO_2	"	"	A	0.15	0.38	0.45	Dead	--	--	--	--	--	--	--	--	--	--	--	--	10% CO_2 reburnout of C
				B	0.16	0.29	--	0.38	0.41	Dead	--	--	--	--	--	--	--	0.26	0.38	0.45	
				C	0.14	--	--	--	--	0.43	Dead	--	--	--	--	--	--	--	--	--	
4682-14	2.8% Pt on C-10% SiO_2	"	"	A	0.15	0.31	0.35	0.38	0.42	Dead	--	--	--	--	--	--	--	--	--	--	10% CO_2 reburnout of C
				B	0.17	0.28	0.325	0.36	0.385	Dead	--	--	--	--	--	--	--	0.26	0.38	0.49	
4682-16	"	"	"	A	0.15	0.32	0.405	0.445	Dead	--	--	--	--	--	--	--	--	--	--	--	10% CO_2 reburnout of C
				B	0.15	0.295	0.355	0.425	Dead	--	--	--	--	--	--	--	--	0.22	0.395	0.55	
4682-22	"	"	"	A	0.12	0.28	0.345	0.39	0.39	Dead	--	--	--	--	--	--	--	--	--	--	10% CO_2 reburnout of C
				B	0.15	0.28	--	0.36	0.38	0.41	Dead	--	--	--	--	--	--	0.29	0.38	0.41	
				C	0.14	--	--	--	--	--	0.43	Dead	--	--	--	--	--	--	--	--	
4682-25	1.5% Pt on C-10% SiO_2	"	0.63	A	0.165	0.34	0.405	0.48	Dead	--	--	--	--	--	--	--	--	--	--	--	10% CO_2 reburnout of C
				B	0.17	0.32	--	0.405	0.45	Dead	--	--	--	--	--	--	--	0.22	0.34	0.41	2% ozonization
				C	0.16	--	--	--	0.42	0.46	Dead	--	--	--	--	--	--	--	--	--	
4682-27	0.55% Pt on C-10% SiO_2	"	0.23	A	0.165	0.45	Dead	--	--	--	--	--	--	--	--	--	--	--	--	--	10% CO_2 reburnout of C
				B	0.17	0.35	Dead	--	--	--	--	--	--	--	--	--	--	0.29	0.40	0.49	28% ozonization
4682-30	1.3% Pt on C-10% SiO_2	"	0.54	A	0.18	0.36	0.41	0.46	Dead	--	--	--	--	--	--	--	--	--	--	--	
				B	0.17	0.32	--	0.40	0.47	Dead	--	--	--	--	--	--	--	0.265	0.38	0.45	10% CO_2 reburnout of C,
				C	0.15	--	--	--	0.42	Dead	--	--	--	--	--	--	--	--	--	--	6% ozonization
4682-35	2.2% Pt on C-10% SiO_2 ~5% T.B.	"	0.92	A	0.13	0.34	Dead	--	--	--	--	--	--	--	--	--	--	--	--	--	10% CO_2 reburnout of C
				B	0.14	0.275	0.34	0.37	Dead	--	--	--	--	--	--	--	--	0.25	0.39	0.46	
				C	0.12	--	--	--	0.385	0.39	0.4.	Dead	--	--	--	--	--	--	--	--	
4682-37	2.2% Pt on C ~ 5% T.B.	"	0.91	A	0.14	0.365	Dead	--	--	--	--	--	--	--	--	--	--	--	--	--	10% CO_2 reburnout of C
				B	0.15	0.30	0.36	0.405	Dead	--	--	--	--	--	--	--	--	0.22	0.37	0.44	
				C	0.14	--	--	--	0.40	0.41	0.45	Dead	--	--	--	--	--	--	--	--	
4682-42	2.4% Pt on C-10% SiO_2	"	1.0	A	0.15	0.285	0.33	0.36	0.38	0.39	Dead	--	--	--	--	--	--	--	--	--	20% CO_2 reburnout of C
				B	0.16	0.265	--	0.34	--	0.38	Dead	--	--	--	--	--	--	0.27	0.35	0.41	
				C	0.13	--	--	--	--	--	0.39	Dead	--	--	--	--	--	--	--	--	
4682-48	0.4% Pt on C-10% SiO_2	"	0.17	A	0.15	Dead	--	--	--	--	--	--	--	--	--	--	--	--	--	--	10% CO_2 reburnout of C,
				B	0.20	Dead	--	--	--	--	--	--	--	--	--	--	--	0.33	0.44	0.49	100% ozonization
4682-49	0.5% Pt on C-10% SiO_2	"	0.20	A	0.18	Dead	--	--	--	--	--	--	--	--	--	--	--	--	--	--	10% CO_2 reburnout of C,
				B	0.21	Dead	--	--	--	--	--	--	--	--	--	--	--	0.27	0.44	0.56	100% ozonization
4682-44	1.9% Pt on C-38% Al_2O_3	"	0.79	A	0.155	Dead	--		--	--	--	--	--	--	--	--	--	--	--	--	No activation treat
				B	0.155	Dead	--	--	--	--	--	--	--	--	--	--	--	0.27	Dead	--	
4682-45	2.7% Pt on C-28% Al_2O_3	"	1.1	A	0.14	Dead	--	--	--	--	--	--	--	--	--	--	--	--	--	--	No activation treat
				B	0.12	Dead	--	--	--	--	--	--	--	--	--	--	--	0.29	Dead	--	
4682-46	2.1% Pt on C-44% Al_2O_3	"	0.88	A	0.15	0.39	Dead	--	--	--	--	--	--	--	--	--	--	--	--	--	No activation treat
				B	0.155	Dead	--	--	--	--	--	--	--	--	--	--	--	0.27	0.46	--	
4588-3	2.7% Pt on C-28% Al_2O_3	"	1.1	A	0.14	Dead	--	--	--	--	--	--	--	--	--	--	--	--	--	--	
				B	0.15	0.47	Dead	--	--	--	--	--	--	--	--	--	--	0.29	0.46	0.52	
																				0.59	
4588-4	2.0% Pt on C-44% Al_2O_3	"	0.83	A	0.145	Dead	--	--	--	--	--	--	--	--	--	--	--	--	--	--	
				B	0.15	Dead	--	--	--	--	--	--	--	--	--	--	--	0.27	>0.60	--	
4588-9	4.0% Pt on C-1% Al_2O_3	"	1.7	A	0.17	0.34	0.40	0.38	Dead	--	--	--	--	--	--	--	--	--	--	--	Al_2O_3 removed by hot
				B	0.16	0.30	--	0.37	--	Dead	--	--	--	--	--	--	--	0.27	0.36	0.40	leaching with H_3PO_4
				C	0.15	--	--	--	--	0.42	Dead	--	--	--	--	--	--	--	--	--	
4588-26	3.9% Pt on C-7% Al_2O_3	"	1.6	A	0.145	0.32	0.38	0.41	Dead	--	--	--	--	--	--	--	--	--	--	--	
				B	0.12	0.255	--	0.36	0.39	Dead	--	--	--	--	--	--	--	0.23	0.36	0.43	
				C	0.12	--	--	--	--	0.42	Dead	--	--	--	--	--	--	--	--	--	
4588-12	2.2% Pt on C-10% SiO_2 ~5% T.B.	"	0.92	A	0.13	0.32	Dead	--	--	--	--	--	--	--	--	--	--	--	--	--	
				B	0.145	0.24	--	0.33	0.375	Dead	--	--	--	--	--	--	--	0.27	0.40	0.48	
				C	0.12	--	--	--	--	0.40	Dead	--	--	--	--	--	--	--	--	--	
4588-14	2.2% Pt on C ~ 5% T.B.	"	"	A	0.12	0.34	Dead	--	--	--	--	--	--	--	--	--	--	--	--	--	
				B	0.13	0.275	Dead		--	--	--	--	--	--	--	--	--	0.23	0.50	>0.70	
				C	0.125	--	0.335	Dead	--	--	--	--	--	--	--	--	--	--	--	--	

(1) Reduction of Pt salt with carbon monoxide followed by activation step except where indicated.
(2) Sintered carbon Teflon electrode prepared using Teflon 42 BX emulsion (7.5 to 22.5%), except where indicated.
(3) A. Butane performance before oxygen treat.
B. Butane performance after oxygen treat.
C. Butane performance after overpolarization.

APPENDIX C-1 (CONT'D)

SUPPORTED PLATINUM CATALYSTS

Reference	Catalyst[1]	Carbon Type	Pt Loading mg/cm²[2]	Run Type[3]	Butane Performance, 14.7 M H_3PO_4, 150°C Polarization from Theory at Indicated ma/cm², Volts 0	5	10	15	20	25	30	35	40	45	50	55	60	O_2 Performance Polarization from Theory at Ind ma/cm², Volts: 0	50	100	Comments
0096-60	2.3% Pt on C	FC-30	0.96	A	0.145	0.315	Dead	--	--	--	--	--	--	--	--	--	--	0.31	0.45	0.50	10% Oxonization of C
				B,C	0.12	0.27	--	0.37	Dead	--	--	--	--	--	--	--	--	--	--	--	after H_2 Reduction
0096-61	2.3% Pt on C - 10% SiO_2	"	"	A	0.16	0.33	0.415	Dead	--	--	--	--	--	--	--	--	--	0.25	0.38	0.48	10% Oxonization of C
				B,C	0.14	0.31	--	0.40	Dead	--	--	--	--	--	--	--	--				after H_2 Reduction
0096-64	"	"	"	A	0.16	Dead	--	--	--	--	--	--	--	--	--	--	--	0.32	0.47	0.54	No Activation Treat;
				B,C	0.17	0.39	Dead	--	--	--	--	--	--	--	--	--	--	--	--	--	10% Oxonization of C after H_2 Reduction
0096-65	2.3% Pt on C	"	"	A	0.17	0.45	Dead	--	--	--	--	--	--	--	--	--	--	0.26	0.40	0.50	2 1/4 Hr. Adsorption;
				B,C	0.16	0.41	0.45	Dead	--	--	--	--	--	--	--	--	--	--	--	--	10% Oxonization of C after H_2 Reduction
0096-102	2.9% Pt on C - 10% SiO_2	"	1.2	A	0.14	0.32	0.32	Dead	--	--	--	--	--	--	--	--	--	0.27	0.43	0.49	5% Oxonization of C
				B,C	0.14	0.27	--	0.37	0.40	Dead	--	--	--	--	--	--	--	--	--	--	after CO, H_2 Reduction
0096-103	2.6% Pt on C - 10% SiO_2	"	1.1	A	0.15	0.315	0.36	0.42	0.38	0.43	Dead	--	--	--	--	--	--	--	--	--	30°C Adsorption
				B	0.16	0.27	--	0.35	0.37	0.39	0.43	Dead	--	--	--	--	--	0.27	0.37	0.45	
				C								0.42	0.44	Dead							
0096-108	2.4% Pt on C - 10% SiO_2	"	1.0	A	0.12	0.33	0.40	Dead	--	--	--	--	--	--	--	--	--	0.31	0.48	--	60°C Adsorption
				B,C	0.12	0.27	--	0.365	0.40	--	--	--	--	--	--	--	--	--	--	--	
0096-120	"	"	"	A	0.14	0.34	0.44	Dead	--	--	--	--	--	--	--	--	--	0.29	0.45	0.52	60°C Adsorption
				B	0.13	0.265	0.33	0.38	--	--	--	--	--	--	--	--	--	--	--	--	
				C	0.11	--	--	--	+0.38	Dead	--	--	--	--	--	--	--	--	--	--	
0096-126	2.3% Pt on C	"	0.96	A	0.14	0.29	0.335	0.38	Dead	--	--	--	--	--	--	--	--	--	--	--	60°C Adsorption
				B,C	0.13	0.23	--	0.32	--	0.385	Dead	--	--	--	--	--	--	0.29	0.48	--	
0096-130	2.5% Pt on C	"	1.0	A	0.13	0.34	0.37	Dead	--	--	--	--	--	--	--	--	--	--	--	--	30°C Adsorption
				B,C	0.13	0.27	--	0.37	Dead	--	--	--	--	--	--	--	--	--	--	--	
0096-140	1.9% Pt on C	"	0.80	A	0.16	0.35	0.41	Dead	--	--	--	--	--	--	--	--	--	--	--	--	0°C Adsorption
				B	0.18	0.31	0.36	0.41	Dead	--	--	--	--	--	--	--	--	0.29	0.42	0.48	
				C	0.14	--	--	0.38	0.41	Dead	--	--	--	--	--	--	--	--	--	--	
0096-141	2.1% Pt on C - 10% SiO_2	"	0.88	A	0.17	0.345	0.41	0.48	Dead	--	--	--	--	--	--	--	--	0.26	0.35	0.43	0°C Adsorption
				B,C	0.18	0.33	0.385	0.43	0.45	Dead	--	--	--	--	--	--	--	--	--	--	
0096-152	2.6% Pt on C - 10% SiO_2	"	1.1	A	0.155	0.315	0.365	0.405	0.44	Dead	--	--	--	--	--	--	--	0.28	0.40	0.48	30°C Adsorption
				B,C	0.11	0.29	--	0.37	0.38	0.415	Dead	--	--	--	--	--	--	--	--	--	
0195-4	"	"	"	A	0.15	0.32	0.39	0.43	0.50	Dead	--	--	--	--	--	--	--	0.24	0.37	0.46	30°C Adsorption
				B,C	0.13	0.275	--	0.36	--	0.41	0.44	Dead	--	--	--	--	--	--	--	--	
0195-60	6.0% Pt - 10Ir on C	FC-30	2.5	A	0.13	0.32	0.40	0.47	Dead	--	--	--	--	--	--	--	--	0.245	0.37	0.44	Slurry Electrode -
				B,C	0.13	0.275	--	0.38	0.40	0.415	Dead	--	--	--	--	--	--	--	--	--	Dried 15 Min. before sintering
0195-61	"	"	"	A	0.17	0.41	Dead	--	--	--	--	--	--	--	--	--	--	0.24	0.38	0.415	Modified Slurry Electrode -
				B,C	0.15	0.31	0.38	0.43	0.45	Dead	--	--	--	--	--	--	--	--	--	--	Dried 30 Min. before sintering
0195-64	"	"	"	A	0.15	0.45	Dead	--	--	--	--	--	--	--	--	--	--	0.24	0.41	0.49	Standard Electrode -
				B,C	0.12	0.30	0.38	0.42	0.445	Dead	--	--	--	--	--	--	--	--	--	--	Dried 60 Min. before sintering
0195-68	"	"	"	A	0.12	0.34	0.40	Dead	--	--	--	--	--	--	--	--	--	0.27	0.37	0.42	Slurry Electrode - Dried
				B,C	0.12	0.24	--	0.33	--	0.38	0.405	Dead	--	--	--	--	--	--	--	--	0 Min. before Sintering
0195-71	"	"	"	A	0.155	0.45	Dead	--	--	--	--	--	--	--	--	--	--	0.22	0.40	0.48	Slurry Electrode - Dried
				B,C	0.14	0.295	0.37	0.43	Dead	--	--	--	--	--	--	--	--	--	--	--	60 Min. before Sintering
0195-74	"	"	"	A	0.12	0.41	Dead	--	--	--	--	--	--	--	--	--	--	0.23	0.40	0.44	Standard Electrode - Dried
				B,C	0.12	0.30	0.37	0.425	Dead	--	--	--	--	--	--	--	--	--	--	--	0 Min. before Sintering
0195-75	"	"	"	A	0.14	0.31	0.375	0.42	Dead	--	--	--	--	--	--	--	--	0.21	0.33	0.38	Slurry Electrode - Blotting
				B,C	0.14	--	--	0.34	--	0.39	0.42	0.43	Dead	--	--	--	--	--	--	--	and Drying Omitted
0195-96	"	"	"	B	0.11	0.25	--	0.31	--	0.355	--	0.395	--	0.425	0.45	Dead	--	0.22	0.30	0.37	Retest of 0195-75
				C	0.12	--	--	--	--	--	--	--	--	--	--	0.435	0.465	--	--	--	after Washing and Drying
0195-130	"	"	"	A	013	0.43	Dead	--	--	--	--	--	--	--	--	--	--	0.25	0.43	0.49	Slurry Electrode, New
				B,C	013	0.30	0.38	0.44	Dead	--	--	--	--	--	--	--	--	--	--	--	Teflon Sample - No Drying before Sintering
0195-132	"	"	"	A	0.155	Dead	--	--	--	--	--	--	--	--	--	--	--	0.24	0.465	0.55	"
				B,C	0.14	0.35	0.455	Dead	--	--	--	--	--	--	--	--	--	--	--	--	
0195-134	"	"	"	A	0.10	0.39	Dead	--	--	--	--	--	--	--	--	--	--	0.24	0.40	0.49	"
				B,C	0.12	0.27	0.34	0.41	0.43	Dead	--	--	--	--	--	--	--	--	--	--	

(1) Reduction of Pt salt with carbon monoxide followed by activation step except where indicated
(2) Sintered carbon Teflon electrode prepared using Teflon 42 BX emulsion (7.5 to 22.5%), except where indicated.
(3) A. Butane performance before oxygen treat.
B. Butane performance after oxygen treat.
C. Butane performance after overpolarization.

APPENDIX C-1(CONT'D)

SUPPORTED PLATINUM CATALYSTS

Reference	Catalyst (1)	Carbon Type	Pt Loading, mg/cm² (2)	Run Type (3)	Butane Performance, 14.7 M H_3PO_4, 150°C — Polarization from Theory at Indicated ma/cm², Volts: 0	5	10	15	20	25	30	35	40	45	50	55	60	65	70	75	80	85	90	O₂ Performance Polarization from Theory at Ind ma/cm², volts: 0	50	100	Comments
[illegible]-72	4.7% Pt on C	PC-13	2.0	A	0.14	0.26	0.32	0.36	0.365	0.39	0.38	Dead	--	--	--	--	--	--	--	--	--	--	--	0.30	0.36	0.43	10% Oxonization of C
				B	0.17	0.23	--	0.30	--	0.35	--	0.385	0.40	0.435	--	--	--	--	--	--	--	--	--	--	--	--	
				C	0.15	--	--	--	--	--	--	--	--	--	0.415	0.43	Dead	--	--	--	--	--	--	--	--	--	
[illegible]-73	4.1% Pt on C + 10% SiO_2	"	1.7	A	0.145	0.30	0.35	0.39	0.42	0.44	Dead	--	--	--	--	--	--	--	--	--	--	--	--	0.25	0.33	0.41	" " " "
				B	0.18	0.27	--	0.37	--	0.41	0.44	0.48	Dead	--	--	--	--	--	--	--	--	--	--	--	--	--	
				C	0.185	--	--	--	--	--	--	--	0.45	0.49	Dead	--	--	--	--	--	--	--	--	--	--	--	
[illegible]-80	1.9% Pt on C	PC-25	0.6	A	0.205	Dead	--	--	--	--	--	--	--	--	--	--	--	--	--	--	--	--	--	0.27	0.43	0.50	5% Oxonization of C
				B	0.205	Dead	--	--	--	--	--	--	--	--	--	--	--	--	--	--	--	--	--	--	--	--	
[illegible]-84	1.7% Pt on C + 10% SiO_2	"	0.7	A	0.17	Dead	--	--	--	--	--	--	--	--	--	--	--	--	--	--	--	--	--	0.28	0.43	0.465	" " " "
				B	0.18	0.44	Dead	--	--	--	--	--	--	--	--	--	--	--	--	--	--	--	--	--	--	--	
[illegible]-132	1.3% Pt on C	99% Graphite	0.4	A	0.24	Dead	--	--	--	--	--	--	--	--	--	--	--	--	--	--	--	--	--	0.22	0.42	0.49	25% CO_2 Burnout of C
				B	0.21	0.42	Dead	--	--	--	--	--	--	--	--	--	--	--	--	--	--	--	--	--	--	--	
[illegible]-135	1.1% Pt on C + 10% SiO_2	"	0.5	A	0.17	Dead	--	--	--	--	--	--	--	--	--	--	--	--	--	--	--	--	--	0.25	0.51	0.58	" " " " "
				B	0.21	Dead	--	--	--	--	--	--	--	--	--	--	--	--	--	--	--	--	--	--	--	--	
[illegible]-[illegible]	1.5% Pt on C	Regal 330R	0.6	A	0.17	0.40	Dead	--	--	--	--	--	--	--	--	--	--	--	--	--	--	--	--	0.33	0.65	--	
				B,C	0.185	0.42	Dead	--	--	--	--	--	--	--	--	--	--	--	--	--	--	--	--	--	--	--	
[illegible]-[illegible]	3.2% Pt on C	Vulcan XC-72	1.3	A	0.18	0.34	0.39	0.48	Dead	--	--	--	--	--	--	--	--	--	--	--	--	--	--	0.25	0.49	>0.65	Impreg. with Pt ammonia complex
				B,C	0.155	0.30	0.37	0.39	Dead	--	--	--	--	--	--	--	--	--	--	--	--	--	--	--	--	--	
[illegible]-[illegible]	5.0% Pt on C	"	2.3	A	0.195	Dead	--	--	--	--	--	--	--	--	--	--	--	--	--	--	--	--	--	0.24	0.48	--	10% Oxonization of C
				B,C	0.16	0.49	Dead	--	--	--	--	--	--	--	--	--	--	--	--	--	--	--	--	--	--	--	
[illegible]-[illegible]	1.3% Pt on C	"	1.4	A	0.18	0.39	0.435	Dead	--	--	--	--	--	--	--	--	--	--	--	--	--	--	--	--	--	--	
				B,C	0.17	0.35	0.385	Dead	--	--	--	--	--	--	--	--	--	--	--	--	--	--	--	--	--	--	
[illegible]-[illegible]	4.0% Pt on C	PC-30C	1.8	A	0.16	Dead	--	--	--	--	--	--	--	--	--	--	--	--	--	--	--	--	--	0.29	0.47	0.53	Final air treat only @ 160°C; Double Adsorption
				B	0.17	0.405	0.405	--	Dead	--	--	--	--	--	--	--	--	--	--	--	--	--	--	--	--	--	
				B,C(4)	0.14	0.30	0.37	0.37	0.39	0.395	0.41	Dead	--	--	--	--	--	--	--	--	--	--	--	--	--	--	
[illegible]-[illegible]	4.4% Pt on C	"	1.8	A	0.15	0.41	0.475	Dead	--	--	--	--	--	--	--	--	--	--	--	--	--	--	--	0.22	0.33	0.42	Double Adsorption
				B,C	0.18	0.31	--	0.385	--	0.425	0.43	0.465	Dead	--	--	--	--	--	--	--	--	--	--	--	--	--	
93278-27	4.4% Pt on C	"	1.8	A	0.17	0.36	0.40	0.42	0.47	Dead	--	--	--	--	--	--	--	--	--	--	--	--	--	0.22	0.33	0.38	Double Adsorption
				B,C	0.16	--	--	--	0.37	0.40	0.42	--	0.41	0.435	Dead	--	--	--	--	--	--	--	--	--	--	--	
				B,C(5)	0.15	--	--	--	--	--	--	--	--	0.41	0.42	0.46	Dead	--	--	--	--	--	--	--	--	--	
[illegible]-21	4.0% Pt on C	"	0.9	A	0.17	0.46	0.48	--	--	--	--	--	--	--	--	--	--	--	--	--	--	--	--	0.23	0.345	0.385	Double Adsorption
				B,C	0.20	--	0.37	0.40	0.44	0.41	0.43	0.43	Dead	--	--	--	--	--	--	--	--	--	--	--	--	--	
[illegible]-[illegible]	4.3% Pt on C	FC-20C	1.7	A	0.095	0.17	0.28	0.31	--	0.375	--	0.38	--	0.40	--	0.42	0.43	0.44	Dead	--	--	--	--	0.23	0.295	0.35	Double Adsorption
				B,C	0.155	--	--	0.28	--	--	--	0.36	--	--	--	0.40	--	0.43	--	0.465	--	0.49	Dead	--	--	--	
[illegible]	3.5% Pt on C	"	1.4	A	0.20	0.30	0.37	0.41	Dead	--	--	--	--	--	--	--	--	--	--	--	--	--	--	0.22	0.33	0.40	Double Adsorption
				B,C	0.185	--	--	0.36	0.38	0.42	0.48	0.45	Dead	--	--	--	--	--	--	--	--	--	--	--	--	--	
				B,C(5)	0.16	--	--	0.39	--	0.43	0.42	0.46	0.45	Dead	--	--	--	--	--	--	--	--	--	--	--	--	
[illegible]	3.5% Pt on C	"	1.2	A	0.13	0.235	0.285	0.34	0.36	0.39	0.39	0.41	0.405	Dead	--	--	--	--	--	--	--	--	--	0.23	0.28	0.33	Double Adsorption
				B,C	0.19	--	--	--	--	--	0.38	--	0.40	--	0.42	--	0.435	--	0.45	Dead	--	--	--	--	--	--	
				B,C(5)	0.16	--	--	--	--	--	0.365	--	--	--	0.405	--	0.425	--	0.43	0.43	0.445	Dead	--	--	--	--	

(1) Reduction of Pt salt with carbon monoxide followed by activation step except where indicated.
(2) Sintered carbon Teflon electrode prepared using Teflon 42 EX emulsion (7.5 to 22.5%), except where indicated.
(3) A - Butane performance before oxygen treat
B - Butane performance after oxygen treat
C - Butane performance after overpolarization
(4) After aging electrode
(5) Isolated gas performance

APPENDIX C-4 (CONT'D)

SUPPORTED PLATINUM CATALYSTS

Reference	Catalyst(2)	Carbon Type	Pt Loading mg/cm²(2)	Run Type(3)	Butane Performance, 14.7 M H_3PO_4, 150°C — Polarization from Theory at Indicated ma/cm², Volts: 0	5	10	15	20	25	30	35	40	45	50	55	60	O2 Performance Polarization from Theory at Ind. ma/cm², volts: 0	50	100	Comments
0195-[illegible]	[illegible] Pt on C	FC-50(6)	2.1	A	0.16	0.295	0.34	0.375	0.41	Dead	--	--	--	--	--	--	--	0.30	0.49	--	Ball milled before prep.
				B,C	0.17	0.255	--	0.36	0.40	Dead	--	--	--	--	--	--	--	--	--	--	
0195-[illegible]	[illegible] Pt on C	"	2.0	A	0.17	0.28	0.33	0.37	0.385	0.41	Dead	--	--	--	--	--	--	0.25	0.39	>0.60	
				B,C	0.175	0.27	--	0.35	--	0.42	Dead	--	--	--	--	--	--	--	--	--	Ball milled before prep.
0195-14	[illegible] Pt on C	"	1.8	A	0.165	0.295	0.35	0.375	0.39	0.42	0.45	Dead	--	--	--	--	--	0.26	0.36	0.45	
				B	0.17	0.25	--	0.335	--	0.36	--	0.42	0.44	0.46	Dead						
				C	--	--	--	--	--	--	--	--	--	--	0.47	0.50	Dead				
0195-24	4.6% Pt on C	"	1.8	A	0.17	0.35	0.44	Dead	--	--	--	--	--	--	--	--	--	0.24	0.335	0.44	Elect 0195-14 After
				B	0.195	0.23	0.35	0.395	0.42	0.46	Dead	--	--	--	--	--	--	--	--	--	Treatment with 1N HCl
				C	0.19	--	--	--	--	--	0.45	Dead	--	--	--	--	--	--	--	--	
0195-[illegible]	4.0% Pt on C-10% SiO_2	"	1.7	A	0.19	0.31	0.36	0.39	0.40	0.42	Dead	--	--	--	--	--	--	--	--	--	
				B	0.175	0.265	--	0.38	0.41	0.49	Dead	--	--	--	--	--	--	0.26	0.36	0.54	
				C	0.17	--	--	--	--	0.435	Dead	--	--	--	--	--	--	--	--	--	
0195-26	4.5% Pt on C-10% SiO_2	"	1.9	A	0.13	0.27	0.32	0.37	0.44	Dead	--	--	--	--	--	--	--	--	--	--	Ball milled before prep.
				B	0.16	0.255	--	Dead	--	--	--	--	--	--	--	--	--	0.30	>0.60	--	
0195-2[illegible]	4.3% Pt on C-10% SiO_2	"	1.8	A	0.155	0.30	0.35	0.395	0.44	Dead	--	--	--	--	--	--	--	0.35	Dead	--	Ball milled before prep.
0195-32	7.1% Pt on C	"	2.1	A	0.14	0.27	--	0.36	--	0.46	Dead	--	--	--	--	--	--	0.26	0.39	0.52	Ball milled before prep.
				B,C	0.15	0.255	--	0.355	--	0.43	Dead	--	--	--	--	--	--	--	--	--	
0195-36	4.0% Pt on C-10% SiO_2	"	1.7	A	0.195	0.30	0.355	0.39	0.415	0.45	0.50	Dead	--	--	--	--	--	--	--	--	
				B	0.19	0.28	--	0.37	--	0.44	--	0.49	--	--	--	--	--	0.25	0.35	0.43	
				C	0.18	--	--	--	--	--	--	--	0.47	0.475	Dead	--	--	--	--	--	
0195-4[illegible]	4.6% Pt on C	"	1.9	A	0.20	0.28	--	0.36	--	0.40	--	0.415	0.45	0.46	Dead	--	--	--	--	--	
				B	0.17	--	--	0.335	--	--	--	0.405	--	0.445	Dead	--	--	0.26	0.34	0.43	
				C	0.18	--	--	--	--	0.375	--	--	--	--	0.45	0.49	Dead	--	--	--	
0195-42	7.1% Pt on C	"	2.1	A	0.20	0.29	--	0.365	--	Dead	--	--	--	--	--	--	--	0.26	0.35	0.45	Ball milled before prep.
				B,C	0.17	--	--	0.37	0.415	0.46	Dead	--	--	--	--	--	--	--	--	--	
0195-51	21.3% Pt on C	"	2.2	A	0.21	0.39	Dead	--	--	--	--	--	--	--	--	--	--	0.26	0.45	>0.6	Adm. of Colloidal Pt
				B,C	0.205	0.355	0.42	Dead	--	--	--	--	--	--	--	--	--	--	--	--	
0195-79	6.4% Pt on C	"	1.8	A	0.18	0.43	Dead	--	--	--	--	--	--	--	--	--	--	0.25	0.42	0.50	Slurry electrode - poor
				B,C	0.17	0.35	--	0.44	0.45	Dead	--	--	--	--	--	--	--	--	--	--	Agglomeration
0195-[illegible]	2.6% Pt on C + 50% $Pt_{0.3}WO_3$	"	2.0	A	0.09	0.17	Dead	--	--	--	--	--	--	--	--	--	--	--	--	--	
				B	0.16	0.33	0.40	Dead	--	--	--	--	--	--	--	--	--	0.25	0.40	0.45	
				C	0.185	--	--	0.385	Dead	--	--	--	--	--	--	--	--	--	--	--	
0195-89	4.9% Pt on C	FC-20	2.9	A	0.12	0.255	0.35	0.37	0.39	0.41	0.43	0.44	0.46	Dead	--	--	--	0.25	0.32	0.39	
				B	0.16	--	--	0.31	--	--	--	0.405	--	0.46	Dead	--	--	--	--	--	19% Ozonization of C
				C	--	--	--	--	--	--	--	--	--	--	0.45	--	Dead	--	--	--	
0195-[illegible]	4.7% Pt on C	FC-50(6)	2.0	A	[illegible]	0.29	0.355	0.395	0.415	0.445	0.47	Dead	--	--	--	--	--	0.25	0.36	0.44	2 Hr. ball milling
				B,C	0.18	0.29	--	0.375	--	0.42	0.45	0.455	0.50	Dead	--	--	--	--	--	--	
0195-[illegible]	[illegible] Pt on C	"	"	A	0.145	0.275	0.33	0.385	0.44	Dead	--	--	--	--	--	--	--	0.25	0.37	0.44	1/2 Hr. ball milling
				B,C	0.175	0.275	--	0.39	--	Dead	--	--	--	--	--	--	--	--	--	--	
0195-[illegible]	10% Pt on C	"	~4.2	A	0.19	0.32	0.37	0.40	0.44	0.485	0.49	Dead	--	--	--	--	--	--	--	--	Combined colloidal Pt
				B	0.20	0.29	--	0.37	--	0.41	--	0.47	0.49	--	--	--	--	0.25	0.33	0.40	and adsorption of
				C	--	--	--	--	--	--	--	--	--	0.475	0.50	Dead	--	--	--	--	chloroplatinate
0195-[illegible]	4.7% Pt on C	"	2.0	A	0.16	0.33	0.39	0.41	0.425	0.455	Dead	--	--	--	--	--	--	--	--	--	8 Hr. ball milling
				B	0.17	0.30	--	0.38	--	0.43	--	0.48	Dead	--	--	--	--	0.25	0.35	0.425	
				C	--	--	--	--	--	--	--	--	0.47	Dead	--	--	--	--	--	--	
0195-[illegible]		"	"	A	[illegible]	0.35	0.375	0.405	0.435	0.47	Dead	--	--	--	--	--	--	0.25	0.33	0.40	24 Hr. ball milling
				B	0.20	0.30	--	0.375	--	0.415	--	0.455	--	--	--	--	--	--	--	--	
				C	--	--	--	--	--	--	--	--	0.45	0.51	Dead	--	--	--	--	--	
01[illegible]-11[illegible]		"	"	A	0.145	0.285	0.32	0.35	0.38	0.41	0.43	0.44	Dead	--	--	--	--	0.24	0.34	0.42	4 Hr. ball milling
				B,C	0.18	0.27	--	0.35	--	0.36	--	0.435	0.445	0.47	Dead	--	--	--	--	--	
[illegible]5-11[illegible]	"	"	"	A	0.175	0.40	0.46	Dead	--	--	--	--	--	--	--	--	--	0.24	0.39	0.45	Slurry electrode
				B,C	0.205	0.32	--	0.42	0.465	0.50	Dead	--	--	--	--	--	--	--	--	--	4 Hr. ball milling
0195-1[illegible]		"	"	A	0.15	0.40	Dead	--	--	--	--	--	--	--	--	--	--	0.26	0.36	--	Slurry electrode
				B,C	0.17	0.35	0.43	0.48	Dead	--	--	--	--	--	--	--	--	--	--	--	1/2 Hr. ball milling
0195-1[illegible]	[illegible] Pt on C	"	1.8	A	[illegible]	0.35	0.405	0.4[illegible]	0.4[illegible]	Dead	--	--	--	--	--	--	--	0.26	0.41	0.50	Double adsorption
				B,C	0.15	0.29	--	0.3[illegible]	--	0.46	0.475	Dead	--	--	--	--	--	--	--	--	Intermed. reduction @ 300°F
0195-1[illegible]	6.0% Pt on C	"	1.3	A	0.195	0.335	0.38	0.41	0.44	Dead	--	--	--	--	--	--	--	0.25	0.37	0.42	Double adsorption
				B,C	0.205	0.30	--	0.38	--	0.415	0.48	Dead	--	--	--	--	--	--	--	--	No intermed. reduction
0195-1[illegible]	4.0% Pt on C	"	2.5	A	0.20	0.30	0.34	0.38	0.405	0.43	0.45	0.47	Dead	--	--	--	--	--	--	--	
				B	0.21	--	--	0.34	--	0.375	--	0.41	--	0.48	Dead	--	--	0.26	0.33	0.39	Double adsorption
				C	0.21	--	--	--	--	--	--	--	--	--	0.48	Dead	-	--	--	--	No intermed. reduction

(1) Reduction of Pt salt with carbon monoxide followed by activation step except where indicated.
(2) Sintered carbon-Teflon electrode prepared using Teflon 42 BM emulsion (7.5 to 22.5%), except where indicated.
(3) A Butane performance before oxygen treat.
B Butane performance after oxygen treat.
C Butane performance after overpolarization.
(6) [illegible] were treated with 10% ozone by weight relative to C, and catalysts were ballmilled after prep. unless otherwise indicated.

SUPPORTED PLATINUM CATALYSTS

Reference	Catalyst[1]	Carbon Type	Pt Loading, mg/cm² [2]	Run Type [3]	Polarization from Theory vs. Indicated mA/cm², Volts: 0	5	10	15	20	25	30	35	40	45	50	55	60	O_2 Performance Polarization from Theory at Indicated mA/cm², volts: 0	50	100	Comments
4588-24	2.1% Pt on C	PC-30	1.3	A	0.13	0.28	0.36	0.40	Dead	--	--	--	--	--	--	--	--	--	--	--	10% CO_2 reburnout of C
				B	0.135	0.27	--	Dead	--	--	--	--	--	--	--	--	--	0.26	> 0.75	--	
4588-33	"	"	"	A	0.135	0.275	0.33	0.375	Dead	--	--	--	--	--	--	--	--	--	--	--	10% CO_2 reburnout of C
				B	0.14	0.275	--	0.40	Dead	--	--	--	--	--	--	--	--	0.28	0.51	--	
4588-35	"	"	"	A	0.16	0.30	0.33	0.38	Dead	--	--	--	--	--	--	--	--	--	--	--	10% CO_2 reburnout of C
				B	0.14	0.28	--	0.36	0.38	Dead	--	--	--	--	--	--	--	0.25	0.38	0.44	
				C	0.14					0.35	Dead										
4588-40	3.1% Pt on C	"	"	A	0.15	0.305	0.37	0.42	Dead	--	--	--	--	--	--	--	--	--	--	--	10% CO_2 reburnout of C
				B	0.16	0.26	--	0.355	0.37	Dead	--	--	--	--	--	--	--	0.28	0.39	0.43	
				C	0.12	--	--	--	--	0.40	--	--	--	--	--	--	--	--	--	--	
4588-46	2.1% Pt on C-10 wt%	"	0.88	A	0.13	Dead	--	--	--	--	--	--	--	--	--	--	--	--	--	--	
				B	0.17	0.38	Dead	--	--	--	--	--	--	--	--	--	--	0.30	0.44	0.50	
4588-37	1.2% Pt on C-10% SiO_2	PC-20 [7]	2.2	A	0.16	0.42	Dead	--	--	--	--	--	--	--	--	--	--	--	--	--	> 100 mesh hand ground C.
				B	0.14	0.39	Dead	--	--	--	--	--	--	--	--	--	--	0.28	> 0.5	--	
4588-42	3.0% Pt on C	"	2.6	A	0.16	0.40	Dead	--	--	--	--	--	--	--	--	--	--	--	--	--	> 100 mesh hand ground C.
				B	0.17	0.37	Dead	--	--	--	--	--	--	--	--	--	--	0.30	> 0.65	--	
4588-48	3.2% Pt on C-10% SiO_2	"	2.2	A	0.12	Dead	--	--	--	--	--	--	--	--	--	--	--	--	--	--	> 100 mesh hand ground C.
				B	0.16	0.41	Dead	--	--	--	--	--	--	--	--	--	--	0.33	> 0.65	--	
4589-4	3.1% Pt on C	"	2.6	A	0.12	0.255	0.32	0.395	0.385	0.38	Dead	--	--	--	--	--	--	--	--	--	Ballatiled before prep.
				B	0.15	0.23	--	0.32	--	0.38	--	--	--	--	--	--	--	0.35	0.40	0.46	
				C	0.155	--	--	--	--	--	0.41	Dead	--	--	--	--	--	--	--	--	
4589-6	3.4% Pt on C-10% SiO_2	"	2.25	A	0.21	0.335	0.44	Dead	--	--	--	--	--	--	--	--	--	--	--	--	Ballatiled before prep.
				B	0.19	0.32	0.42	Dead	--	--	--	--	--	--	--	--	--	0.31	0.43	0.52	
4589-9	3.1% Pt on C	"	2.6	A	0.135	0.31	Dead	--	--	--	--	--	--	--	--	--	--	--	--	--	No activation treat
				B	0.18	0.26	Dead	--	--	--	--	--	--	--	--	--	--	0.36	0.45	0.53	Ballatiled before prep.
4589-10	3.4% Pt on C-10% SiO_2	"	2.25	A	0.12	0.30	0.365	Dead	--	--	--	--	--	--	--	--	--	--	--	--	Ballatiled before prep.
				B	0.19	0.31	0.38	0.46	Dead	--	--	--	--	--	--	--	--	0.32	0.42	0.48	
4589-11	"	"	2.25	A	0.21	0.37	Dead	--	--	--	--	--	--	--	--	--	--	--	--	--	No activation treat
				B	0.19	0.36	0.43	Dead	--	--	--	--	--	--	--	--	--	0.29	0.39	0.50	Ballatiled before prep.
4588-13	3.1% Pt on C	"	2.6	A	0.15	0.29	0.36	0.38	0.39	Dead	--	--	--	--	--	--	--	--	--	--	Ballatiled before prep.
				B	0.18	0.27	--	0.37	0.39	Dead	--	--	--	--	--	--	--	0.33	0.38	0.45	
				C	0.18	--	--	--	--	0.43	Dead	--	--	--	--	--	--	--	--	--	
4589-19	4.2% Pt on C-10% SiO_2	"	2.4	A	0.155	0.265	0.37	0.36	0.45	Dead	--	--	--	--	--	--	--	--	--	--	Cellulose milled
				B	0.145	0.25	--	0.38	0.40	Dead	--	--	--	--	--	--	--	0.28	0.38	0.48	
				C	0.15	--	--	--	0.39	0.48	Dead	--	--	--	--	--	--	--	--	--	
4589-21	4.0% Pt on C-15% SiO_2	"	2.0	A	0.15	0.25	0.30	0.35	0.36	0.38	0.40	0.40	Dead	--	--	--	--	--	--	--	10% contamination of C
				B	0.17	0.25	--	0.38	--	0.37	--	0.40	0.42	Dead	--	--	--	0.31	0.36	0.41	
				C	0.16	--	--	--	--	--	--	--	--	0.42	0.455	0.49	Dead	--	--	--	
4589-27	4.9% Pt on C-10% SiO_2	"	2.9	A	0.14	0.27	0.32	0.37	0.38	0.405	0.425	0.43	Dead	--	--	--	--	--	--	--	10% contamination of C
				B	0.16	0.28	--	0.38	--	0.38	--	0.39	0.41	0.44	Dead	--	--	0.27	0.32	0.395	
				C	0.155	--	--	--	--	--	--	--	--	--	0.44	0.48	0.49	--	--	--	
4589-40	3.2% Pt on C-10% SiO_2	"	2.2	A	0.12	0.32	0.40	0.48	Dead	--	--	--	--	--	--	--	--	--	--	--	
				B,C	0.17	0.32	--	0.42	0.49	Dead	--	--	--	--	--	--	--	0.31	0.46	0.55	
4589-42	3.0% Pt on "	"	2.6	A	0.17	0.275	0.36	0.40	0.41	0.44	Dead	--	--	--	--	--	--	--	--	--	
				B	0.165	0.26	--	0.36	--	0.42	0.52	Dead	--	--	--	--	--	0.26	0.35	0.43	
				C	0.17	--	--	--	--	--	0.45	0.45	Dead	--	--	--	--	--	--	--	
4589-43	4.0% Pt on C-15% SiO_2	"	1.0	A	0.17	0.33	0.375	0.375	Dead	--	--	--	--	--	--	--	--	--	--	--	10% contamination of C
				B	0.145	0.29	--	0.37	0.41	Dead	--	--	--	--	--	--	--	0.32	0.37	0.43	
				C	0.17	--	--	--	--	0.45	0.43	--	--	--	--	--	--	--	--	--	
4589-47	4.9% Pt on C-10% SiO_2	"	1.6	A	0.165	0.315	0.37	0.41	Dead	--	--	--	--	--	--	--	--	--	--	--	10% contamination of C
				B	0.15	0.28	--	0.385	0.42	Dead	--	--	--	--	--	--	--	0.40	0.40	0.55	
				C	0.15	--	--	--	--	0.46	Dead	--	--	--	--	--	--	--	--	--	
4589-1	4.0% Pt on C	"	2.3	A	0.12	0.27	0.36	0.375	0.39	0.43	Dead	--	--	--	--	--	--	--	--	--	15% CO_2 burnout of C,
				B	0.17	0.25	--	0.35	--	0.46	Dead	--	--	--	--	--	--	0.35	0.44	0.48	ballatiled before prep.
4589-	3.3% Pt on C-15% SiO_2	"	2.3	A	0.16	0.35	0.415	0.46	0.53	Dead	--	--	--	--	--	--	--	--	--	--	15% CO_2 burnout of C,
				B,C	0.17	0.28	0.40	Dead	--	--	--	--	--	--	--	--	--	0.28	0.48	> 0.65	ballatiled before prep.
4594-1	4.0 Pt on C	"	2.5	A	0.13	0.27	0.34	0.38	0.375	0.395	Dead	--	--	--	--	--	--	--	--	--	15% CO_2 burnout of C,
				B,C	0.19	0.26	--	0.33	0.37	0.39	Dead	--	--	--	--	--	--	0.37	0.50	--	ballatiled before prep.
4594-24	3.9% Pt on C	"	"	A	0.16	0.25	0.30	0.335	0.355	0.375	0.425	0.41	0.42	Dead	--	--	--	--	--	--	10% contamination of C
				B	0.16	0.22	--	0.295	--	0.35	--	0.39	--	0.42	Dead	--	--	0.31	0.37	0.42	
				C	0.175	--	--	--	--	--	--	--	--	--	0.405	0.43	Dead	--	--	--	
4594-34	3.15 Pt on C	"	1.3	A	0.20	0.32	0.38	0.43	0.49	Dead	--	--	--	--	--	--	--	--	--	--	20% contamination of C
				B	0.21	0.31	--	0.41	0.44	Dead	--	--	--	--	--	--	--	0.33	0.36	0.45	
				C	--	--	--	--	--	0.445	Dead	--	--	--	--	--	--	--	--	--	
4594-38	2.8% Pt on C-10% SiO_2	"	1.2	A	0.17	0.33	0.40	Dead	--	--	--	--	--	--	--	--	--	--	--	--	20% contamination of C
				B	0.21	0.32	--	0.35	0.44	Dead	--	--	--	--	--	--	--	0.36	0.39	0.48	
4594-36	3.1% Pt on C-10% SiO_2	"	2.3	A	0.18	0.29	0.36	0.40	0.44	0.49	Dead	--	--	--	--	--	--	--	--	--	20% contamination of C
				B	0.18	0.285	--	0.36	--	0.415	--	0.48	Dead	--	--	--	--	0.26	0.37	0.47	
				C	0.19	--	--	--	--	--	--	--	0.48	Dead	--	--	--	--	--	--	

(1) Reduction of Pt salt with carbon monoxide followed by activation step except where indicated.
(2) Sintered carbon Teflon electrode prepared using Teflon 42 DE emulsion (7.3 to 12.5%), except where indicated.
(3) A - Before performance before oxygen treat
B - Before performance after oxygen treat
C - Before performance after overpolarization.
(7) All PC-20K carbons were ballatiled after preparation unless other grinding procedure is listed.

SUPPORTED PLATINUM CATALYSTS

Reference	Catalyst[1]	Carbon Type	Pt Loading, mg/cm²[2]	Run Type[3]	Butane Performance, 14.7 N H_3PO_4, 150°C Polarization from Theory at Indicated ma/cm², Volts												O_2 Performance Polarization from Theory at Indicated ma/cm², volts:			Comments
					0	5	10	15	20	25	30	35	40	45	50	55	e0	0	50	100	
[illegible]	6.3% Pt on [illegible]	FC-50[4]	1.9	A	0.17	0.34	0.39	0.41	Dead	--	--	--	--	--	--	--	--	--	--	--	
				B	0.17	0.25	--	0.33	--	0.37	0.40	0.41	Dead	--	--	--	--	0.32	0.43	0.53	
				C	0.18	--	--	--	--	--	--	--	0.39	0.43	0.45	0.46	Dead	--	--	--	
[illegible]	6.3% Pt on [illegible]	"	"	B	0.135	--	--	0.315	.335	--	--	Dead	--	--	--	--	--	--	--	--	Second day operation of 0096-42.
				C	0.145	--	--	--	--	--	--	0.34	0.37	0.37	0.39	--	0.42	--	--	--	
[illegible]	6.8% Pt on C-10% ZrO_2	"	1.7	A	0.18	0.35	0.395	0.44	0.45	Dead	--	--	--	--	--	--	--	--	--	--	
				b	0.21	0.30	--	0.39	--	0.435	Dead	--	--	--	--	--	--	0.24	0.34	0.42	
				C	0.21	--	--	--	--	--	0.42	0.43	0.46	Dead	--	--	--	--	--	--	
[illegible]	6.3% Pt on C	"	1.9	A	0.16	0.28	0.35	0.36	0.38	0.41	0.40	Dead	--	--	--	--	--	--	--	--	
				B	0.18	0.26	--	0.34	--	0.38	--	0.405	0.42	Dead	--	--	--	0.31	0.38	0.45	
				C	0.17	--	--	--	--	--	--	--	--	0.41	0.435	0.44	0.45	--	--	--	
[illegible]		"	2.8	A	0.17	0.305	0.35	0.38	0.41	0.43	0.46	0.48	0.50	Dead	--	--	--	--	--	--	1-1/2 x Standard loading.
				B	0.20	--	--	0.33	--	--	--	0.40	--	0.43	--	0.47	Dead	0.30	0.38	0.48	
[illegible]		"	0.5	A	0.16	0.44	Dead	--	--	--	--	--	--	--	--	--	--	--	--	--	1/4 x Standard loading.
				B,C	0.20	0.33	0.42	Dead	--	--	--	--	--	--	--	--	--	0.30	0.46	0.56	
[illegible]		"	"	A	0.20	0.46	Dead	--	--	--	--	--	--	--	--	--	--	--	--	--	"
				B,C	0.21	0.39	0.45	Dead	--	--	--	--	--	--	--	--	--	0.27	0.42	0.51	
[illegible]		"	"	A	0.16	0.385	Dead	--	--	--	--	--	--	--	--	--	--	--	--	--	"
				B,C	0.19	0.35	0.40	0.45	Dead	--	--	--	--	--	--	--	--	0.31	0.44	0.52	
[illegible]		"	"	A	0.19	0.40	Dead	--	--	--	--	--	--	--	--	--	--	--	--	--	"
				B,C	0.22	0.34	0.42	0.45	Dead	--	--	--	--	--	--	--	--	0.27	0.37	0.42	
[illegible]		"	"	A	0.17	0.34	0.38	Dead	--	--	--	--	--	--	--	--	--	--	--	--	"
				B,C	0.195	0.31	0.35	0.39	Dead	--	--	--	--	--	--	--	--	0.30	0.44	0.52	
[illegible]		"	"	A	0.21	0.395	Dead	--	--	--	--	--	--	--	--	--	--	--	--	--	"
				B,C	0.21	0.37	0.44	Dead	--	--	--	--	--	--	--	--	--	0.27	0.45	0.52	

(1) Evaporation of Pt salt with carbon suspension followed by activation step except where indicated.
(2) Sintered carbon Teflon electrode prepared using Teflon 41 BK emulsion (7.5 to 22.5%), except where indicated.
(3) A. Butane performance before oxygen treat.
B. Butane performance after oxygen treat.
C. Butane performance after overpolarization.
(4) All FC-50C's were treated with 15% arsine by weight relative to C, and catalysts were ballmilled after prep, unless otherwise indicated.

APPENDIX C-2

PREPARATION OF ALUMINO SILICATE ON CARBON SUBSTRATES

Test No.	Solution A	Solution B	Order of Addition	Temp of Stirring, °C	Time of Stirring, min	Time of Filtration, min	Time of Washing, min	Amount of Wash, ml	pH at End of Wash	Amount Recovered of Alumino Silicate on Carbon, gms	Comments
6261-30-1	22 ml H_2O 1 gm $NaAlO_2$ .100 gm NaOH 2.54 gm Na Silicate 1 gm "B" Carbon	--	--	80	--	--	--	≅ 200	≅ 9-12	2.4801	
6261-32-1	22.5 ml H_2O 1 gm $NaAlO_2$ .100 gm NaOH 2.54 gm Na Silicate 1 gm "B" Carbon	--	--	80	40	--	--	≅ 140 cc	≅ 9-12	2.2953	
6261-32-2	Same as above 32-1	--	--	60	60	--	--	≅ 220 cc	≅ 9-12	2.2843	
6261-33-1	22 ml H_2O 2.54 gm Na Silicate 1.007 gm NaOH 1 gm $NaAlO_2$ 1.0026 gm "B" Carbon	--	--	25	20	--	--	305	≅ 9.7	2.2814	
6261-33-2	Same as above except 1.0053 gm "B" Carbon	--	--	40	10	--	--	280	≅ 9.8	2.3063	
6261-33-3	Same as above except 1.0033 gm "B" Carbon	--	--	50	24	--	--	335	≅ 9.5	2.3010	
6261-39-1	22.1 ml H_2O 2.54 gm Na Silicate 1.008 gm NaOH ≅1.0 gm "B" Carbon	110 ml H_2O 1 gm $NaAlO_2$	B to A	25	.5	5.0	--	≅ 50	≅ 10.0	--	Some product passed through filter.
6261-39-2	Same as Above	Same as Above	B to A	25	.5	15 sec	--	--	--	--	Some product passed through filter.
6261-37-1	4.1 ml H_2O .1136 gm Na Silicate .1 gm NaOH .0270 gm "B" Carbon	1.1 ml H_2O 0.1 gm $NaAlO_2$	B to A	25	20	≪1	18	70 cc	9-10	1.1429	
6261-37-2	11 ml H_2O .254 gm Na Silicate .100 gm NaOH .2654 gm "B" Carbon	11.0 ml H_2O 0.1 g $NaAlO_2$	B to A	25	20	16	66	80	9.2	1.11.	
6261-30-3a	110 ml H_2O 2.54 gm Na Silicate 1.008 gm NaOH 1.0270 gm "B" Carbon	110 ml H_2O 1.0 gm $NaAlO_2$	B to A	25	5	104	⩾60	220 cc	9.5/12.0	2.0045	

NOTE: "A" Carbons were CO_2 burned out PC-30 carbon.
"B" Carbons had 100 m^2/gm surface area.
"B" Carbon had 110 m^2/gm surface area.

APPENDIX C-1 (CONT'D)

PREPARATION OF ALUMINO SILICATE ON CARBON SUPPORTATES

Test No.	Solution A	Solution B	Order of Addition	Temp of Stirring, °C	Time of Stirring, min	Time of Filtration, min	Time of Washing, min	Amount of Wash, ml	pH at End of Wash	Amount Recovered of Alumino Silicate on Carbon, gms	Comments
4265-38-3b	Same as above except "B" Carbon = 1.0020 gm	Same as Above	B to A	25	5	14	55	220	11.5	1.9560	Some material lost through filter.
4265-39-3c	Same as Above except "B" Carbon = .9951 gm	Same as Above	B to A	25	5	12	40	265	9.7	1.927e	
4255-39-4	110 ml H_2O 256 gm Na Silicate 1.08 gm NaOH 1.0091 gm "B" Carbon	110 ml H_2O 1.0 gm $NaAlO_2$	B to A	25	20	5	23	225	10	2.1647	
4265-40-5	110 ml H_2O 2.56 gm Na Silicate 1.08 gm NaOH .9980 gm "B" Carbon	110 ml H_2O 1.0 gm $NaAlO_2$	B to A	25	120	1.5	5	135	9.5	2.2161	.0441 gm of material passed through filter.
4265-40-6	110 ml H_2O 2.56 gm Na Silicate 0.9917 gm "B" Carbon	110 ml H_2O 1.0 gm $NaAlO_2$ 1.08 gm NaOH	B to A	25	20	5	31	350	9.0	2.2021	.0483 gm of material passed through filter.
4265-41-7	110 ml H_2O 2.56 gm Na Silicate	110 ml H_2O 1.0 gm $NaAlO_2$ 1.08 gm NaOH 1.0037 gm "B" Carbon	B to A	25	20	12	44	295	11.0	2.0705	
4265-41-8	1.1 ml H_2O 0.1103 gm NaOH 0.2315 gm Na Silicate	1.1 ml H_2O 0.1 gm $NaAlO_2$	B to A	25	.5	--	--	--	--	--	Combination of solutions A + B poured through 1 gm carbon on filter. Formed white layer on top of carbon.
4265-41-9	11.0 ml H_2O 2.56 gm Na Silicate 1.08 gm NaOH	11.0 ml H_2O 1.0 gm $NaAlO_2$	B to A	25	.5	--	70	175	10.0	2.2190	Same as above.
4265-42-12	110 ml H_2O 0.256 gm Na Silicate 0.108 gm NaOH 0.9985 gm "B" Carbon	110 ml H_2O 0.1 gm $NaAlO_2$	B to A	25	20	.5	1	55	9.0	0.9516	
4265-43-1	55 ml H_2O 0.64 gm Na Silicate 0.27 gm NaOH 5.0051 gm "B" Carbon	55 ml H_2O 0.25 gm $NaAlO_2$	B to A	25	20	.75	3	130	9.4	4.9717	
4265-43-2	55 ml H_2O 1.28 gm Na Silicate 0.54 gm NaOH 5.0066 gm "B" Carbon	55 ml H_2O 0.50 gm $NaAlO_2$	B to A	25	20	.75	8	180	9.6	5.5970	
4265-44-3	55 ml H_2O 2.56 gm Na Silicate 1.08 gm NaOH 5.0061 gm "B" Carbon	55 ml H_2O 1.0 gm $NaAlO_2$	B to A	25	--	1	11	220	10.0	6.2328	

NOTE: All carbons were CO_2 burned out "C-30 carbon.
"A" Carbon had 195 m^2/gm surface area.
"B" Carbon had 110 m^2/gm surface area

APPENDIX D-1

PREPARATION OF MIXED SODIUM, POTASSIUM PHOSPHATE MELT

Sample Number	Weight of Original Mixture (gms)	Weight of Resultant Melt (gms)	Percent Weight Loss
1	43.67	40.70	6.8
2	49.03	45.56	7.7
3	53.20	49.68	6.2

APPENDIX D-2

ANODIC BUFFER ACTION OF MIXED PHOSPHATE MELT AT 250°C

Current Density, ma/cm^2	Polarization from Hydrogen Theory, volts			
	(1)	(2)	(3)	(4)
50	0.04	0.02	0.01	0.06
100	0.05	0.05	0.04	0.07
200	0.11	0.10	0.07	0.08
300	0.11	0.12	0.11	0.11
400	0.55	0.14	0.12	0.11

(1) and (2) dry hydrogen duplicate runs.

(3) hydrogen sparged through water at 50°C.

(4) hydrogen sparged through water at 80°C.

APPENDIX D-3

CATHODIC BUFFER ACTION OF MIXED PHOSPHATE MELT AT 250°C

Current Density, ma/cm^2	Polarization from Hydrogen Theory, volts		
	(1)	(2)	(3)
25	0.01	0	0.02
50	0.02	0	0.02
100	0.04	0.01	0.03
150	0.06	0.01	0.04

(1) dry hydrogen.

(2) hydrogen sparged thr ugh water at 60°C.

(3) hydrogen sparged through water at 90°C.

APPENDIX D-4

BUTANE PERFORMANCE ON SINTERED PLATINUM-TEFLON ELECTRODES IN THE MIXED PHOSPHATE MELT AT 250°C

Water Bath Temp, °C	Polarization from Butane Theory at Indicated ma/cm^2, volts						
	5	10	50	100	200	300	400
80	0.23	0.25	0.31	0.35	0.37	0.33	0.29-0.46
80	0.22	0.23	0.27	0.27	0.35	0.27	0.17-0.29
80	0.23	0.25	0.34	0.37	0.37	--	--
80	--	--	0.40	0.45	0.44	0.32	--
60	0.41	0.42	0.45	0.52	0.55-0.59	--	--

APPENDIX D-5

OXYGEN PERFORMANCE ON SINTERED PLATINUM-TEFLON ELECTRODES IN THE MIXED PHOSPHATE MELT

Oxygen Humidified With Water at	Polarization from Oxygen Theory at Indicated ma/cm^2, volts						
	0	10	25	50	100	150	200
No humidification	0.06	0.21	0.23	0.25	0.22	--	(1)
60°C	0.08	0.13	0.17	0.18	0.22	0.31	0.39
80°C	0.08	0.13	0.13	0.17	0.18	0.18	0.19
90°C	0.09	0.10	0.16	0.17	0.19	0.17	0.18

(1) Dry oxygen was not tested beyond 100 ma/cm^2.

Security Classification

DOCUMENT CONTROL DATA - R&D

(Security classification of title, body of abstract and indexing annotation must be entered when the overall report is classified)

1. ORIGINATING ACTIVITY (Corporate author)	2a. REPORT SECURITY CLASSIFICATION
Esso Research and Engineering Company Government Research Laboratory Linden, New Jersey	Unclassified 2b GROUP

3. REPORT TITLE

HYDROCARBON-AIR FUEL CELL

4. DESCRIPTIVE NOTES (Type of report and inclusive dates)

Semi-Annual - 1 January 1966 - 31 July 1966

5. AUTHOR(S) (Last name, first name, initial)

Heath, Carl E.; Horowitz, Hugh H.; Ciprios, George; Okrent, Eugene H.; Asher, William J.; Batzold, John S.; Beltzer, Morton; Broyde, Barret; Zimmerman, Abraham, A.

6. REPORT DATE	7a. TOTAL NO. OF PAGES	7b. NO. OF REFS
October 1966	111	68

8a. CONTRACT OR GRANT NO.	9a. ORIGINATOR'S REPORT NUMBER(S)
DA 36-039 AMC-03743(E) b. PROJECT NO. AMC Code: 1C622001A053-04 c. d.	9b. OTHER REPORT NO(S) (Any other numbers that may be assigned this report) ECOM-03743-9

10. AVAILABILITY/LIMITATION NOTICES

Each transmittal of this document outside the Department of Defense must have prior approval of CG, U.S. Army Electronics Command, Fort Monmouth, N.J. ATTN: AMSEL-KL-PB

11. SUPPLEMENTARY NOTES	12. SPONSORING MILITARY ACTIVITY
	U.S. Army Electronics Command Fort Monmouth, New Jersey 07703 ATTN: AMSEL-KL-PB

13. ABSTRACT

Studies aimed at the development of a direct hydrocarbon-air fuel cell system for moderate temperature and pressure operation indicates that anode electrocatalysis is the key problem area. Consequently, research during this report period emphasized studies aimed at (1) improving platinum catalyst utilization and (2) developing a non-noble metal hydrocarbon catalyst. Two classes of compounds which meet the electrocatalyst requirements, the tungsten bronzes and the eta-phase carbides, were investigated. None of the carbides tested showed significant activity. However, a $Ni_{0.237}WO_3$ tungsten bronze has shown catalytic activity on hydrogen in 90°C sulfuric acid without any evidence of corrosion.

Work aimed at improving noble metal utilization through the use of improved supports, co-supports and decomposition techniques has resulted in an improved butane catalyst. Tests in 150°C phosphoric acid yielded a current density of 80 ma/cm^2 at a loading of only 3.2 mg Pt/cm^2. An alternate route to improved utilization is the use of an intermediate temperature electrolyte (250-275°C). These electrolytes should significantly improve power densities with noble metals and some are sufficiently non-corrosive to be useful with non-noble metal catalysts. Pyrophosphoric acid and mixed alkali metal hydrogen phosphates have sustained high current densities at both the hydrocarbon anode and oxygen cathode.

At 250°C the butane electrode was polarized only 0.35 volts at 200 ma/cm^2 while the oxygen electrode was only 0.18 volts polarized. Based upon these results, efforts to improve catalyst utilization through the use of supports and intermediate temperature electrolytes warrants further work.

DD FORM 1 JAN 64 1473

Security Classification

14. KEY WORDS	LINK A		LINK B		LINK C	
	ROLE	WT	ROLE	WT	ROLE	WT
Hydrocarbon Oxidation Adsorption Mechanism Catalyst Utilization Electrochemical Activity Non-Noble Catalysts Buffer Electrolytes Limiting Currents Noble Metal Alloy Catalysts Electrode Structure Catalyst Supports						

INSTRUCTIONS

1. ORIGINATING ACTIVITY: Enter the name and address of the contractor, subcontractor, grantee, Department of Defense activity or other organization *(corporate author)* issuing the report.

2*a*. REPORT SECURITY CLASSIFICATION: Enter the overall security classification of the report. Indicate whether "Restricted Data" is included. Marking is to be in accordance with appropriate security regulations.

2*b*. GROUP: Automatic downgrading is specified in DoD Directive 5200.10 and Armed Forces Industrial Manual. Enter the group number. Also, when applicable, show that optional markings have been used for Group 3 and Group 4 as authorized.

3. REPORT TITLE: Enter the complete report title in all capital letters. Titles in all cases should be unclassified. If a meaningful title cannot be selected without classification, show title classification in all capitals in parenthesis immediately following the title.

4. DESCRIPTIVE NOTES: If appropriate, enter the type of report, e.g., interim, progress, summary, annual, or final. Give the inclusive dates when a specific reporting period is covered.

5. AUTHOR(S): Enter the name(s) of author(s) as shown on or in the report. Enter last name, first name, middle initial. If military, show rank and branch of service. The name of the principal author is an absolute minimum requirement.

6. REPORT DATE: Enter the date of the report as day, month, year; or month, year. If more than one date appears on the report, use date of publication.

7*a*. TOTAL NUMBER OF PAGES: The total page count should follow normal pagination procedures, i.e., enter the number of pages containing information.

7*b*. NUMBER OF REFERENCES: Enter the total number of references cited in the report.

8*a*. CONTRACT OR GRANT NUMBER: If appropriate, enter the applicable number of the contract or grant under which the report was written.

8*b*, 8*c*, & 8*d*. PROJECT NUMBER: Enter the appropriate military department identification, such as project number, subproject number, system numbers, task number, etc.

9*a*. ORIGINATOR'S REPORT NUMBER(S): Enter the official report number by which the document will be identified and controlled by the originating activity. This number must be unique to this report.

9*b*. OTHER REPORT NUMBER(S): If the report has been assigned any other report numbers *(either by the originator or by the sponsor)*, also enter this number(s).

10. AVAILABILITY/LIMITATION NOTICES: Enter any limitations on further dissemination of the report, other than those imposed by security classification, using standard statements such as:

(1) "Qualified requesters may obtain copies of this report from DDC."

(2) "Foreign announcement and dissemination of this report by DDC is not authorized."

(3) "U. S. Government agencies may obtain copies of this report directly from DDC. Other qualified DDC users shall request through _____."

(4) "U. S. military agencies may obtain copies of this report directly from DDC. Other qualified users shall request through _____."

(5) "All distribution of this report is controlled. Qualified DDC users shall request through _____."

If the report has been furnished to the Office of Technical Services, Department of Commerce, for sale to the public, indicate this fact and enter the price, if known.

11. SUPPLEMENTARY NOTES: Use for additional explanatory notes.

12. SPONSORING MILITARY ACTIVITY: Enter the name of the departmental project office or laboratory sponsoring *(paying for)* the research and development. Include address.

13. ABSTRACT: Enter an abstract giving a brief and factual summary of the document indicative of the report, even though it may also appear elsewhere in the body of the technical report. If additional space is required, a continuation sheet shall be attached.

It is highly desirable that the abstract of classified reports be unclassified. Each paragraph of the abstract shall end with an indication of the military security classification of the information in the paragraph, represented as *(TS)*, *(S)*, *(C)*, or *(U)*.

There is no limitation on the length of the abstract. However, the suggested length is from 150 to 225 words.

14. KEY WORDS: Key words are technically meaningful terms or short phrases that characterize a report and may be used as index entries for cataloging the report. Key words must be selected so that no security classification is required. Identifiers, such as equipment model designation, trade name, military project code name, geographic location, may be used as key words but will be followed by an indication of technical context. The assignment of links, rules, and weights is optional.